

Fig. 3. Temperature polarization.

increase in mass flux and temperature (vapor enthalpy depends on temperature).

The temperature polarization coefficient (τ) defined in Eq. (2) can be obtained by substituting T_1 and T_2 from Eqs. (9) and (10):

$$\tau = 1 - \left(\frac{JH_{v}\{(T_1 + T_2)/2\}}{T_f - T_p} \left(\frac{1}{h_f} + \frac{1}{h_p}\right)\right)$$
(11)

Spacers can improve the flow characteristics at the membrane surface [3,4] by promoting regions of turbulence due to the formation of eddies and wakes when the fluid passes spacer strands. As a consequence, the film heat transfer coefficient is increased. Then, the membrane surface temperature T_1 is raised to $T_1^{\rm s}$, and T_2 is reduced to $T_2^{\rm s}$ (see Fig. 3) (the superscript 's' indicates the spacer filled channel condition). In such a situation heat and mass transfer models are written as

$$J = C^{8}(P_{1}^{3} - P_{2}^{3}) \tag{12}$$

and

$$h_{\rm f}^{\rm s}(T_{\rm f}-T_{\rm l}^{\rm s})=JH_{\rm v}\left\{\frac{T_{\rm l}^{\rm s}+T_{\rm 2}^{\rm s}}{2}\right\}=h_{\rm p}^{\rm s}(T_{\rm 2}^{\rm s}-T_{\rm p})$$
 (13)

or

$$T_{\rm i}^{\rm s} = T_{\rm f} - \frac{J^{\rm s}}{h_{\rm f}^{\rm s}} H_{\rm v} \left\{ \frac{T_{\rm i}^{\rm s} + T_{\rm i}^{\rm s}}{2} \right\} \tag{14}$$

$$T_2^s = T_p + \frac{J^s}{h_p^s} H_v \left\{ \frac{T_1^s + T_2^s}{2} \right\}$$
 (15)

The heat and mass transfer models are used to derive the mass flux enhanced model for the spacer filled channel. The first step in the derivation is to consider the ratio of mass flux between empty and spacer filled channels as expressed below.

$$\frac{J^{s}}{J} = \frac{C^{s}(P_{1}^{s} - P_{2}^{s})}{C(P_{1} - P_{2})}$$
 (16)

Both membrane distillation coefficients, C and C^s depend on the membrane morphology; such as the porosity, pore size, membrane tortuosity, membrane thickness and also depend on the vapor properties such as molecular weight, mean free path, and mean membrane temperature [8,10]. Such properties would be unchanged and we can assume that the membrane distillation coefficients are unaffected by the spacer. Then, Eq. (16) can be rewritten as

$$\frac{J^s}{J} = \frac{P_1^s - P_2^s}{P_1 - P_2} \tag{17}$$

This can be further simplified for the special case when the feed and permeate solutions are the distilled water, the flow rates on both sides are equal, and the bulk temperature difference between feed and permeate side is less than 10°C. We can then assume that the film heat transfer coefficients on both sides are equal $(h_f^s = h_p^s = h^s)$, and the vapor pressure polarization coefficient (f) is equal to the temperature polarization coefficient (τ) [1]. With this assumption, Eq. (17) can be expressed by Eq. (18):

$$\frac{J^{s}}{J} = \frac{\tau^{s}}{\tau} \tag{18}$$

and

$$\tau^{s} = \frac{T_{1}^{s} - T_{2}^{s}}{T_{f} - T_{p}} \tag{19}$$

 T_1^s and T_2^s are given by Eqs. (14) and (15). When $h_f^s = h_p^s$, the average membrane temperature $(T_1^s + T_2^s)/2$ can be replaced by the average bulk temperature $(T_f + T_p)/2$. This assumption can be proven from the heat transfer model, Eq. (13), as shown below.

From Eq. (13): $h_{\rm f}^{\rm s}(T_{\rm f}-T_{\rm l}^{\rm s})=h_{\rm p}^{\rm s}(T_{\rm 2}^{\rm s}-T_{\rm p})$, when $h_{\rm f}^{\rm s}=h_{\rm p}^{\rm s}$; Eq. (13) can be written by

$$T_{\rm f} - T_{\rm i}^{\rm s} = T_{\rm 2}^{\rm s} - T_{\rm p} \tag{20}$$

Eq. (20) is rearranged:

$$T_1^s + T_2^s = T_f + T_p$$

So

$$\frac{T_1^s + T_2^s}{2} = \frac{T_f + T_p}{2} \tag{21}$$

Combination of Eqs. (14), (15), (18), (19) and (21) gives Eq. (22) shown below:

$$J^{s} = \frac{J}{\tau} \left[\frac{T_{f} - (J^{s}/h^{s})H_{v}\{(T_{f} + T_{p})/2\}}{-T_{p} - (J^{s}/h^{s})H_{v}\{(T_{f} + T_{p})/2\}}}{T_{f} - T_{p}} \right]$$
(22)

After rearranging Eq. (22), the model predicting mass flux enhancement due to the effect of the spacer is obtained:

$$\frac{J^{s}}{J} = \frac{1}{(\tau + [\{2J/h^{s}(T_{f} - T_{p})\}H_{v}\{(T_{f} + T_{p})/2\}])}$$
(23)

In Eq. (23), the values of J and τ are known from the empty channel experiments. The vapor enthalpy of water (H_v) is determined by [11,12]

$$H_{\rm v} = 1.7535T + 2024.3\tag{24}$$

where T is the temperature (K) and H_v the vapor enthalpy of water (kJ kg⁻¹).

For the same conditions as described above, the temperature polarization coefficient for the empty channel in Eq. (11) becomes

$$\tau = 1 - \frac{2J}{h(T_f - T_p)} H_v \left\{ \frac{T_f + T_p}{2} \right\}$$
 (25)

where h is the heat transfer coefficient for the empty channel, calculated from heat transfer correlations such as the Graetz-Leveque equation, Eq. (26) [13]:

$$Nu = 1.86 \left(Re Pr \frac{d_{\rm h}}{L} \right)^{0.33} \tag{26}$$

Combining Eqs. (23) and (25), the mass flux enhanced by the spacers is expressed as

$$\frac{J^{s}}{J} = \frac{1}{1 - [(2JH_{v}\{(T_{f} + T_{p})/2\}/(T_{f} - T_{p})\}\{(1/h) - (1/h^{s})\}]}$$
(27)

The film heat transfer coefficient for the spacer filled channels, h^s in Eq. (27), is determined from heat transfer correlations for the spacer filled channel. Da Costa [14] obtained mass transfer correlations for spacer filled channels which can be used by assuming an analogy between heat and mass transfer. Thus, the heat transfer correlations can be written by:

• for spacers inducing directional flow change:

$$Nu = 0.664k_{\rm dc} Re^{0.5} Pr^{0.33} \left(\frac{2d_{\rm h}}{l_{\rm m}}\right)^{0.5}$$
 (28)

and

$$k_{\rm dc} = 1.654 \left(\frac{d_{\rm f}}{h}\right)^{-0.039} \varepsilon^{0.75} \left(\sin\left(\frac{\theta}{2}\right)\right)^{0.086} (29)$$

 for spacers that do not induce change in flow direction (one set of filaments is parallel to and the other is transverse to flow directions):

$$Nu = 0.664 Re^{0.5} Pr^{0.33} \left(\frac{d_{\rm h}}{l_{\rm m}}\right)^{0.5}$$
 (30)

where Nu is the Nusselt number, Re the Reynolds number, and Pr the Prandtl number, other symbols are defined in the nomenclature.

The Re for the spacer filled flat channel is expressed by

$$Re = \frac{\rho u^{s} d_{h}}{\mu} \tag{31}$$

where u^s is the velocity when the spacer fills the channel, ρ the density, and μ the viscosity.

The velocity u^s can be calculated by [4]

$$u^{s} = \frac{Q}{A\varepsilon} \tag{32}$$

where Q is the volumetric flow rate, and A the cross sectional area of empty channel.

The diameter d_h can be calculated by [15]

$$d_{\rm h} = \frac{4\varepsilon}{(2/h_{\rm sp}) + (1 - \varepsilon)S_{\rm vsp}} \tag{33}$$

where h_{sp} is the spacer thickness, and S_{vsp} the specific surface of the spacer.

$$S_{\text{vsp}} = \frac{4}{d_{\text{f}}} \tag{34}$$

According to [14], spacer voidage is calculated by

$$\varepsilon = 1 - \frac{\pi d_{\rm f}^2}{2l_{\rm m}h_{\rm sp}\sin\theta} \tag{35}$$

When the value of the heat transfer coefficient for the spacer filled channels is large, the temperature polarization coefficient in the channels approaches unity.

Table 1 Characteristics of coarse and fine spacers

Spacer	$h_{\rm sp} \times 10^3$ (m)	$d_{\rm f} \times 10^3 ({\rm m})$	$l_{\rm m} \times 10^3 (\rm m)$	Voidage e	S _{vsp} (m ⁻¹)	$d_{\rm h} \times 10^3 \; (\rm m)$	Angle θ (°)
Coarse	2.1	1.15	4.85	0.796	3478	1.92	80
Fine	1.15	0.55	2.8	0.852	7273	1.21	90

At this condition, we obtain the maximum mass flux enhanced by the effect of spacers (J_{max}^{s}). Eq. (18) can be changed to Eq. (36), giving

$$\frac{J_{\max}^s}{I} = \frac{1}{\tau} \tag{36}$$

Eq. (36) shows that the effect of spacers on mass flux enhancement will be most evident for DCMD systems which have poor fluid dynamic arrangements (low temperature polarization coefficient). For DCMD systems which have good fluid dynamics (high temperature polarization coefficient), τ falls in the range of 0.4–0.7 [8]. Thus, the probable maximum ratio of mass flux enhanced by the spacers and mass flux for the empty channel would be in the range 1.43–2.5.

3. Experimental

The model was tested by comparison with the results obtained using an unsupported flat sheet membrane in a direct contact membrane distillation module. The membrane was Millipore GVHP (PVDF) with a nominal pore size of $0.2 \,\mu\text{m}$, a porosity of 80%, membrane thickness of $125 \,\mu\text{m}$, and thermal conductivity of $0.14 \, \text{W} \, \text{m}^{-1} \, \text{K}^{-1}$.

The membrane module was made from perspex (polymerized methylmethacrylate) with a flow channel 40 mm wide, 100 mm long, and 2.5 mm high. The effective membrane area was 0.004 m². In all experiments, the membrane module was placed in the vertical position. Distilled water was used as the feed and permeate solutions.

The feed solution was heated and maintained at the required temperatures in a thermostatic water bath, and the permeate solution was maintained at the required temperature by a cooler. Both feed and permeate solutions were pumped into the bottom of the module and flowed co-currently. The process solutions were circulated through closed thermostatic systems.

The temperatures of the process streams were measured by thermocouples at the entrance $(T_{f,in}, T_{p,in})$ and exit $(T_{f,out}, T_{p,out})$ of the module. Average values of the temperatures T_f and T_p were calculated by

$$T_{\rm f} = \frac{T_{\rm f,in} + T_{\rm f,out}}{2} \tag{37}$$

$$T_{\rm p} = \frac{T_{\rm p,in} + T_{\rm p,out}}{2} \tag{38}$$

In the experiments, the bulk temperature difference was 10°C, while the average temperature of T_f varied from 40 to 50°C and T_p from 30 to 40°C. The experiments were carried out for two different flow rates: 12 and 19 ml s⁻¹.

The spacers used in this work were coarse (80 MIL type) and fine spacer, the geometric characteristics of these spacers are summarized in Table 1.

The values of mass flux for the empty channel (J) and the values of experimental mass flux for spacer filled channels (J_{exp}^s) were obtained experimentally. The values of τ for empty channels were determined from Eqs. (25) and (26) (all physical properties evaluated at mean bulk temperature). Eq. (23) or Eq. (27) was used to estimate the mass flux enhanced by the spacers (J_{exp}^s) which was then compared with J_{exp}^s .

4. Results and discussion

The model was tested with the two types of spacers. In Figs. 4-7, J_{cal}^s , J_{exp}^s , J_{max}^s , J at flow rates 12 and 19 ml s⁻¹ for coarse and fine spacers are shown versus the average bulk temperatures. Eq. (27) was used to estimate the mass flux achieved by the spacers on the basis of the empty channel experimental data and Eq. (36) was used to estimate the maximum possible mass flux enhanced by the spacers. For the coarse spacer (80 MIL type) (Figs. 4 and 5), the model predicted the mass flux close to the measured mass

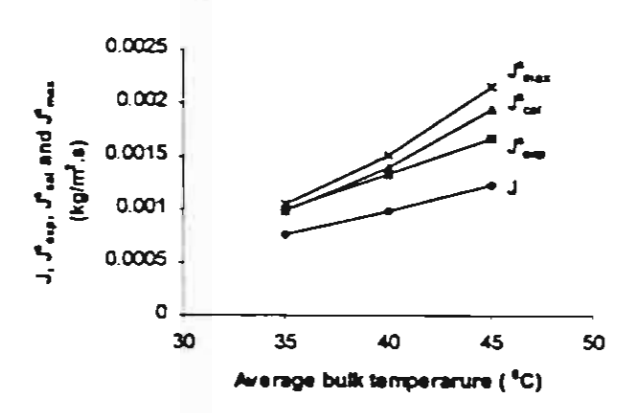


Fig. 4. J_{cul}^s , J_{exp}^s , J_{max}^s , J versus average bulk temperature at the flow rate of $12 \, \text{ml s}^{-1}$ for coarse spacer.

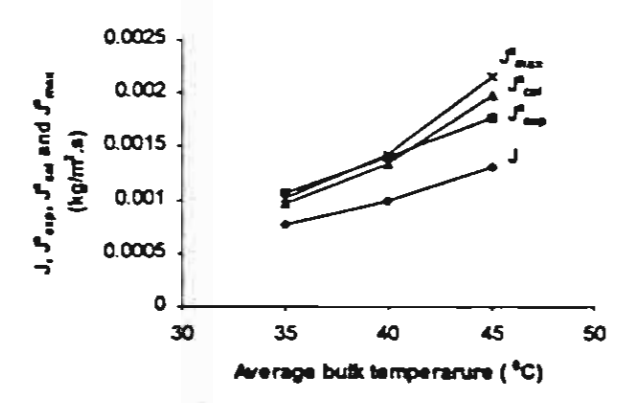


Fig. 5. $J_{\rm cal}^s$, $J_{\rm cap}^s$, $J_{\rm max}^s$, J versus average bulk temperature at the flow rate of 19 ml s⁻¹ for coarse spacer.

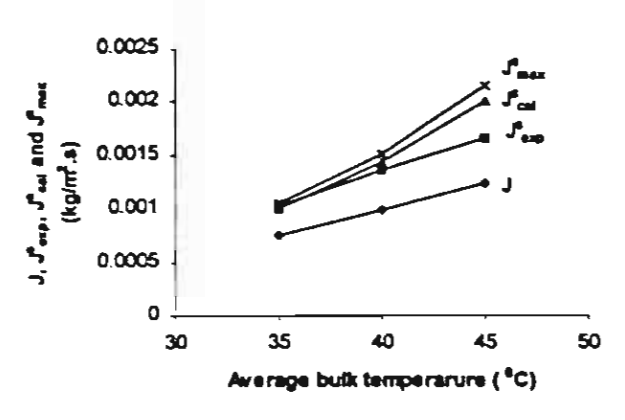


Fig. 6. J_{cup}^s , J_{sup}^s , J_{max}^s , J versus average bulk temperature at the flow rate of $12\,\text{ml s}^{-1}$ for fine spacer.

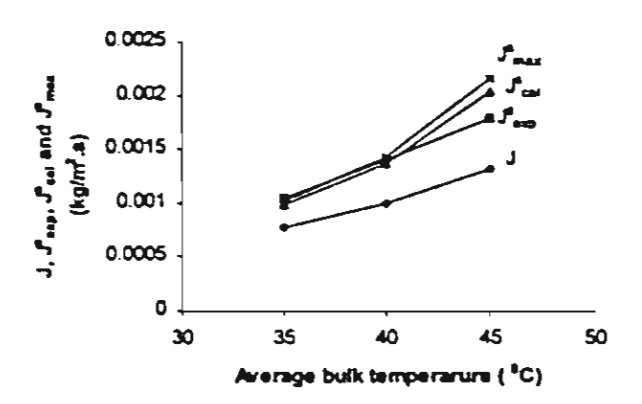


Fig. 7. J_{cal}^{A} , J_{cap}^{B} , J_{max}^{B} , J versus average bulk temperature at the flow rate of 19 ml s⁻¹ for fine spacer.

fluxes. The differences between calculated and measured mass fluxes varied in a range of -9.0 to +16.5%.

For the fine spacers (Figs. 6 and 7), the differences between calculated and measured mass fluxed were in the range of -6.0 to +20.5%. From Figs. 4–7, both $J_{\rm cal}^s$ and $J_{\rm exp}^s$ were close to $J_{\rm max}^s$ because the coarse and fine spacers used can generate large eddies and wakes and thereby give high heat transfer coefficients (9300–17,600 W m⁻² K⁻¹). Da Costa [14] showed that for mass transfer, optimal spacers have hydrodynamic angles in the range of 70–90° and voidages of 60–70%. The characteristics of the spacers used in this study fall into the same ranges.

Figs. 8 and 9 show the temperature polarization coefficients for empty and spacer filled channels at

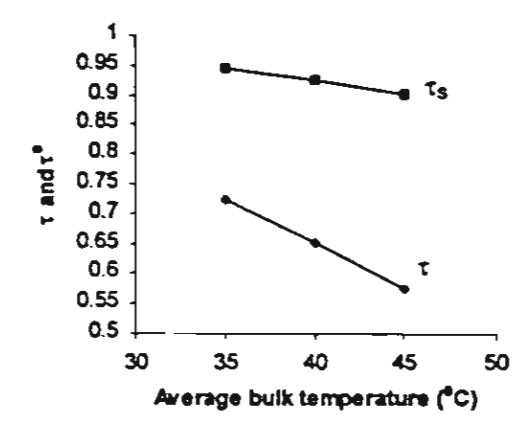


Fig. 8. The temperature polarization coefficients τ and τ^a at the flow rate of $12\,\mathrm{ml}\,s^{-1}$ for coarse spaces.

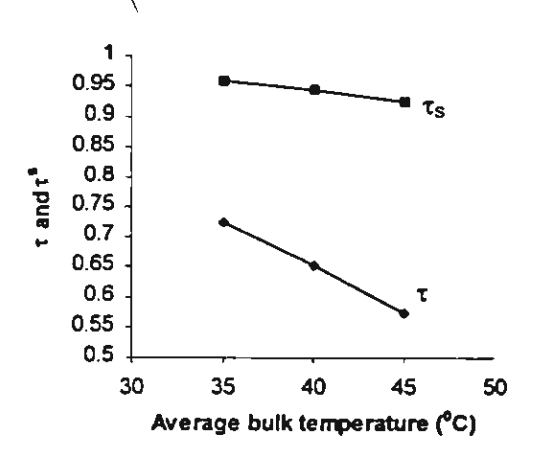


Fig. 9. The temperature polarization coefficients τ and τ^s at the flow rate of $12\,\text{ml}\,\text{s}^{-1}$ for fine spacer.

flow rate of $12 \, \mathrm{ml \, s^{-1}}$ calculated from Eqs. (25) and (18), respectively. From the figures, it is evident that the temperature polarization coefficients are substantially raised when spacers are used. Similar trends are observed at the higher flow rate of $19 \, \mathrm{ml \, s^{-1}}$. The values of τ^s falls in the range of 0.9–0.97 and τ in the 0.57–0.76 range.

When spacers are used in the channels, the temperatures at the membrane surfaces are changed. Pena et al. [16] showed that the membrane distillation coefficient decreases with the average membrane temperature. However, for the case where the heat transfer coefficients of both sides are equal, the average membrane temperature is equal to the average bulk temperature. Thus, the assumption of a constant membrane distillation coefficient is satisfied in these experiments.

Heat transfer correlations for spacer filled channels obtained from an analogy with mass transfer [14] were satisfactory for mass flux predictions in this work. We may conclude that there is analogy between heat transfer and mass transfer in the spacer filled channel. The mass flux enhancement model can be also applied to predict the mass flux enhanced when the flow rate is increased in the empty channel. The heat transfer coefficient for the spacer filled channel in Eq. (27) is replaced by the heat transfer coefficient for the empty channel at the higher flow rate. Both situations rely on the principle of reduction of the temperature polarization due to the increased heat transfer coefficient. In this study, the feed was water

only. However, the observations and model should be valid for modest levels of inorganic and organic solutes based on our earlier work comparing DCMD for solute feed and water feed [17].

5. Conclusions

DCMD in spacer-filled channels is shown to achieve fluxes 31-41% higher than without spacers. A model, based on the analogy between heat and mass transfer using correlations for spacer mass transfer, gives good predictions of spacer enhancement in DCMD. The differences between calculated and measured mass flux fall in the range of -9.0 to +16.5% for a coarse spacer and -6.0 to +20.5% for a fine spacer. The temperature polarization coefficients are substantially increased and approach to unity when the spacers are used in the channels.

Acknowledgements

The authors would like to thank the Thailand Research Fund and the Royal Golden Jubilee Ph.D. Program for financial support. Phattaranawik wishes to thank the UNESCO Center for Membrane Science & Technology for hospitality.

References

- L. Martinez-Diez, M.I. Vazquez-Gonzalez, Temperature and concentration polarization in membrane distillation of aqueous salt solution, J. Membr. Sci. 156 (1999) 265-273.
- [2] L. Martinez-Diez, M.I. Vazquez-Gonzalez, F.J. Florido-Diaz, Study of membrane distillation using channel spacers, J. Membr. Sci. 144 (1998) 45-56.
- [3] A.R. Da Costa, A.G. Fane, C.J.D. Fell, A.C.M. Franken, Optimal channel spacer design for ultrafiltration, J. Membr. Sci. 62 (1991) 275-291.
- [4] A.R. Da Costa, A.G. Fane, D.E. Wiley, Spacer characterization and pressure drop modelling in spacer-filled channels, J. Membr. Sci. 62 (1991) 275-291.
- [5] R.W. Schofield, A.G. Fane, C.J.D. Fell, Gas and vapour transport though microporous membrane. II. Membrane distillation, J. Membr. Sci. 53 (1990) 173-185.
- [6] K.W. Lawson, D.R. Lloyd, Membrane distillation, J. Membr. Sci. 124 (1997) 1-25.
- [7] R.W. Schofield, A.G. Fane, C.J.D. Fell, Heat and mass transfer in membrane distillation, J. Membr. Sci. 33 (1987) 299-313.

- [8] R.W. Schofield, Membrane distillation, Ph.D. Thesis, University of New South Wales, 1989.
- [9] J. Phattaranawik, R. Jiraratananon, Direct contact membrane distillation: effect of mass transfer on heat transfer, J. Membr. Sci., accepted for publication.
- [10] M. Tomaszewska, M. Gryta, A.W. Morawski, Mass transfer of HCl and H₂O across the hydrophobic membrane during membrane distillation, J. Membr. Sci. 166 (2000) 149–157.
- [11] J.M. Smith, H.C. Van Ness, Introduction to Chemical Engineering Thermodynamics, 4th Edition, McGraw-Hill, New York, 1990.
- [12] R.H. Perry, Perry's Chemical Engineers' Handbook, 6th Edition, McGraw-Hill, New York, 1984.

- [13] J.P. Holman, Heat Transfer, McGraw-Hill, New York,
- [14] A.R. Da Costa, Fluid flow and mass transfer in spacer-filled channels for ultrafiltration, Ph.D. Thesis, School of Chemical Engineering and Industrial Chemistry, University of New South Wales, 1993.
- [15] G. Schock, A. Miquel, Mass transfer and pressure loss in spiral-wound modules, Desalination 64 (1987) 339-352.
- [16] L. Pena, M. Paz Godino, J.I. Mengual, A method to evaluate the net membrane distillation coefficient, J. Membr. Sci. 143 (1998) 219-233.
- [17] R.W. Schofield, A.G. Fane, C.J.D. Fell, Factors affecting flux in membrane distillation, Desalination 77 (1990) 279-294.

ARTICLE IN PRESS



journal of MEMBRANE SCIENCE

35

42

43

45

Journal of Membrane Science 5477 (2002) 1-17

www.elsevier.com/locate/memsci

Heat transport and membrane distillation coefficients in direct contact membrane distillation

J. Phattaranawik^a, R. Jiraratananon^{a,*}, A.G. Fane^b

Department of Chemical Engineering, King Monghut's University of Technology Thonburi, Toonghru, Bangkok 10140, Thailand
UNESCO Centre for Membrane Science & Technology, School of Chemical Engineering and Industrial Chemistry,
The University of New South Wales, Sydney, NSW 2052, Australia

Received 20 June 2002; received in revised form 25 September 2002; accepted 11 October 2002

Abstract

12

13

15

16

17 18

20

22

25

28

30

This work aims to provide detailed understanding of heat transport in direct contact membrane distillation (DCMD). The influence of mass transfer on heat transfer rates and on the heat transfer coefficient was identified, and the relative significance of each heat transfer mechanism was evaluated. The role of spacers in heat transfer improvement was analyzed. Alternative methods to evaluate the membrane thermal conductivity were also proposed.

The heat transfer analysis of the experimental results showed that the effects of mass transfer on the heat transfer rates and on the film heat transfer coefficients were negligible. The heat transfer due to the vapor flow (q_v) in the membrane was equal to or greater than the heat conduction (q_c) for the membranes studied and increased with the feed temperature. When the feed temperature was lower than 323 K, the heat loss due to heat conduction across the membrane was the major contribution of the total heat transfer in the membrane. In addition, the temperature distributions in the membranes were closely linear. The membrane distillation (MD) coefficients for each membrane were constant over the flow rates and temperatures studied. The flow pattern in the spacer-filled channel was probably transition flow rather than turbulent flow. The alternative models for calculating the membrane thermal conductivity showed better agreement than the commonly used model.

© 2002 Published by Elsevier Science B.V.

Keywords: Effect of mass transfer, Heat transport; Membrane distillation; Membrane distillation coefficient; Spacers

1. Introduction

Membrane distillation (MD) is a hybrid process that uses membranes and operates on the basis of evaporation. Unlike most other membrane processes, MD does not require a mechanical pressure pump and is not limited by the osmotic pressure. In MD, mass is transported by the difference in vapor pressures between feed and permeate. The most common configuration of

E-mail address: ratana.jir@kmutt.ac.th (R. Jiraratananon).

MD is direct contact membrane distillation (DCMD) in which both heated feed and cold permeate streams are in direct contact with the porous, hydrophobic membrane. The difference in the temperature and composition of solutions in the layers adjoining the membrane between the feed and permeate streams creates the vapor pressure driving force for DCMD. On the other hand, the chemical potential resulting from the temperature difference plays an important role in both heat and mass transport. The DCMD process takes place at atmospheric pressure and at temperatures that are much lower than the normal boiling point of the feed solutions. The vaporization at the hot

0376-7388/02/\$ - see front matter © 2002 Published by Elsevier Science B.V. PII: S0376-7388(02)00498-2

^{*} Corresponding author. Tel.: +66-2-470-9222; fax: +66-2-428-3534.

Nomenclati	ire
С	membrane distillation coefficient
	$(kg m^{-2} s^{-1} Pa^{-1})$
C_{pv}	specific heat of vapor (kJ kg ⁻¹ K ⁻¹)
$d_{\mathbf{f}}$	filament size (m)
$d_{\mathrm{h.s}}$	hydraulic diameter of spacer-filled
	channel (m)
D	hydraulic diameter of empty
	channel (m)
h	heat transfer coefficient for low
	mass transfer rate (W m ⁻² K ⁻¹)
h*	heat transfer coefficient for high
	mass transfer rate (W $m^{-2} K^{-1}$)
$h_{\rm f}$ and $h_{\rm p}$	heat transfer coefficients at feed
	and permeate sides
H	spacer thickness (m)
$H_{\mathbf{v}}\{T\}$	vapor enthalpy at temperature
	$T(kJkg^{-1})$
J	mass flux $(kg m^{-2} s^{-1})$
k	thermal conductivity coefficient
	$(W m^{-1} K^{-1})$
k _{dc}	correction factor for spacer
l _m	mesh size (m)
Nu	Nusselt number
Pr	Prandit number
<i>q</i> c	heat transfer by conduction convective heat transfer rates across
q_{f} and q_{p}	the boundary layer at feed and
	permeate sides (kW m ⁻²)
-m m	heat transfer rates due to mass
$q_{ m f}^{ m m}$ and $q_{ m p}^{ m m}$	transfer across the thermal
ı	boundary layers of feed and
_	permeate sides (kW m ⁻²) heat transfer due to vapor
$q_{\rm v}$	
	flowing through the membrane (kW m ⁻²)
Re	(kW m ⁻²) Reynolds number
	temperatures at membrane surface
T_1 and T_2	on feed and permeate sides (K)
$T_{\rm f}$ and $T_{\rm p}$	bulk temperatures of feed and
It and Ip	permeate (K)
	• • • •
Greek lette	
δ	membrane thickness
ε	membrane porosity
θ	spacer hydrodynamic angle

τ	temperature polarization coefficient
φ	spacer voidage
φ	rate factor
$\psi_{\rm T}$	correction factor of high mass
	transfer rate effect for heat transfer
Subsc	ripts
g	air
m	membrane
s	solid
foil	aluminum foil

feed-membrane surface interface produces the vapor, which is then driven across the membrane by various mass transport mechanisms, and condenses at the membrane surface-cold permeate solution interface. The hydrophobicity of the membrane protects against liquid penetration through the membrane. Thus, only vapor or gas phase is allowed to enter the membrane pores.

49

50

51

52

53

54 55

58

59

60

61

62

63

64

67

68

69

70

71

72

73

75

79

80

The heat transfer with simultaneous mass transfer takes place in DCMD, resulting in complex heat transfer mechanisms. As a consequence, the mass transfer can affect both heat transfer rates and heat transfer coefficients [1,2]. The heat transfer model has been proposed to describe the heat transfer mechanisms in DCMD and facilitates the evaluation of the membrane surface temperatures. In most literatures, the heat transfer model for DCMD was developed based on the assumption of linear temperature profile and isenthalpy flow of vapor. However, there are different heat transfer models derived based on other assumptions. Gryta and Tomaszewska [3] derived the heat transfer model by assuming non-isenthalpy flow of vapor and non-linear temperature distribution and used the temperature on membrane surface on the permeate side as thermodynamic reference temperature. Although better agreement between the measured mass fluxes and the predicted fluxes was achieved, the significance of each heat transfer mechanism was not mentioned. Izquierdo-Gil et al. [4] achieved the heat transfer model from the conservation of enthalpy flux and the terms of heat flux due to mass flux were first introduced to MD. Both works showed better agreements between experimental and calculation results. However, the previous models did not mention the de-

ARTICLE IN PRESS

J. Phattaranawik et al. / Journal of Membrane Science 5477 (2002) 1-17

tails and importance of heat transfer mechanisms involved. Furthermore, such models cannot identify the influence of mass transfer on heat transfer rates. Recently, Phantaranawik and Jiraratananon [5] proposed the heat transfer model that can identify the influence of mass transfer on heat transfer rates and significance of each heat transfer mechanism in DCMD. However, the experimental data employed in [5] were taken from Lawson and Lloyd's work [6], which covered only turbulent flow condition and one membrane material (polypropylene). In addition, the thermal conductivity of the membrane used in the calculation was too low, 0.024 W m⁻¹ K⁻¹ [5,6]. Hence, the calculation results did not cover all membrane material and flow conditions.

90

91

92

93

95

97

99

100

101

102

103

106

107

108

109

110

111

112

113

115

116

117

118

119

120

121

125

126

127

128

Spacers may be applied as the turbulent promoter in DCMD to increase both heat and mass transfer [7,8]. The maximum flux enhancement was obtained by approximately 50%. On the other hand, the spacers in the UF processes improved fluxes by three- to five-fold [9,10]. In addition, turbulent or upper transition flow regime was found in the spacer-filled channels for UF and RO [9,11] although the Reynolds numbers were still in laminar regime. However, the flow characteristic for spacer-filled channels in DCMD has not been investigated.

From above discussion, the influence of mass transfer on heat transfer rates and on heat transfer coefficients for DCMD was ignored in most works. However, high mass transfer rate theory [1,2] suggests that high mass transfer rates have strong effect on heat transport, especially the transfer coefficients (momentum, heat, and mass). In addition, the significance of each heat transfer mechanism has not been described clearly. Accordingly, the understanding in the heat transfer of DCMD is still incomplete.

This paper intends to illustrate the details of all heat transfer mechanisms in feed stream, inside the membrane, and in permeate stream. The main objectives of this work are to: (1) study the effect of mass transfer on heat transfer rates and heat transfer coefficients; (2) determine the significance of each heat transfer mechanism for both laminar and turbulent flow conditions; (3) prove the validity of the assumptions of linear temperature profile inside the membrane and isenthalpic flow of vapor; (4) identify the flow condition in spacer-filled channels.

2. Theory

2.1. Heat transfer model and temperature distribution inside the membrane

The heat transfer in DCMD relies on the complex relation between simultaneous heat and mass transfer, which are transported in the same direction from hot feed to cold permeate. The schematic diagram of heat and mass transfer for DCMD is illustrated in Fig. 1. The difference between the bulk temperatures and the temperatures at the liquid-vapor interface or membrane surfaces on both sides of the membrane is termed temperature polarization, which appears in all configurations of membrane distillation. The temperature polarization coefficient [12] defined in Eq. (1) is used to measure the magnitude of this phenomenon. Furthermore, the temperature polarization can be regarded as a defect of the DCMD process, which should be minimized. The use of spacers, as the turbulent promoters [7,8], and turbulent flow [6] are appropriate methods to decrease the effect of this phenomenon.

$$\tau = \frac{T_1 - T_2}{T_f - T_p} \tag{1}$$

 T_1 and T_2 are the membrane surface temperatures on the heated feed and cold permeate sides, respectively, whereas T_f and T_p are the bulk temperatures of feed and permeate streams. The temperature polarization coefficient is, therefore, the ratio of the actual driving force to the overall driving force.

Mass transport across the membrane in DCMD is generally described by various mass transfer models based on the dusty gas model [13], such as the Knudsen model, the Poiseuille model, the Knudsen-

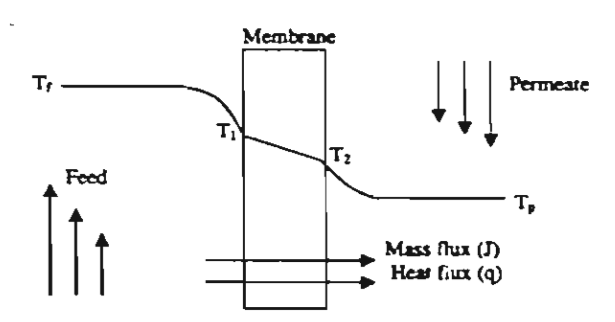


Fig. 1. Heat and mass transfer in DCMD.

3

130

131

133

143

144

145

146

149

150

151

155

ARTICLE IN PRESS

J. Phattaranawik et al./Journal of Membrane Science 5477 (2002) 1-17

Poiseuille transition models, and the molecular diffusion model [6,12,14]. The selection of the most appropriate model depends on the properties of vapor and membrane, i.e. the mean free path and mean pore size. However, in most cases, the models suggest that the mass flux may be written as a linear function of the vapor pressure difference across the membrane, given by

$$J = C(P_1 - P_2) \tag{2}$$

where J is the mass flux, C the membrane distillation coefficient, and P_1 and P_2 the partial pressure of vapor (water) at the membrane surfaces on the feed and permeate sides, respectively. According to the mass transfer models, the membrane distillation coefficient (C) is a function of the membrane properties (pore size, thickness, porosity, and membrane tortuosity), properties of the vapor transported across the membrane (molecular weight and diffusivity), and temperatures.

The original expression for heat transfer with simultaneous mass transfer is derived from energy conservation [1,2], Eq. (3)

$$q = JH\{T\} - k\frac{\mathrm{d}T}{\mathrm{d}X} \tag{3}$$

where q is the total heat flux, J the mass flux, $H\{T\}$ the enthalpy at temperature T, k the thermal conductivity, and x the distance in direction of heat transfer. In addition, the term for convective heat transfer should replace the conduction term in Eq. (3) to illustrate the heat transport in the feed and permeate streams. Thus, Eq. (3) becomes Eq. (4)

190
$$q = JH\{T\} + h(T_{bulk} - T_{gar})$$
 (4)

where h is the convective heat transfer coefficient, T_{bulk} the bulk temperature, and T_{sur} the surface temperature.

As seen in Fig. 1, energy transport in DCMD is divided into three regions; feed, membrane, and permeate regions. The mechanisms of heat transfer in the feed and permeate streams can be described by Eq. (4), and Eq. (3) is used to explain the heat transfer across the membrane. The heat transfer model [5] can be visualized by the electrical analog shown in Fig. 2. The heat transfer in each region with model elements were mentioned in our previous work [5].

To achieve the temperature distribution inside the membrane, the heat transfer mechanisms in the mem-

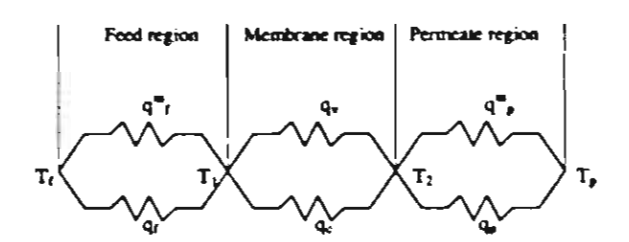


Fig. 2. The electrical analogy of heat transfer model for DCMD.

brane have to be considered. The heat transport across the membrane (q_m) can be divided in to two possible mechanisms, conduction across the membrane material (q_c) together with a heat due to vapor flowing through the membrane (q_v) . With the assumption of non-linear temperature distribution and non-isenthalpic flow, the heat transfer equation inside the membrane is given by

$$q_{\rm m} = JH_{\rm v}\{T\} - k_{\rm m}\frac{{\rm d}T}{{\rm d}X} \tag{5}$$

where $H_v\{T\}$ is the vapor enthalpy at temperature T, and k_m is the thermal conductivity of the membrane that is contributed from both polymer material (k_s) and gases (k_g) which are usually air and water vapor. In some cases, the presence of vapor mixtures, for example acid or alcohol vapor mixed up with water vapor, causes problems in calculating k_g because it is difficult to approximate the mole fraction of each vapor in the membrane. In the case of the air—water vapor mixture, there is a small difference between their thermal conductivities. Consequently, the mixture can be assumed to be a single component (air).

Generally, the reference temperature (T_0) is 273 K, so $H_v\{T\}$ can be written in the forms below

$$H_{v}\{T\} = C_{pv}T + (H_{v}\{T_{0}\} - C_{pv}T_{0})$$
 (6) 228

Here, C_{pv} is specific heat of vapor and liquid, and $H_v\{T_0\}$ is vapor enthalpy evaluated at the reference temperature, T_0 .

By assuming that $k_{\rm m}$ is constant over the range of temperatures considered with steady-state conditions, both heat and mass flux are constant in all regions. The temperature distribution in the membrane is obtained by substituting Eq. (6) into Eq. (5), separating the variables, and integrating the equation for the boundary conditions, x = 0, $T = T_1$ and x = x, T = T. The ex-

293

294

296

297

298

300

301

302

303

304

309

310

311

312

313

pression representing the temperature distribution in the membrane is shown in Eq. (7).

١

$$241 \quad T = (\alpha + T_1) \exp(\gamma x) - \alpha \tag{7}$$

242 where

$$\alpha = \frac{JH_{v}\{T_{0}\} - q_{m} - JC_{pv}T_{0}}{JC_{pv}}$$
 (8)

244 and

246

247

248

249

250

254

255

256

257

258

259

369

264

265

267

268

269

270

271

272

$$\gamma = \frac{JC_{pv}}{k_m}$$
 (9)

The term γx represents the ratio of heat transport contributed by mass transfer inside the membrane to heat conduction through the membrane. Eq. (7) also reveals that the temperature profile in the membrane is an exponential function of the distance (x) due to the assumption of non-isenthalpic flow of water vapor. Although the positive sign of γx gives an increasing function with distance, the value of α calculated by Eq. (8) is negative which results in decreasing temperatures across the membrane evaluated by Eq. (7). The typical values of α and γ are approximately $-2000 \, \text{K}$ and $70 \, \text{m}^{-1}$ (at $T_f = 323 \, \text{K}$, GVHP membrane, and laminar flow). At $x = \delta$ (membrane thickness), $T = T_2$ and the equation used to calculated q_m in Eq. (8) appears in Eq. (10)

$$q_{\rm m} = \frac{C_{\rm pv}/T_1 \exp(\gamma \delta) - C_{\rm pv}/T_2}{\exp(\gamma \delta) - 1}$$
263 + $J(H_{\rm v}\{T_0\} - C_{\rm pv}T_0)$ (10)

At steady-state conditions, heat fluxes in each region are transported with identical rates, which allows us to obtain the expressions that can be used to evaluate the membrane surface temperatures (T_1 and T_2), details are given in [5].

2.2. The influence of mass transfer on heat transfer rate and significance of each heat transfer mechanism

The significance of the mechanisms is determined after the membrane surface temperatures T_1 and T_2 are obtained from the heat transfer model. The mass fluxes are obtained from the experimental measurements, and the heat transfer coefficients are calculated from the heat transfer correlations for heat exchangers.

The methods to calculate the effect of mass transfer on heat transfer in the feed and the permeate streams $(q_f^m \text{ and } q_p^m)$ were described in [5]. The heat transfer due to vapor flowing through the membrane (q_v) is calculated by

$$q_{\rm v} = JH_{\rm v}\{T\} \tag{11}$$

The heat conduction across the membrane can be determined from the difference between $q_{\rm m}$ and $q_{\rm v}$. The membrane distillation coefficients are calculated by Eq. (2), and the vapor pressures of water at the membrane surface temperatures are calculated by the Antoine equation for water. In addition, the enthalpies of water vapor and liquid are determined from the equations fitted from the enthalpy data of saturated water vapor and liquid taken from the thermodynamic property table [15,16] in the range of temperature 273–373 K, expressed as

$$H_{v}\{T\} = 1.7535(T) + 2024.3$$
 (12) 295

2.3. Thermal conductivity of membrane

As mentioned previously, the thermal conductivity of the membrane is contributed from both polymer (k_s) and air (k_g) . For homopolymers, k_s is mainly dependent upon the temperature, spatial arrangement, the degree of crystallinity and shape of the crystallites [17,18]. However, the thermal conductivity of crystalline polymers is a weak function of temperature because the polymer chains in crystalline structure hardly move or vibrate when energy is absorbed. For instance, the thermal conductivities for polyvinylidenedifluoride (PVDF), polytetrafluoroethylene (PTFE), and polypropylene (PP) tested by the standard method ASTM C177, are reported in a narrow range: PVDF 0.17-0.19 W m-1 K-1 (at 296 K) and 0.21 W m⁻¹ K⁻¹ (at 348 K); PTFE $0.25-0.27 \,\mathrm{W}\,\mathrm{m}^{-1}\,\mathrm{K}^{-1}$ (at 296 K) and $0.29 \,\mathrm{W}\,\mathrm{m}^{-1}\,\mathrm{K}^{-1}$ (at 348 K); PP 0.11-0.16 W m-1 K-1 (at 296 K) and 0.2 W m⁻¹ K⁻¹ (at 348 K) [19-21]. The thermal conductivities of air and water vapor are reported as 0.026 W m-1 K-1 (at 298 K) and 0.03 W m-1 K-1 (at 348 K) for air, and 0.020 W m⁻¹ K⁻¹ (at 298 K) and 0.022 W m⁻¹ K⁻¹ (at 348 K) [22] for water vapor. Fortunately, there is a very small difference between the thermal conductivities of vapor and air. Thus, it is

J. Phattaranawik et al./Journal of Membrane Science 5477 (2002) 1-17

possible to assume that the gases in the pores behave as one component.

There are three models that can be used to predict the thermal conductivity of two-phase composite material, based on molecular orientation: (1) the Isostrain or parallel model [23] (Eq. (13)); (2) Isostress or series model [23] (Eq. (14)); (3) flux law model [24] (Eq. (15)).

330 Isostrain model:

331
$$k_{\rm m} - (1 - \varepsilon)k_{\rm s} + \varepsilon k_{\rm g}$$
 (13)

332 Isostress model:

$$k_{\rm m} = \left[\frac{\varepsilon}{k_{\rm g}} + \frac{(1-\varepsilon)}{k_{\rm s}}\right]^{-1} \tag{14}$$

334 Flux law model:

$$k_{\rm m} = k_{\rm g} \left[\frac{1 + (1 - \varepsilon)\beta_{\rm s-g}}{1 - (1 - \varepsilon)\beta_{\rm s-g}} \right]$$
 (15)

338 where

$$\beta_{s-g} = \frac{k_s/k_g - 1}{k_s/k_g + 2}$$

where ε is membrane porosity. Eq. (13) is often utilized for MD, and Eqs. (14) and (15) are the alternative expressions to calculate the membrane thermal conductivity.

342 2.4. The influence of mass transfer343 on heat transfer coefficient

Transfer of mass across the thermal boundary layers possibly distorts the temperature profiles in the thermal boundary layers [1,2] of both feed and permeate streams. Generally, convective heat transfer correlations are developed based on the assumption of small rate of mass transfer, Eq. (16). When a high rate of mass transfer exists in the system being considered, all transfer coefficients (momentum, heat, and mass) depend on the mass transfer rate (Eq. (17)) [1].

353
$$Nu = f(Re, Pr, \text{ channel geometry})$$
 (16)

Nu =
$$f\left(Re, Pr, \frac{J_A C_{pA} + J_B C_{pB}}{h}, \text{ channel geometry}\right)$$
356 (17)

The effect of high mass transfer on film heat transfer coefficients can be assessed by the correction factor (ψ_T) in Eq. (18) [1,2], which may be evaluated by the film theory or the penetration theory, and the boundary layer theory. However, only the film theory is discussed in this work due to its simple solution, Eqs. (18) and (19)

$$\psi_{\mathsf{T}} = \frac{h^*}{h} = \frac{\phi}{\exp(\phi) - 1} \tag{18}$$

where

$$\phi = -\frac{J_A C_{pA}}{h} \tag{19}$$

In Eq. (19), ϕ , J_A , $C_{\rm pA}$, and h are the rate factor, the molar flux, the heat capacity of species A, and heat transfer coefficient at low mass transfer calculated by ordinary Nusselt number correlations, respectively. h^* in Eq. (18) is the apparent heat transfer coefficient including the effect of high mass transfer rates. The minus sign in Eq. (19) is due to the water removed from the feed side [1,2]. The typical values of ψ_T are estimated in Section 4.3.

2.5. The spacers for DCMD

Net-type spacers are often put into the flow channels in membrane processes such as reverse osmosis and ultrafiltration to improve the mass transfer and to reduce the effect of concentration polarization and fouling [9,25]. Spacer geometry and the flow moving through the spacer is shown in Fig. 3. Spacers also have benefits in MD [7,8] since they destabilize the flow and create eddy currents in the laminar regime so that momentum, heat, and mass transfer are enhanced.

The heat transfer correlation for DCMD with spacers was obtained from the mass transfer correlation for UF [26] under the assumed analogy between heat and mass transfer

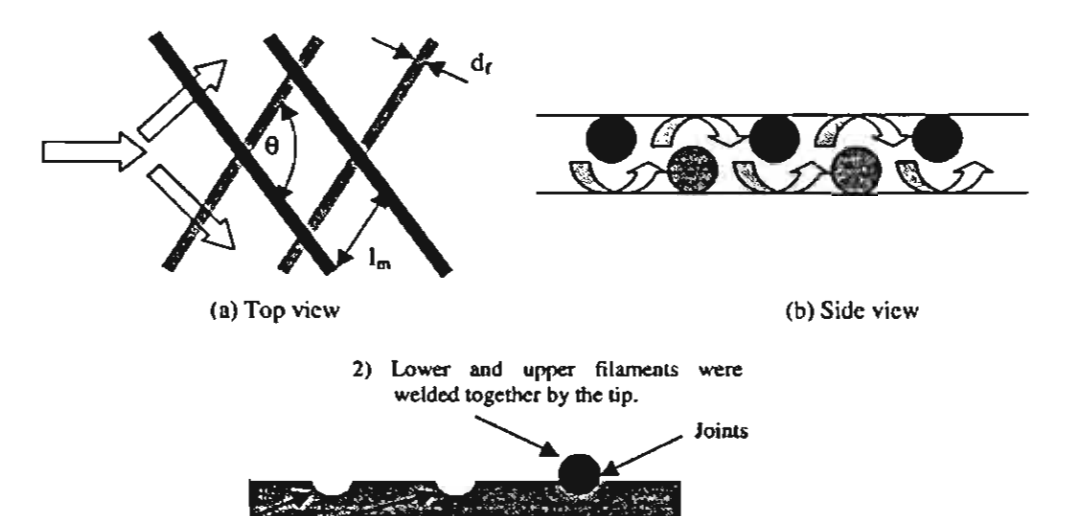
$$Nu = k_{\rm dc} 0.664 Re_{\rm s}^{0.5} Pr^{0.33} \left(\frac{2d_{\rm h,s}}{l_{\rm m}}\right)^{0.5}$$
 (20)

here

$$k_{\rm dc} = 1.654 \left(\frac{d_{\rm f}}{H}\right)^{-0.039} \varphi^{0.75} \left(\sin\left(\frac{\theta}{2}\right)\right)^{0.086}$$
 392

Here, $k_{\rm dc}$ is the correction factor for spacer geometry, 393 $d_{\rm h,s}$ the hydraulic diameter for the spacer-filled channel, $d_{\rm f}$ filament size, $l_{\rm m}$ the mesh size, H the spacer 395

J. Phattaranawik et al./Journal of Membrane Science 5477 (2002) 1-17



1) Lower filaments were melted by the hot tip to create the indentations.

(c) Spacer fabrication

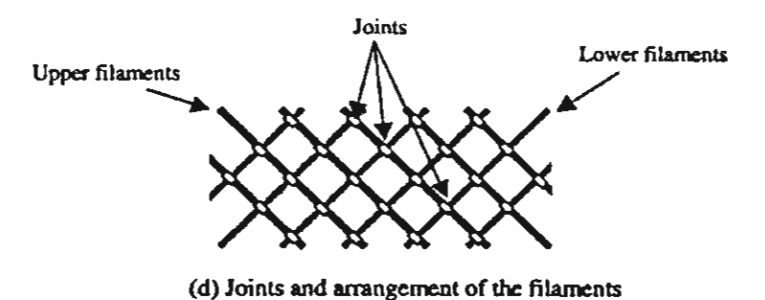


Fig. 3. Flow direction in spacer-filled channel and spacer fabrication.

thickness, φ the spacer voidage, and θ the hydrodynamic angle. In this work, DCMD experiments with the spacers were carried out to identify the flow conditions in the spacer-filled channels.

3. Experimental 400

396

397

398

399

401

402

403

404

405

The membrane modules for laminar and turbulent flow conditions were made from polymethylmethacrylate (PMMA). The dimensions and the characteristics of both modules are shown in Table 1. In the experiments, both modules were placed in the vertical position in order to eliminate the effects of free convection. Distilled water was used as the feed and permeate solutions. The membranes used were PVDF (nos. 1 and 2), and PTFE (no. 3), and their reported properties are summarized in Table 2. In addition, membranes 410 nos. 4 and 5 are also included for the discussion in 411 Section 4.1.

The feed solution was heated and maintained at 413 the required temperature in a 281 thermostatic water 414 bath (Nickel-Electro: model NE4D) with sensitivity 415 ±0.1 K and uniformity ±0.01 K. The low temperature 416 circulator for the permeate solution was supplied by 417 Vision Scientific (model VS-1205CW) with unifor- 418

J. Phattaranawik et al./Journal of Membrane Science 5477 (2002) 1-17

Table 1
Membrane module characteristics and channel dimensions

Membrane module	Width (m)	Length (m)	Height (m)	Hydraulic diameter of channel (m)	Effective membrane area (m²)
Laminar flow	5 × 10 ⁻²	1 × 10 ⁻¹	5 × 10 ⁻³	9.09 × 10 ⁻³	5 × 10 ⁻³
Turbulent flow	3×10^{-3}	1×10^{-1}	3×10^{-3}	3×10^{-3}	3 × 10 ⁻⁴

Table 2 Membrane properties [4]

No.	Membrane material	Pore size (µm)	Thickness (µm)	Porosity (ε)	Ł _{m.,r} (W m. −1 K −1)	Manufacturer
1	PVDF (GVHP)	0.22*	126	0.62	0.041	Millipore
2	PVDF (HVHP)	0.45*	116	0.66	0.040	Millipore
3	PTFE	0.24	70	0.7ª	_	Sartorious
4	PTFE	0.2*	64	0.9	0.031	Gore
5	PIFE	0.45°	77	0.89	0.027	Gore

Note: $k_{m,r}$ are the reported membrane thermal conductivities [4]; GVHP and HVHP are code names of the PVDF membranes produced by Millipore.

mity ±0.1 K. The feed and permeate solutions were pumped co-currently into the top of the modules by precision brushless drives (model 7741) supplied by Cole-Parmer (Master Flex), and the flow rates were measured by a glass variable area flow meter (model 10A1197) supplied by ABB Fisher & Porter for the hot feed stream and by a polycarbonate flow meter (model RMB-85) provided by Dwyer for the cold permeate stream. The solution temperatures were measured by digital thermometers supplied by Testo (model Testo 935). The process solutions were circulated through closed thermostatic systems. The bulk temperatures of feed solutions were varied from 313 to 343 K with 10 K increments, and the permeate temperatures were constant at 293 K.

The experiments were divided into three parts. (1) The experiments for obtaining the most suitable heat transfer correlations for laminar and turbulent flow modules used. (2) DCMD experiments were performed with the empty channels. The measured mass fluxes at various operating conditions were used to calculate the influence of mass transfer on heat transfer rates and on heat transfer coefficients, to assess the significance of each heat transfer mechanism, and to evaluate the membrane distillation coefficient (C). (3) DCMD experiments with two types of the spacers to identify the flow characteristic in the spacer-filled channel and study the enhancement of heat and mass transfer by the spacers.

3.1. Determination of appropriate heat transfer correlations

To eliminate the mass transfer, the membranes were replaced by the aluminum foil with thickness of 40 μ m and thermal conductivity of 229 W m⁻¹ K⁻¹. In this part, Reynolds numbers for both sides were kept equal, and the experiments were conducted with four different flow rates (*Re*), shown in Table 3. The calculated overall heat transfer coefficients from the heat transfer correlations (U_{corre} , Eq. (21)) and the experimental overall heat transfer coefficient (U_{exp} , Eq. (22)) were compared, and standard deviations [27] of the differences were considered to determine the best heat transfer correlation for each flow condition

$$U_{\text{corre}} = \frac{1}{[(1/h_{\text{h}}) + (\delta_{\text{foil}}/k_{\text{foil}}) + (1/h_{\text{c}})]}$$
(21)

Table 3

The experimental conditions for determining the appropriate heat transfer correlations

Temperature	(K)	Reynolds numbers		
Feed	Permeate	Laminar	Turbulent	
313-343	293	762	12,217	
313-343	293	1142	15,708	
313-343	293	1523	17,453	
313343	293	2094	19,198	

^{*} Manufacturer's data.

Table 4
Heat transfer correlations for laminar flow

Correlation		Reference
$Nu = 1.86 \left(\frac{RePr}{L/D}\right)^{1/3}$	(23)	[28]
$Nu = 4.36 + \frac{0.036RePr(D/L)}{1 + 0.0011(RePr(D/L))^{0.8}}$	(24)	[3]
$Nu_{\text{cooling}} = 11.5(RePr)^{0.23}(D/L)^{0.5},$ $Nu_{\text{beanng}} = 15(RePr)^{0.23}(D/L)^{0.5}$	(25)	[27]
$Nu = 0.13Re^{0.64} Pr^{0.38}$	(26)	[27]
$Nu = 1.95 \left(\frac{RePr}{L/D}\right)^{1/3}$	(27)	[29]*
$Nu = 0.097 Re^{0.73} Pr^{0.13}$	(28)	[27]
$Nu = 3.66 + \frac{0.104 Re Pr(D/L)}{1 + 0.0106 (Re Pr(D/L))^{0.8}}$	(29)	[29]

Average Nusselt number.

$$U_{\exp} = \frac{Q}{A \Delta T_{\ln}}$$
 (22)

64 where

467

466

469

470

471

472

473

474 475

476

477

478

479

480

481

482

483

484

$$\Delta T_{\text{hs}} = \frac{(T_{\text{h,in}} - T_{\text{c,in}}) - (T_{\text{h,out}} - T_{\text{c,out}})}{\ln[(T_{\text{h,in}} - T_{\text{c,in}})/(T_{\text{h,out}} - T_{\text{c,out}})]}$$

In Eqs. (21) and (22), Q is the heat transfer rate, $\delta_{\rm foil}$ the foil thickness, $k_{\rm foil}$ the foil thermal conductivity, $h_{\rm h}$ the heat transfer coefficient of hot solution, and $h_{\rm c}$ the heat transfer coefficient of the cold solution. The heat transfer correlations tested for both flow conditions are shown in Tables 4 and 5.

In Tables 4 and 5, L is the channel length and D the hydraulic diameter of the membrane module. The entrance effect term, (1 + (6D/L)) [34], is considered for most correlations in Table 5. The most appropriate heat transfer correlations obtained were used to evaluate the heat transfer coefficients in the subsequent experiments.

3.2. The DCMD experiments with the empty channels

The same heat transfer coefficients for both feed and permeate streams were employed in order to compare the effect of mass transfer on each side. However, the same flow rates cannot provide the same heat transfer coefficients due to the large difference between the bulk feed and permeate temperatures. Accordingly, the flow rates of the feed side were reset in order to equalize the heat transfer coefficients of both sides. The chosen correlations from Section 3.1 were used to calculate both the experimental conditions (fluid velocity) and the heat transfer coefficients. The experiments for this part were performed with three different flow rates (heat transfer coefficients) for each flow condition, shown in Table 6.

3.3. The DCMD experiments with spacer-filled channels

The operating conditions used in this part were similar to those previously described for laminar flow conditions (Table 6) except that spacers were put in both feed and permeate channels. To minimize the bypass flow the spacer thickness was equal to the channel height, that is, 5 mm for both spacers. The spacers were made 'in house' from polypropylene rod 3 mm in diameter. A welding rod with a sharp tip was electrically heated and used to fabricate the spacers. Spacer thickness (H) should be less than double the filament diameters since vertically directional flow change is required (see Fig. 3b). The hot tip was used to create indents of approximately 1 mm in the lower filaments. Then, the upper filaments were placed across the indents and the tip was used to weld both filaments together (see Fig. 3c). The welding positions and arrangement of upper and lower filaments are displayed in Fig. 3d. Dimensional errors in fabricating spacers were controlled to levels less than 8% (Table 7). The relationship in Eq. (37) [26] was used to evaluate the mesh size (l_m) at the required voidage (φ) and hydrodynamic angle (θ). Both voidage and mesh size are necessary for spacer fabrication. The geometric characteristics of the spacers are summarized in Table 7.

$$l_{\rm m} = \frac{\pi d_{\rm f}^2}{2(1 - \varphi)H\sin\theta} \tag{37}$$

In Eq. (37) d_f is the diameter of the spacer filament and H the spacer thickness. The mass fluxes obtained from the experiments with spacers were compared to those from the experiments performed under laminar and turbulent flow conditions so as to estimate the heat transfer coefficients and identify the flow characteristic for spacer-filled channels.

to 489 vc- 490 ri- 49

- 490 - 491 - 492 / 493

495

496

0W 493 494

> 1- 497 1- 498 th 499 ss 500 cl 501

in 503 cri- 504 cer 505 ent 506 is 507

re- 508 la- 509 oss 510 nts 511 ar- 512

/ed 513 ac- 514 7). 515 /al- 516

(φ) 517
nesh 518
net- 519
d in 520

J. Phattaranawik et al./Journal of Membrane Science 5477 (2002) 1-17

Table 5 Heat transfer correlations for turbulent flow

Correlation		Reference
$Nu = \left(1 + \frac{6D}{L}\right) \left(\frac{(f/8)RePr}{1.07 + 12.7(f/8)^{1/2}(Pr^{2/3} - 1)}\right)$	(30)	[29]
$Nu = \left(1 + \frac{6D}{L}\right) \left(\frac{(f/8)(Re - 1000)Pr}{1 + 12.7(f/8)^{1/2}(Pr^{2/3} - 1)}\right)$	(31)	[30]
$Nu = 0.023 \left(1 + \frac{6D}{L} \right) Re^{0.3} Pr^{1/3}$	(32)	[31]
$N_{\rm H} = 0.036 {\rm Re}^{0.3} Pr^{1/3} \left(\frac{D}{L} \right)^{0.055}$	(33)	[32]
$Nu = \left(1 + \frac{6D}{L}\right) \left(\frac{(f/8)RePr}{1.2 + 13.2(f/8)^{1/2}(Pr^{2/3} - 1)}\right)$	(34)	[33]
$Nu = \left(1 + \frac{6D}{L}\right) \left(\sqrt{\frac{f}{8}}\right) \left[12.48Pr^{2/3} - 7.853Pr^{1/3} + 3.613\ln(Pr) + 5.8 + 2.78\ln\left(\frac{Re\sqrt{f/32}}{45}\right)\right]^{-1}$	(35)	[33]
$Nu = 0.027 \left(1 + \frac{6D}{L}\right) Re^{0.3} Pr^{1/3} \left(\frac{\mu_{\text{book}}}{\mu_{\text{ext}}}\right)^{0.14}$	(36)	[32]

Note: $f = (0.79 \ln(Re) - 1.64)^{-2}$ for all correlations.

Table 6
Operating conditions and heat transfer coefficients calculated by Eq. (24) for laminar flow and by Eq. (32) for turbulent flow

Run	Temperature (K)		erature (K) Laminar flow (Eq. (24))				Turbulent flow (Eq. (32))			
	Feed	Permeste	Fluid velocity (m s ⁻¹)			Heat transfer coefficient		velocity (m s ⁻¹)	Heat transfer coefficient	
			Feed	Permeste	(W m-2 K	·')	Feed	Permente	(W m ⁻² K ⁻¹)	
ī	313	293	0.063	0.063	1054.3		2_59	3.50	17,026.3	
2	323	293	0.063	0.063	1054.3	(4)	2.32	3.50	17,026.3	
3	333	293	0.060	0.063	1054.3	100	2.13	3.50	17,026.3	
4	343	293	0.060	0.063	1054.3		1.94	3.50	17,026.3	
5	313	293	0.083	0.084	1281.9		3.06	4.09	19,261.0	
6	323	293	0.083	0.084	1281.9	11	2.78	4.09	19,261.0	
7	333	293	0.083	0.084	1281.9	8	2.50	4.09	19,261.0	
8	343	293	0.083	0.084	1281.9	1120	2.22	4.09	19,261.0	
9	313	293	0.100	0.105	1498.9		3.52	4.67	21,432.4	
10	323	293	0.100	0.105	1498.9		3.14	4.67	21,432.4	
11	333	293	0.100	0.105	1498.9		2.87	4.67	21,432.4	
12	343	293	0.097	0.105	1498.9		2.59	4.67	21,432.4	

Table 7 Characteristics of spacers

No.	Voidage (p)	Hydrodynamic angle (θ)	Hydraulic diameter (m)	l _m (m)
1 2	0.612 0.623(±8%)	45(±7%) 90(±5%)	2.7 × 10 ⁻³ (±5%) 2.8 × 10 ⁻³ (±5%)	$ \begin{array}{c} 11 \times 10^{-3}(\pm 7\%) \\ 8 \times 10^{-3}(\pm 7\%) \end{array} $

Note: Spacer thickness = $5(\pm 8\%)$ mm.

570

571

572

573

574

575

576

580

581

582

J. Phattaranawik et al./Journal of Membrane Science 5477 (2002) 1-17

4. Results and discussion

531

532

533

534

535

536

537

538

539

540

544

545

546

547

549

550

552

553

554

555

556

557

559

560

561

4.1. Thermal conductivities of the membranes

The values of $k_{\rm m,r}$ taken from [4] were compared with the calculated membrane thermal conductivities $(k_{\rm m,c})$ by various models. As shown in Table 8, the Isostress model, Eq. (14), provided the best agreement for all membranes. On the other hand, the Isostrain model (Eq. (13)) which is usually used to calculate the membrane thermal conductivity in most MD studies provided very large discrepancies. Therefore, the Isostress model (Eq. (14)) appeared to be the most appropriate model for calculating the membrane thermal conductivity, and also suggests that the thermal conductivity of the PTFE (no. 3) was 0.0382 W m⁻¹ K⁻¹.

4.2. The most suitable heat transfer correlations

For repeated runs of each experiment, the measured temperatures: $T_{\rm h,in}$, $T_{\rm h,out}$, $T_{\rm c,in}$, and $T_{\rm c,out}$ fluctuated slightly within 4% of the average values (or ± 0.8 K at 293 K). As a result, the average error of measured overall heat transfer coefficients was less than 7%. $U_{\rm exp}$ ranged from 480 to 1240 W m⁻² K⁻¹ for laminar flow and 7100–16,000 W m⁻² K⁻¹ for turbulent flow. The thermal resistances of the foil were approximately 1.1% of the total resistance due to foil thinness and high thermal conductivity.

Table 9 compares the standard deviations of heat transfer correlations. The most suitable heat transfer correlations for each flow condition were chosen at the minimum standard deviation. Thus, Eq. (24) in Table 4 and Eq. (32) in Table 5 were selected for laminar flow and turbulent flow conditions, respectively. The average discrepancies between $U_{\rm exp}$ and $U_{\rm corre}$ calculated

by the chosen correlations were about 6% for laminar flow and 9% for turbulent flow. Subsequently, the selected correlations were used to calculate the required operating conditions and to evaluate the corresponding convective heat transfer coefficients for both flow conditions (Table 6). It should be noted that high standard deviation was found for Eq. (23), which is the commonly used Seider-Tate equation for laminar flow. On the other hand, the commonly used Dittus-Boelt equation was the most suitable for turbulent condition.

4.3. The influence of mass transfer on heat transfer rates and heat transfer coefficients, significance of each heat transfer mechanism, and membrane distillation coefficients

The importance of each heat transfer mechanism was determined and interpreted in the forms of percentage compared to the total heat transfer rates. The influence of mass transfer on heat transfer rates was described by percentage of q_f^m and percentage of q_p^m . As seen in Figs. 4 and 5, the maximum percentages at 343 K was 7.2% for q_f^m and 2.8% for q_p^m . Both $q_{\rm f}^{\rm m}$ and $q_{\rm p}^{\rm m}$ increase with the feed temperatures due to higher mass fluxes. In Fig. 5, the heat transfer coefficients slightly affected both q_f^m and q_p^m because the increase of the heat transfer coefficients raised $q_i^{\rm m}$ and q_p^m , and q_f and q_p in the same portions. The impact of mass transfer on the heat transfer coefficients in the feed stream can be assessed by the correction factor (ψ_T) calculated by Eqs. (18) and (19), and Fig. 16. For PTFE at 343 K, ψ_T was approximately 1.009 for $h = 1054.29 \,\mathrm{W \, m^{-2} \, K^{-1}}$ and 1.0015 for $h = 21.432.4 \,\mathrm{W\,m^{-2}\,K^{-1}}$. As a result, the effect of mass transfer on the heat transfer coefficients was only 0.9 and 0.15% of the coefficients calculated by the

Table 8
Calculations of membrane thermal conductivities

No.	Membrane	k _{m,r} (W m ⁻¹ K ⁻¹)	Isostrain model		Isostress model		Flux law model	
			k _{m,c} (W m ⁻¹ K ⁻¹)	Error (%)	$k_{\rm m,c} (W {\rm m}^{-1} {\rm K}^{-1})$	Error (%)	$k_{\rm m,c} \ ({\rm W m^{-1} K^{-1}})$	Error (%)
ī	PVDF	0.041	0.0858	109.17	0.0412	0.56	0.046	12.55
2	PVDF	0.040	0.0797	99.20	0.0393	1.81	0.044	9.25
3	PTFE	_	0.0946	_	0.0382	_	0.044	_
4	PTFE	0.031	0.0502	61.94	0.0307	0.88	0.032	4.45
5	PTFE	0.027	0.0524	94.15	0.0310	14.93	0.033	21.69

Note: k_s (polymer) = 0.18 and 0.25 W m⁻¹ K⁻¹ for PVDF and PTFE, respectively; k_g (air) = 0.028 W m⁻¹ K⁻¹ for all calculations.

Table 9
Standard deviations of the heat transfer correlations

	S.D. $(W m^{-2} K^{-1})$	
Laminar flow		
Eq. (23)	314.72	
Eq. (24)	53.69 ^a	
Eq. (25)	252.04	
Eq. (26)	57.58	
Eq. (27)	290.49	
Eq. (28)	71.87	
Eq. (29)	171.96	
Turbulent flow		
Eq. (30)	2196.33	
Eq. (31)	2065.97	
Eq. (32)	1334.81*	
Eq. (33)	1591.62	
Eq. (34)	1634.49	
Eq. (35)	1401.31	
Eq. (36)	2157.94	

Minimum S.D.

596

509

600

801

602

603

604

805

606

correlations with no or low mass transfer, respectively. Under the condition of the calculation (PTFE at 343 K and turbulent condition) the mass fluxes were about $0.014 \, \mathrm{kg} \, \mathrm{m}^{-2} \, \mathrm{s}^{-1}$ (50.41 m⁻² h⁻¹). Therefore, in this study the mass transfer in DCMD did not affect either heat transfer rates or heat transfer coefficients.

Figs. 6 and 7 show that the percentage of heat transfer due to vapor transport inside the membrane (q_v) varied from 40 to 62% for GVHP and also increased with the feed temperatures because of the higher mass fluxes. The similar trends were found for HVHP and

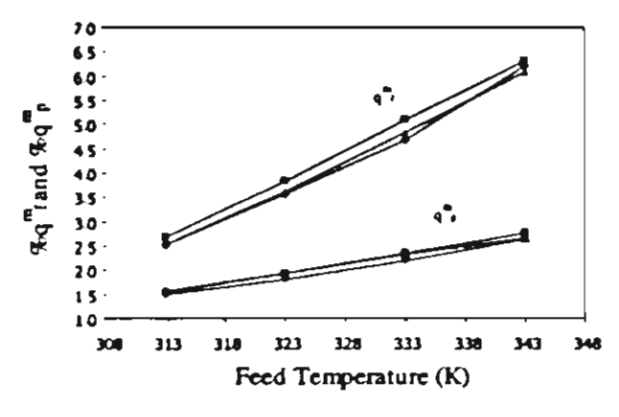


Fig. 4. Percentages of q_1^m and q_p^m at various feed temperatures for laminar flow, $h=1498.87~\mathrm{W}~\mathrm{m}^{-2}~\mathrm{K}^{-1}$; (\spadesuit) GVHP 0.22 $\mu\mathrm{m}$; (\blacksquare) HVHP 0.45 $\mu\mathrm{m}$; (\spadesuit) PTFE 0.2 $\mu\mathrm{m}$.

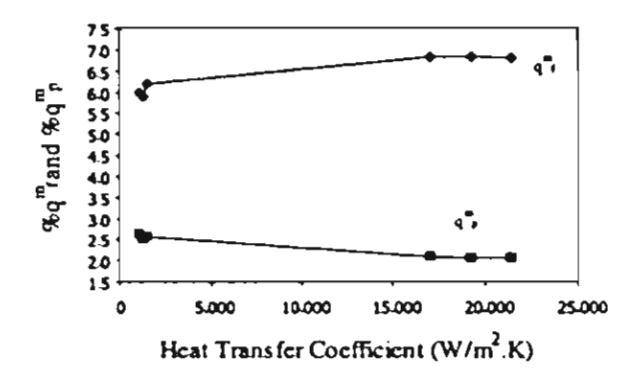


Fig. 5. Percentages of q_T^m and q_p^m at various heat transfer coefficients (flow rate, flow conditions), $T_f = 343 \,\text{K}$, for GVHP 0.22 μ m; $(\Phi) q_T^m$ and $(\blacksquare) q_p^m$.

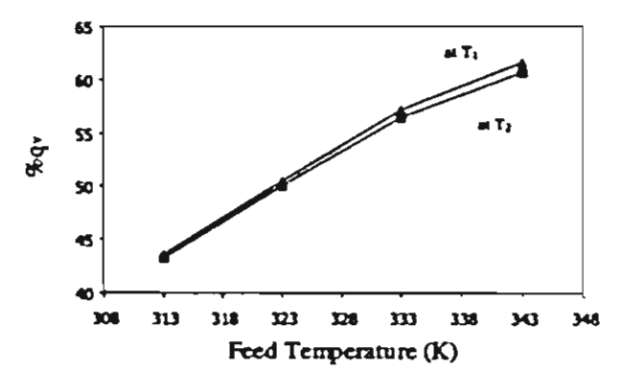


Fig. 6. Percentages of q_v at various feed temperatures for HVHP 0.45 $\mu m_v h = 1498.87 \text{ W m}^{-2} \text{ K}^{-1}$.

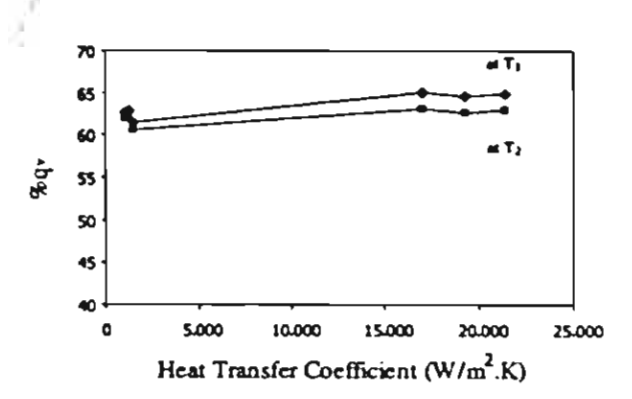


Fig. 7. Percentages of q_v at various heat transfer coefficients (flow rate), $T_f \approx 343$ K, for HVHP 0.45 μ m.

PTFE with the maximum percentage of q_v of 63.4% (PTFE and turbulent flow). In Fig. 7, the significance of q_v seems independent of the film heat transfer coefficients used. Thus, the significance of q_v was comparable to heat conduction across the membrane (q_c) . Compared to the previous simulation [5], with polypropylene membranes, the maximum percentage of q_v was 92% and q_v was the major component of heat transfer inside the membranes, and the heat conduction (q_c) could be disregarded. q_f^m , q_p^m and q_v in present work were rather lower than those in the previous simulation [5] due to difference in the membrane materials and properties. However, the present results are judged to be more reasonable because of the use of the membrane properties experimentally determined [4]. Fig. 6 also reveals that the heat loss by heat conduction (q_c) was larger than q_v when the feed temperature was lower than 323 K. To minimize the proportion of the heat loss in the membrane, higher feed temperature and low thermal conductivity membranes are required.

606

609

610

611

612

613

614

615

618

619

620

621

622

623

628

629

630

631

632

633

635

636

Figs. 8 and 9 reveal that the temperature polarization coefficients (τ) for laminar and turbulent flow decreased with increasing feed temperature due to higher energy consumption from the vaporization at the feed membrane surface at higher temperatures. Significantly higher τ values for turbulent flow can be seen by comparing Figs. 8 and 9. This is illustrated more clearly in Fig. 10, which shows the effect of heat transfer coefficients (a flow regime) on τ . The tem-

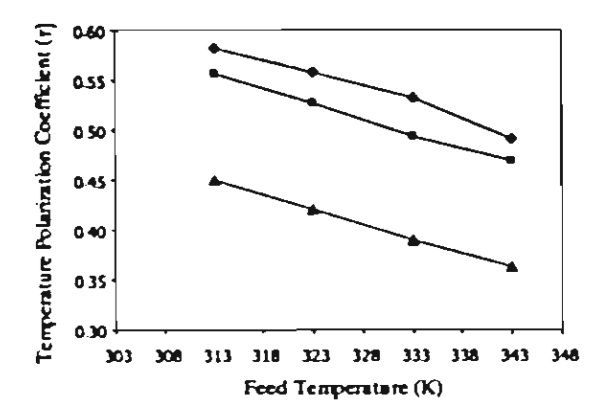


Fig. 8. Temperature polarization coefficients at various feed temperatures for laminar flow condition, $h=1498.87\,\mathrm{W\,m^{-2}\,K^{-1}};$ (Φ) GVHP 0.22 $\mu\mathrm{m}$; (Ξ) HVHP 0.45 $\mu\mathrm{m}$; (Δ) PTFE 0.2 $\mu\mathrm{m}$.

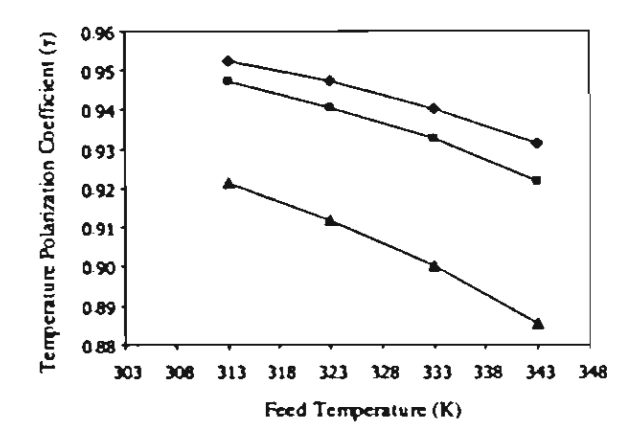


Fig. 9. Temperature polarization coefficients at various feed temperatures for turbulent flow condition, $h = 21,423.4 \,\mathrm{W \, m^{-2} \, K^{-1}};$ (Φ) GVHP 0.22 μ m; (\blacksquare) HVHP 0.45 μ m; (\triangle) PTFE 0.2 μ m.

perature polarization was reduced by higher flow rates due to the decrease in the thermal resistances of convection in the boundary layers.

The membrane distillation coefficients (C) were evaluated by Eq. (2). The analysis results showed that MD coefficients were not affected by flow rates (heat transfer coefficients) and membrane temperatures studied (Fig. 11). The constant slopes of the straight lines in Fig. 11 mean the MD coefficients that are $3.459 \times 10^{-7} \,\mathrm{kg}\,\mathrm{m}^{-2}\,\mathrm{s}^{-1}\,\mathrm{Pa}^{-1}$ for GVHP, $4.169 \times 10^{-7} \,\mathrm{kg}\,\mathrm{m}^{-2}\,\mathrm{s}^{-1}\,\mathrm{Pa}^{-1}$ for HVHP, and

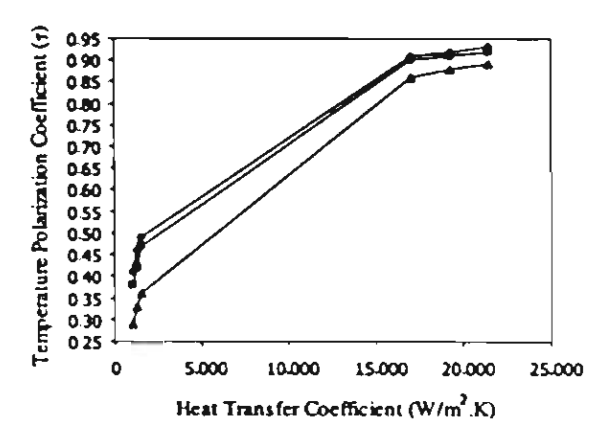


Fig. 10. Temperature polarization coefficients at various heat transfer coefficients (flow rates, flow conditions), $T_f=343\,\mathrm{K};\ (\spadesuit)$ GVHP 0.22 $\mu\mathrm{m};\ (\blacksquare)$ HVHP 0.45 $\mu\mathrm{m};\ (\triangle)$ PTFE 0.2 $\mu\mathrm{m}.$

650

651

652

653

660

661

662

863

664

665

666

667

671

677

673

674

J. Phattaranawik et al./Journal of Membrane Science 5477 (2002) 1-17

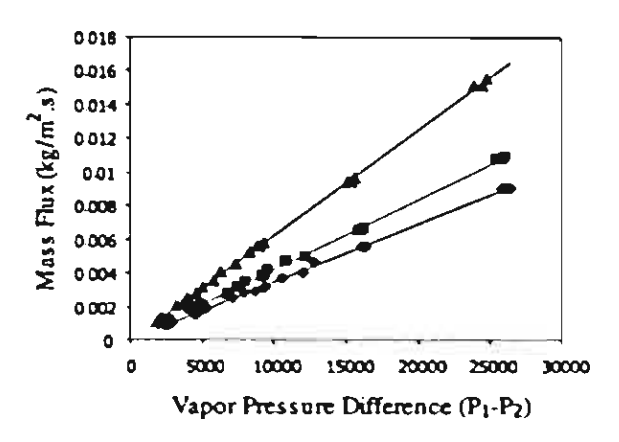


Fig. 11. Mass fluxes at various driving force; (♦) GVHP 0.22 μm; (■) HVHP 0.45 μm; (▲) PTFE 0.2 μm.

 $6.245 \times 10^{-7} \,\mathrm{kg} \,\mathrm{m}^{-2} \,\mathrm{s}^{-1} \,\mathrm{Pa}^{-1}$ for PTFE. The MD coefficient for the HVHP is lower than that reported in the previous work [12] by 15.1% due to differences in the calculation methods. The MD coefficients as defined in Eq. (2) represent the mass transfer coefficient across the membrane region. As a result, changes in flow rates in feed and permeate streams should not affect MD coefficients. In the range of the membrane temperatures studied (303-318 K), the temperatures did not influence the MD coefficients. There are two possible reasons to explain why MD coefficients are not dependent on the temperatures. First, the change in the average membrane temperatures was less than 5% from 303 to 318 K. Second, the majority of mass transfer occurred within the transition region [6]. Consequently, the MD coefficients consist of two major contributions: a Knudsen diffusion part (CK) that decreases with temperature to the power of -0.5 [12,14] and a molecular diffusion part (CM), that increases with temperature to the power of 1,34 [6]. These components would counterbalance and therefore, the net values of MD coefficients were almost constant over the temperature range used in these experiments.

The temperature distributions inside the membranes were estimated by Eqs. (7)–(9). Fig. 12 shows the distributions of each membrane for turbulent flow condition, and the similar trends are obtained for laminar flow condition. Figs. 13 and 14 display the influence of the feed temperatures and flow rates on the temperature profiles, respectively. In Fig. 14, higher

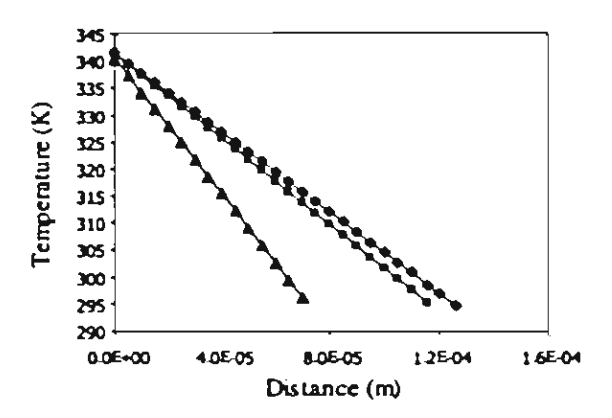


Fig. 12. Temperature distributions for each membrane at $T_f = 343 \text{ K}$, $\lambda = 21,423.4 \text{ W m}^{-2} \text{ K}^{-1}$; $(\Phi) \text{ GVHP 0.22 } \mu\text{m}$; $(\blacksquare) \text{ HVHP 0.45 } \mu\text{m}$; $(\triangle) \text{ PTFE 0.2 } \mu\text{m}$.

trans-membrane temperatures were obtained at higher flow rates leading to higher mass fluxes. Although the temperature profile is expressed in the form of an exponential function, the calculated temperature profiles are nearly linear for all membranes and experimental conditions studied. The possible reason is that the membranes are relatively thin (very short distance). Therefore, the assumption of the linear temperature profile in the membranes used in previous work [3,27] were valid.

If heat transfer due to mass transfer in the feed and permeate streams $(q_l^m \text{ and } q_p^m)$ are neglected, the simplified equations to calculate the membrane surface

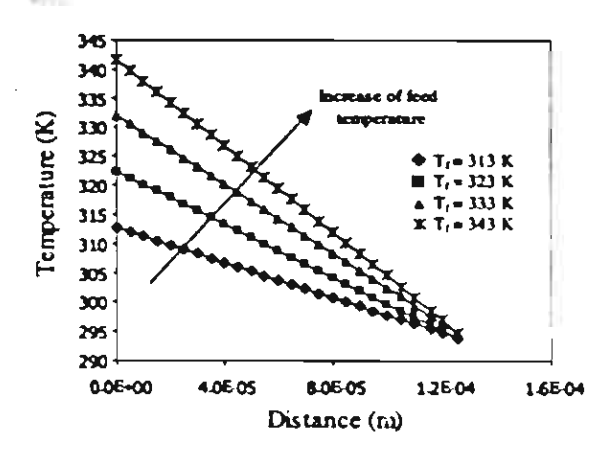


Fig. 13. Effect of feed temperatures on temperature distributions for GVHP, $h=21.423.4\,W\,m^{-2}\,K^{-1}$.

690

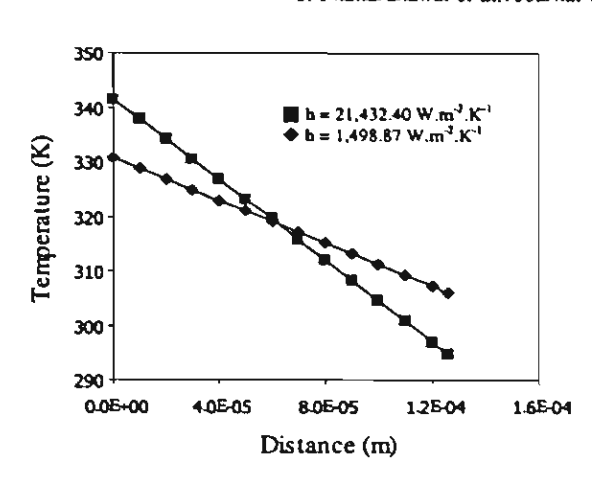


Fig. 14. Effect of film heat transfer coefficients (flow rates) on temperature distributions for GVHP.

temperatures are given by Eqs. (38) and (39). The arrangement in both expressions helps describe the phenomenon of polarization. The second terms in such expressions can be regarded as the polarization terms.

692

693

694

695

696

698

699

700

701

703

704

705

706

$$T_1 = T_f - \frac{q_v + q_c}{h_f} \tag{38}$$

$$T_2 = T_p + \frac{q_v + q_c}{h_p}$$
 (39)

Since the temperature distributions in the membranes appeared to be the straight lines (Figs. 12-14), the heat conduction can be rewritten in the simple form

$$q_{\rm c} = k_{\rm m} \left(\frac{T_1 - T_2}{\delta} \right) \tag{40}$$

From Fig. 6, q_v slightly drops with decreasing temperature across the membrane. As a result, q_v can be assumed constant at the average membrane temperature: $(T_1 + T_2)/2$, given by

$$q_{\rm v} = JH_{\rm v}\{T_{\rm m}\} = JH_{\rm v}\left\{\frac{T_1 + T_2}{2}\right\}$$
 (41)

After substituting Eqs. (40) and (41) into Eqs. (38) 708 and (39), the expressions for evaluating the membrane 709 surface temperatures are shown below 719

$$T_{l} = T_{f} - \frac{JH_{v}\{(T_{1} + T_{2})/2\} + k_{m}\{(T_{1} - T_{2})/\delta\}}{h_{f}}$$
713 (42)

$$T_2 = T_p + \frac{JH_v\{(T_1 + T_2)/2\} + k_m\{(T_1 - T_2)/\delta\}}{h_p}$$
(43) 715

The temperature polarization coefficient can be obtained by the combination of Eqs. (1), (42) and (43) for the simple case of the same film heat transfer coefficients $(h_f = h_p = h)$ [8], expressed as

$$\tau = \frac{1 - [2JH_{\rm v}\{T_{\rm m}\}/h(T_{\rm f} - T_{\rm p})]}{1 + (2k_{\rm m}/\delta h)}$$
(44)

721

$$T_{\rm m} = \frac{T_{\rm f} + T_{\rm p}}{2}$$

Usually, the heat transfer model is arranged in the complicated forms [3,27] which cannot provide the clear picture of temperature polarization. Therefore, the alternative method is proposed in order to offer both simple calculation and better illustration of temperature polarization. Initially (n = 0), the membrane surface temperatures $T_{1,n=0}$ and $T_{2,n=0}$ are approximated by Eqs. (45) and (46). The number 2 in Eqs. (45) and (46) refers to the comparable importance of heat conduction and heat due to vapor flow. Subsequently, $T_{1,n=1}$ and $T_{2,n=1}$ are obtained by replacing $T_{1,n=0}$ and $T_{2,n=0}$ into Eqs. (47) and (48). The calculations are repeated until the differences between T_{n+1} and

$$T_{\rm h}$$
 are smaller than 0.01%. 736
$$T_{\rm 1,h=0} = T_{\rm f} - \frac{2JH_{\rm v}(T_{\rm f} + T_{\rm p})/2}{h_{\rm f}}$$
 (45)

$$T_{2,n=0} = T_p + \frac{2JH_v(T_f + T_p)/2}{h_p}$$
 (46)

$$T_{1,n+1} = T_{\rm f} - \frac{JH_{\rm v}\{(T_{1,n} + T_{2,n})/2\}}{+k_{\rm m}\{(T_{1,n} - T_{2,n})/\delta\}}$$

$$h_{\rm f}$$
(47)

$$T_{2,n+1} = T_{p} + \frac{JH_{v}\{(T_{1,n} + T_{2,n})/2\}}{+k_{m}\{(T_{1,n} - T_{2,n})/\delta\}}$$

$$(48)$$

When the spacers are put in the flow channels, the mass fluxes were increased (compared to laminar flow at the same flow rates). Fig. 15 shows that the mass

15

716

717

718

719

725

726

727

728

729

733

734

735

ARTICLE IN PRESS

J. Phattaranawik et al./Journal of Membrane Science 5477 (2002) 1-17

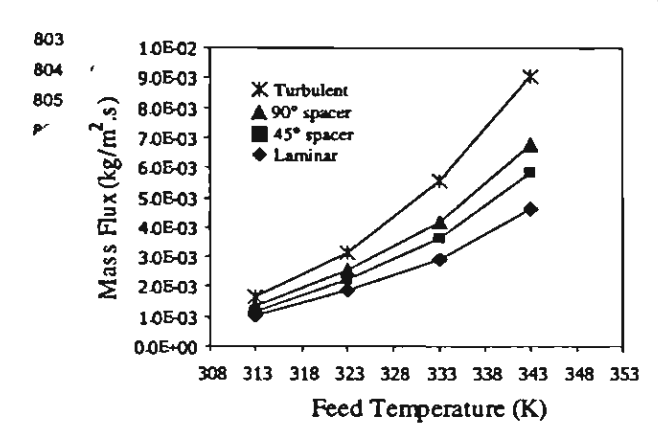


Fig. 15. Mass fluxes at various feed temperatures under laminar flow ($h = 1498.87 \, \text{W m}^{-2} \, \text{K}^{-1}$), 90° spacer, 45° spacer, and turbulent flow (17,026.3 W m⁻² K⁻¹) for GVHP 0.22 μ m.

745

746

747

748

749

750

751

752

753

754

755

756

757

75A

750

760

761

762

763

764

765

766

767

768

769

770

771

772

773

774

fluxes enhanced by spacers were between the fluxes obtained from laminar and turbulent flow conditions. In addition, the mass fluxes increased by 90° spacers were higher than those increased by 45° spacers due to higher generated eddy [26] in 90° spacers. The mass fluxes enhanced by both spacers are much lower than those obtained from turbulent flow condition. Consequently, the flow characteristic of spacer-filled channels in DCMD was likely to be in the lower transition regime rather than turbulent regime. Compared to other membrane processes, the turbulent flow was obtained in RO and UF performed with spacers [9,11], and upper transition regime was found in UF with the zigzag spacers [10]. The flow characteristic in spacer-filled channel of UF was concluded to be the upper transition regime (close to turbulent flow) or turbulent flow. The difference in conclusions between DCMD and UF or RO can be explained by theory of high mass transfer rate convection to be mentioned in our next work.

Fig. 15 demonstrates that the values of the heat transfer coefficients for spacer-filled channels fell between those calculated by the correlations for laminar flow and turbulent flow or $1500-17,000~\rm W~m^{-2}~K^{-1}$ for the chosen correlations in this work, and can be estimated by Fig. 16. The preliminary calculations based on the assumption of constant MD coefficient gave the values of the heat transfer coefficients for spacer-filled channel in the range of $2000-5500~\rm W~m^{-2}~K^{-1}$. However, the heat transfer coefficients for spacer-filled

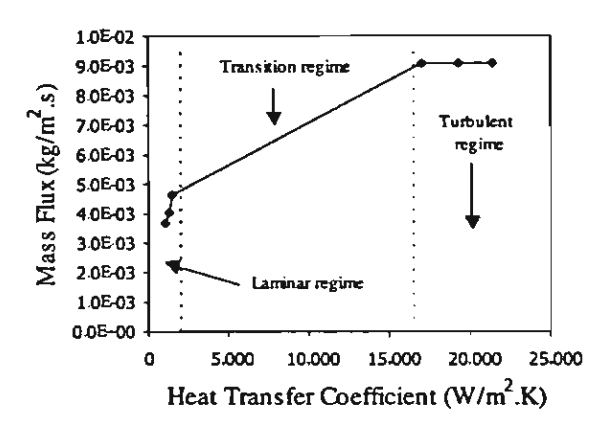


Fig. 16. Mass fluxes at various heat transfer coefficients for GVHP at 343 K.

channels in this work were considerably less than those calculated by Eq. (20) at the same Reynolds numbers.

5. Conclusions

The heat transfer model based on the simultaneous heat and mass transfer was used to identify the significance of each heat transfer mechanism and the influence of mass transfer on heat transfer rates. The theory of high mass transfer rate convection was used to assess the effect of mass transfer on heat transfer coefficients. The maximum effects of mass transfer on heat transfer rates in the feed and permeate streams were only 7.2 and 3.2%, respectively. The calculation results proved that the effects of mass transfer on heat transfer rates and on heat transfer coefficient can be neglected. The significance of heat conduction in the membranes and of heat transfer due to vapor flowing was comparable. The assumption of linear temperature profile inside the membranes and vapor flowing with constant enthalpy was valid for all membranes studied. The MD coefficients remained unchanged with the operating conditions employed in this work and depended only on the membrane properties. Therefore, the MD coefficient can be considered as the characteristic values for each membrane. In this work, the MD coefficients were 3.459×10^{-7} , 4.169×10^{-7} , and $6.245 \times 10^{-7} \text{ kg m}^{-2} \text{ s}^{-1} \text{ Pa}^{-1}$ for GVHP, HVHP, and PTFE, respectively.

775 776

778

783

784

793

794

795

796

797

798

REA

851

852

853

854

855

856

857

858

859

860

861

862

864

865

866

867

868

869

870

871

872

873

874

876

877

878

879

880

881

882

883

RR4

885

886

887

888

889

890

891

892

893

894

895

896

898

899

900

901

903

904

For the experiments with the spacers, 26-56% increase in mass fluxes were achieved, compared with the fluxes performed under laminar flow. Furthermore, the flow characteristic in the spacer-filled channels was likely to fall in the lower transition regime rather than the turbulent regime. The heat transfer coefficients for spacer-filled channels were estimated in the range of 2000-5500 W m⁻² K⁻¹, or were enhanced by approximately 2.5 times of the heat transfer coefficients for laminar flow.

813 Acknowledgements

803

805

806

807

808

809

810

811

812

822

823

824

825

826

827

828

829

830

831

832

633

834

835

836

837

838

839

840

841

842

843

The authors would like to thank The Thailand Research Fund and The Royal Golden Jubilee Ph.D. Program for financial support. J. Phattaranawik wishes to thank the UNESCO Centre for Membrane Science & Technology for hospitality.

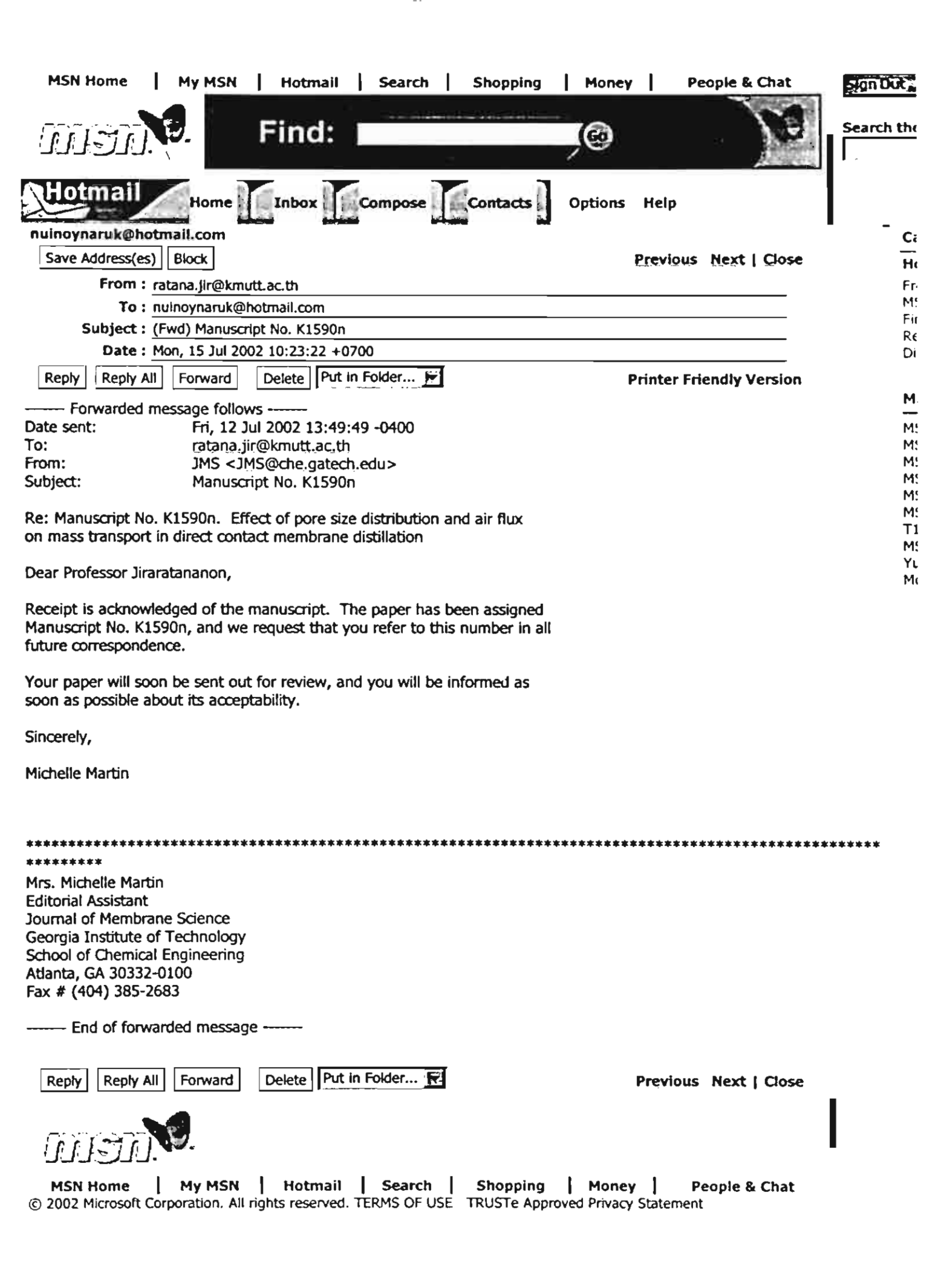
819 References

- [1] R.B. Bird, W.E. Stewart, E.N. Lightfoot, Transport Phenomena, Wiley, New York, 1960.
 - [2] A.F. Mills, Mass Transfer, 2nd ed., Prentice-Hall, Englewood Cliffs, NJ, 2001.
 - [3] M. Gryta, M. Tomaszewska, Heat transport in membrane distillation process, J. Membr. Sci. 144 (1998) 211-222.
 - [4] M.A. Izquierdo-Gil, M.C. Garcia-Payo, C. Fernandez-Pineda, Air gap membrane distillation of sucrose aqueous solution, J. Membr. Sci. 155 (1999) 291-307.
 - [5] J. Phattaranawik, R. Jiraratananon, Direct contact membrane distillation: effect of mass transfer on heat transfer, J. Membr. Sci. 188 (2001) 137-143.
 - [6] K.W. Lawson, D.R. Lloyd, Membrane distillation. IL Direct contact MD, J. Membr. Sci. 120 (1996) 123-133.
 - [7] L. Martinez-Diez, M.I. Vazquez-Gonzalez, F.J. Florido-Diaz, Study of membrane distillation using channel spacers, J. Membr. Sci. 144 (1998) 45-56.
 - [8] J. Phattaranawik, R. Jiraratananon, A.G. Fane, C. Halim, Mass flux enhancement using spacer-filled channels in direct contact membrane distillation, J. Membr. Sci. 187 (2001) 193-201.
 - [9] A.R. Da Costa, A.G. Fane, C.J.D. Fell, A.C. M Franken, Optimal channel spacer design for ultrafiltration, J. Membr. Sci. 62 (1991) 275–291.
- [10] J. Schwinge, D.E. Wiley, A.G. Fane, R. Guenther, Characterization of a zigzag spacer for ultrafiltration, J. Membr. Sci.
 172 (2000) 19-31.
- [11] G. Schock, A. Miquel, Mass transfer and pressure loss in spiral wound modules, Desalination 64 (1987) 339-352.

- [12] R.W. Schofield, A.G. Fane, C.J.D. Fell, Heat and mass transfer in membrane distillation, J. Membr. Sci. 33 (1987) 299– 313.
- [13] E.A. Mason, A.P Malinauskas, in: S.W. Churchill (Ed.), Gas Transport in Porous Media: The Dusty-Gas Model, Elsevier, Amsterdam, 1983.
- [14] R.W. Schofield, A.G. Fane, C.J.D. Fell, Gas and vapour transport though microporous membrane. II. Membrane distillation. J. Membr. Sci. 53 (1990) 173-185.
- [15] J.M. Smith, H.C. Van Ness, Introduction to Chemical Engineering Thermodynamics, 4th ed., McGraw-Hill, New York, 1990.
- [16] R.H. Perry, Perry's Chemical Engineers' Handbook, 6th ed., McGraw-Hill, New York, 1984.
- [17] Y.K. Godovsky, Thermophysical Properties of Polymers, Springer, Berlin, 1992.
- [18] A.B. Strong, Plastics: Material and Processing, 2nd ed., Prentice-Hall, Englewood Cliffs, NJ, 2000.
- [19] J. Brandrup, E.H. Immergut, Polymer Handbook, 3rd ed., Wiley, New York, 1989.
- [20] C.A. Harper, Handbook of Plastics, Elastomers and Composites, 3rd ed., McGraw-Hill, New York, 1996.
- [21] D.W. Van Krevelch, Properties of Polymers, 3rd ed., Elsevier, Amsterdam, 1990.
- [22] C.L. Yaws, Handbook of Transport Property Data: Viscosity, Thermal Conductivity, and Diffusion Coefficients of Liquids and Gases, Gulf Publishing, Houston, 1995.
- [23] S.B. Warner, Fiber Science, Prentice-Hall, Englewood Cliffs, NJ, 1995.
- [24] S.M. Lee, International Encyclopedia of Composites, vol. 5, VCH Publishers, New York, 1991.
- [25] A.R. Da Costa, A.G. Fane, D.E. Wiley, Ultrafiltration of whey protein solutions in spacer-filled flat channels, J. Membr. Sci. 76 (1993) 245-254.
- [26] A.R. Da Costa, A.G. Fane, D.E. Wiley, Spacer characterization and pressure drop modeling in spacer-filled channels for ultrafiltration, J. Membr. Sci. 87 (1994) 79-98.
- [27] M. Gryta, M. Tomaszewska, A.W. Morawski, Membrane distillation with laminar flow, Sep. Purif. Technol. 11 (1997) 93-101.
- [28] E.N. Sieder, G.E. Tate, Heat transfer and pressure drop of liquid in tubes, Ind. Eng. Chem. 28 (1936) 1429-1435.
- [29] L.C. Thomas, Heat Transfer, Prentice-Hall, Englewood Cliffs, NJ, 1992.
- [30] K.P. Hagan, Heat Transfer with Application, Prentice-Hall, Englewood Cliffs, NJ, 1990.
- [31] F.W. Dittus, L.M.K. Boelter, Publications on Engineering, vol. 2, University of California, Berkeley, 1930.
- [32] M.N. Ozisik, Heat Transfer (A Basic Approach), McGraw-Hill, New York, 1985.
- [33] S. Aravinth, Prediction of heat and mass transfer for fully developed turbulent fluid flow through tubes, Int. J. Heat. Mass Transfer 43 (2000) 1399-1408.
- [34] J.R. Welty, C.E. Wicks, R.E. Wilson, Fundamentals of Momentum, Heat and Mass Transfer, 3rd ed., Wiley, New York, 1984.

Manuscripts submitted to <u>Journal of</u> Membrane Science

- Manuscript No. K1590n: Effect of pore size distribution and air flux on mass transport in direct contact membrane distillation.
- Manuscript No. K1621n: Heat and mass transfer enhancement by net-type spacers in direct contact membrane distillation



Effect of Pore Size Distribution and Air Flux on Mass Transport in Direct Contact Membrane Distillation

J. Phattaranawik ^a, R. Jiraratananon ^{a,*}, and A.G. Fane ^b

^a Department of Chemical Engineering, King Mongkut's University of Technology Thonburi, Toongkru,

Bangkok, 10140, Thailand

b UNESCO Centre of Membrane Science & Technology, School of Chemical Engineering and Industrial

Chemistry, The University of New South Wales, Sydney, NSW, 2052, Australia

Abstract

The concept of mass transfer regions within the membranes was introduced to study the mass

transport in membrane distillation processes. Mass transfer model for direct contact membrane distillation

(DCMD) was derived to examine the influence of pore size distribution and air fluxes on water vapor fluxes

across the membranes. The pore size distributions of the membranes were determined by field emission

electron microscopy (FESEM) and the image analysis program. DCMD experiments with pure water were

carried out under laminar and turbulent flow conditions so as to compare the experimental results with the

predictions.

The calculation results showed that Knudsen and transition regions were found in the membranes

studied, while the transition region was the major contribution to mass transport. The model including the

effect of pore size distribution and air fluxes predicted water fluxes with the average discrepancy 5% of the

experimental results. The mass transfer analysis indicated that the influence of pore size distribution and air

fluxes on water fluxes was insignificant. Therefore, the mass transfer model with the assumptions of air

trapped in membrane pores and single pore size is adequate to describe mass transport in DCMD. The

concept of mass transfer regions was also applied to analyze the effect of pore size distribution on flux in

vacuum membrane distillation and gas permeation.

* Corresponding author. Tel.: +66-2-470-9222;

1. Introduction

The transport of vapors or gases inside porous membrane with isothermal condition can be described by 3 major mechanisms based on the Dusty Gas Model [1]: Knudsen diffusion, viscous flow, and molecular diffusion. The combinations of these transport modes such as Knudsen-viscous transition [2] and Knudsen-molecular diffusion transition [3] offered better agreement with the experimental results. The selection of the most suitable mechanism strongly depends on the comparison of mean free path (λ) and pore diameter (d_p). For a single gas system if the mean free path is much smaller than the pore size ($\lambda \ll d_p$), molecule-molecule collisions influence mass transport which can be described by viscous flow. On the other hand, when the mean free path of the gas is much larger than the pore size, molecular-wall collisions become more important and the gas transport is described by Knudsen diffusion.

For porous membrane, the gradients of total pressure, concentration, and partial pressure result in viscous flow, molecular diffusion, and Knudsen diffusion, respectively [1]. In DCMD, total pressure is constant at 1 atm because both feed and permeate solutions are employed under atmospheric pressure. Consequently, viscous flow is theoretically omitted [3,4,5]. Slip flow (viscous slip) and pressure diffusion [6] can also be neglected. Only diffusion slip [6] contributed from ordinary and Knudsen diffusion exists for the combined mode. Surface diffusion [1] can be ignored due to low molecule-membrane interaction.

Due to pore size distribution of the membranes, more than one mechanism of mass transport can simultaneously occur. Most literatures have employed the average pore size in the gas transport model to calculate the fluxes. Recently, the effect of shape of pore size distribution was studied with Gaussian (symmetric) and logarithmic (asymmetric) distribution [4] in which non-symmetrical distribution achieved better agreement with the experimental results. However, the influence of pore size distribution on mass transfer has not been completely elucidated. In MD, air possibly moves counter to water flux. As a result, water flux is probably affected. The effect of air flux has not been assessed and the validity of the air trapped assumption has not been proved. Therefore, this work aims to propose the mathematical models to examine the influence of both pore size distribution and air flux in DCMD.

2. Theory

In DCMD, mass transport across the membrane with non-uniform pore sizes occurs in three regions [6]: Knudsen region, transition region, and continuum region. Location of each region along the pore size distribution is represented by Fig.1. The Knudsen number (Kn.no) used to indicate the borders of the regions is defined as the ratio of the mean free path of the gas to the pore diameter, i.e. Kn.no = λ / d_p .

For the binary mixture of water vapor and air, the mean free path of water in air (λ_{w-a}) is evaluated at the average membrane temperature (T_m) [7,8]:

$$\lambda_{w-a} = \frac{k_B T_m}{\pi \left(\frac{\sigma_w + \sigma_a}{2}\right)^2 P_T \sqrt{1 + \frac{m_w}{m_a}}} \tag{1}$$

In Eq.(1), k_B is Boltzman constant (1.381×10⁻²³ J.K⁻¹), P_T is total pressure (1.013×10⁵ Pa or 1 atm for DCMD), σ_w and σ_a are collision diameters for water vapor (2.641×10⁻¹⁰ m) and air (3.711×10⁻¹⁰ m) [9,10]. m_w and m_a are molecular weights of water and air. At the typical membrane temperature of 60 °C, the mean free path in DCMD system is 0.11 μm .

In Knudsen region (Kn.no. > 1, or $d_p < \lambda$), the transport mode is Knudsen diffusion. For transition region (0.01 < Kn.no < 1, or $\lambda < d_p < 100\lambda$) with constant total pressure, mass transport takes place via the combination of Knudsen and ordinary diffusion in series, whereas ordinary diffusion is used to describe the mass transport in continuum region (Kn.no < 0.01, or $d_p > 100\lambda$). The mass transport of gases through porous media based on the concept of mass transfer regions (Fig.1) can be visualized by the electrical analog shown in Fig.2. In addition, the electrical circuit for Schofield's model [11] and Dusty-Gas Model for DCMD [1,5] can be displayed in Fig.3.

For this work, the lognormal distribution is used to represent the shape of pore size distribution:

$$n\{d_{p}\} = \frac{1}{SD_{log}d_{p}\sqrt{2\pi}} exp\left(-\frac{1}{2}\left(\frac{\ln(d_{p}/\overline{d}_{m})}{SD_{log}}\right)^{2}\right)$$
(2)

where $n\{d_p\}$ is a number of pores at pore diameter d_p , \overline{d}_m is mean pore diameter, and SD_{log} is the standard deviation of lognormal function.

According to the typical mean free path obtained above, the continuum region occurs when the pore size is bigger than 11 μ m (or 100 λ). The area under lognormal curve from transition-continuum region border to infinity (∞) is less than 1%. As a result, importance of the continuum region on mass fluxes can be ignored. Therefore, the total fluxes contributed from the Knudsen and transition regions are determined by integrating the fluxes in each region over the pore size distribution:

$$\bar{J}_{\tau} = \frac{\int\limits_{d_{p}=0}^{d_{p}=\infty} J\{d_{p}\} \frac{\pi d_{p}^{2}}{4} n\{d_{p}\} dd_{p}}{\int\limits_{0}^{\infty} \frac{\pi d_{p}^{2}}{4} n\{d_{p}\} dd_{p}} = \frac{\int\limits_{d_{p}=0}^{d_{p}=\lambda} J_{Kn}\{d_{p}\} \frac{\pi d_{p}^{2}}{4} n\{d_{p}\} dd_{p}}{\int\limits_{0}^{\infty} \frac{\pi d_{p}^{2}}{4} n\{d_{p}\} dd_{p}} + \frac{\int\limits_{d_{p}=\lambda}^{d_{p}=\infty} J_{tr}\{d_{p}\} \frac{\pi d_{p}^{2}}{4} n\{d_{p}\} dd_{p}}{\int\limits_{0}^{\infty} \frac{\pi d_{p}^{2}}{4} n\{d_{p}\} dd_{p}}$$
(3)

To simplify Eq. (3), the average pore sizes for each region (\overline{d}_{Kn} and \overline{d}_{tr}) are employed and the molar fluxes for each region are evaluated at the average pore sizes which are determined at the position of 50% of number of pores in each region, see Fig.1. Consequently, Eq.(3) can be rewritten as:

$$\bar{J}_{T} = \frac{\bar{J}_{Kn} \{\bar{d}_{Kn}\}_{d_{p}=0}^{d_{p}=\lambda} \frac{\pi d_{p}^{2}}{4} n\{d_{p}\} dd_{p}}{\int_{0}^{\infty} \frac{\pi d_{p}^{2}}{4} n\{d_{p}\} dd_{p}} + \frac{\bar{J}_{tr} \{\bar{d}_{tr}\}_{d_{p}=\lambda}^{d_{p}=\infty} \frac{\pi d_{p}^{2}}{4} n\{d_{p}\} dd_{p}}{\int_{0}^{\infty} \frac{\pi d_{p}^{2}}{4} n\{d_{p}\} dd_{p}}$$

$$(4)$$

In Eq. (4),
$$\frac{\int\limits_{d_p=0}^{d_p=\lambda}(\pi d_p^2/4)n\{d_p\}dd_p}{\int\limits_{0}^{\infty}(\pi d_p^2/4)n\{d_p\}dd_p} \quad \text{and} \quad \frac{\int\limits_{d_p=\lambda}^{d_p=\infty}(\pi d_p^2/4)n\{d_p\}dd_p}{\int\limits_{0}^{\infty}(\pi d_p^2/4)n\{d_p\}dd_p} \quad \text{are the fractions of the membrane}$$

area occupied by Knudsen and transition regions. However, Eq. (4) is still complicated and computer simulation is necessary to achieve the solutions. Thus, in this work the fractions of the membrane area are approximated by the fractions of number of pores in each region, shown by Eqs. (5) and (6). As a result, the fractions of pore numbers are directly determined by the cumulative distribution function of lognormal distribution (Φ).

$$\frac{d_{p}=\lambda}{\int_{0}^{d_{p}=0} (\pi d_{p}^{2}/4) n\{d_{p}\} dd_{p}} \approx \frac{\int_{0}^{d_{p}=\lambda} n\{d_{p}\} dd_{p}}{\int_{0}^{\infty} n\{d_{p}\} dd_{p}} = \frac{n_{Kn}}{n_{T}} = F_{Kn} = \Phi \left\{ \frac{\ln(\lambda/\overline{d}_{m})}{SD_{kog}} \right\}$$
(5)

$$\frac{\int_{0}^{d_{p}=\infty} (\pi d_{p}^{2}/4) n\{d_{p}\} dd_{p}}{\int_{0}^{d_{p}=\lambda} (\pi d_{p}^{2}/4) n\{d_{p}\} dd_{p}} \approx \frac{\int_{0}^{d_{p}=\infty} n\{d_{p}\} dd_{p}}{\int_{0}^{\infty} n\{d_{p}\} dd_{p}} = \frac{n_{tr}}{n_{T}} = F_{tr} = 1 - \Phi \left\{ \frac{\ln(\lambda/\overline{d}_{m})}{SD_{log}} \right\}$$
(6)

Substitution of Eqs. (5) and (6) in to Eq. (4) yields the expression of mass transfer derived from the concept of mass transfer regions in the membranes with pore size distributions:

$$\overline{J}_{T} = \Phi \left\{ \frac{\ln(\lambda / \overline{d}_{m})}{SD_{log}} \right\} \overline{J}_{Kn} + \left(1 - \Phi \left\{ \frac{\ln(\lambda / \overline{d}_{m})}{SD_{log}} \right\} \right) \overline{J}_{Tr}$$
 (7)

The cumulative distribution function in Eq. (7) can be considered as the weight fractions indicating the importance of each region. Other distribution functions can also be applied.

In the Knudsen region (Kn.no>1), the gas transport occurs due to free-molecule flow [6] and the mass transfer is described by Knudsen diffusion expressed by Eq.(8). Theoretically, the air fluxes do not affect water fluxes in Knudsen region since each gas molecule moves independently towards the pore wall.

$$\begin{split} \overline{J}_{Kn} &= \frac{D_{Kn}}{RT\delta} (P_{w,1} - P_{w,2}) \\ \text{where} \quad D_{Kn} &= \frac{4}{3} \frac{\varepsilon \overline{d}_{Kn}}{\chi} \sqrt{\frac{RT_m}{2\pi m_w}} \end{split} \tag{8}$$

where \overline{J}_{Kn} is the molar flux in Knudsen region, ε is membrane porosity, χ is membrane tortuosity, δ is membrane thickness, R is gas constant, m_w is molecular weight of water, T_m is membrane temperature. $P_{w,1}$ and $P_{w,2}$ are water vapor pressures evaluated at membrane surface temperatures T_1 and T_2 .

In the transition region, the mean free path of gas is comparable to the pore size. Collision between molecules is as important as the collision between molecules and the pore wall. The mass transfer equation for the transition region is based on the momentum balance including momentum transferred by gas molecule to other molecule as well as to the pore wall (see Fig.4). The combination of molecular and Knudsen diffusion in series is used to describe the mass transfer for this region. The Knudsen diffusion for the transition region can be written by [6]:

$$(J_{w})_{Kn} = -\frac{D_{Kn}}{RT} \nabla P_{w} \Big|_{wall}$$
where
$$D_{Kn} = \frac{4}{3} \frac{\varepsilon \overline{d}_{tr}}{\chi} \sqrt{\frac{RT_{m}}{2\pi m_{w}}}$$
(9)

The derivation of molecular diffusion including the air flux effect (Ja) may be initiated by Fick's law:

$$(J_{w})_{mol} = -\frac{\varepsilon D_{w-a}}{\chi RT} \nabla P_{w} \big|_{mol-mol} + \gamma_{w} \big((J_{w})_{mol} + J_{a} \big)$$
(10)

The air probably moves counter to the water fluxes or from permeate side to feed side due to its partial pressure gradient. Consequently, the influence of the air flux (J_a) should appear in form of the counter molecular diffusion. The relationship between $(J_w)_{mol}$ and J_a can be determined by Graham's law:

$$\frac{J_a}{(J_w)_{mol}} = -\sqrt{\frac{m_w}{m_a}} = -\alpha \tag{11}$$

After substituting Eq. (11) and $y_w = \frac{P_w}{P_T}$ into Eq. (10), the expression for molecular diffusion with the effect of air flux is obtained:

$$(J_{w})_{mol} = -\frac{(\varepsilon/\chi)D_{w-a}}{RT\left(1 - \frac{P_{w}}{P_{T}}(1 - \alpha)\right)}\nabla P_{w}|_{mol-mol}$$
(12)

The serial connection of two resistances shown in Fig. 4 allows writing the expression below:

$$\frac{\nabla P_{w}}{\bar{J}_{Tr}} = \frac{\nabla P_{w}|_{mol-mol}}{(J_{w})_{mol}} + \frac{\nabla P_{w}|_{wall}}{(J_{w})_{Kn}}$$
(13)

The diffusive flux for water vapor is obtained from the combination of Eqs.(9), (12), and (13), expressed by Eq. (14).

$$\overline{J}_{Tr} = -\frac{1}{RT} \left(\frac{P_T - (1 - \alpha)P_w}{(\epsilon/\chi)P_T D_{w-a}} + \frac{1}{D_{Kn}} \right)^{-1} \nabla P_w$$
 (14)

Integration of Eq. (14) provides the steady state flux of water vapor for transition region given by Eq. (15).

$$\bar{J}_{Tr} = \frac{(\epsilon/\chi)P_TD_{w-a}}{(1-\alpha)\delta RT_m} ln \left(\frac{D_{Kn}(P_T - (1-\alpha)P_{w,2}) + (\epsilon/\chi)P_TD_{w-a}}{D_{Kn}(P_T - (1-\alpha)P_{w,1}) + (\epsilon/\chi)P_TD_{w-a}} \right)$$
(15)

The value of D_{w-a} is evaluated by the empirical formulas for the temperature rage 273 – 373 K, given by [10]:

$$P_T D_{w-a} [Pa.m^2 / s] = 1.895 \times 10^{-5} T^{2.072}$$
 (16)

The factor α reveals the effect of air fluxes in DCMD. In case of diffusion through a stagnant gas film, α is equal to 0 and Eq. (15) becomes the Knusen-molecular diffusion transition model [3]. However, Eq. (15) is not valid for equimolar counterdiffusion ($\alpha = 1$) and is based on the assumption of isothermal situation in the membranes. The effect of air fluxes in air gap membrane distillation (AGMD) or sweeping

gas membrane distillation (SGMD) that employs air as the sweeping gas may be more significant than DCMD due to more availability of air source in the permeate.

In short, the mass transfer model consists of Eq. (7) as the core of the model, while \bar{J}_{Kn} and \bar{J}_{Tr} are represented by Eqs. (8) and (15), respectively.

In case that the pore size distribution and air flux effects are ignored, mass transfer is described by the model for transition region because the typical mean pore size of the membrane falls in transition region, and the mass transfer model is given by;

$$\bar{J}_{T} = \frac{(\varepsilon/\chi)P_{T}D_{w-a}}{\delta RT_{m}} ln \left(\frac{D_{Kn}(P_{T} - P_{w,2}) + (\varepsilon/\chi)P_{T}D_{w-a}}{D_{Kn}(P_{T} - P_{w,1}) + (\varepsilon/\chi)P_{T}D_{w-a}} \right)$$
(17)

where
$$D_{Kn} = \frac{4}{3} \frac{\epsilon \overline{d}_m}{\chi} \sqrt{\frac{RT_m}{2\pi m_w}}$$

The water vapor pressure $P_{w,1}$ and $P_{w,2}$ are evaluated by Antoine equation at the membrane surface temperatures T_1 and T_2 . The heat transfer model [12] facilitates the determination of the membrane surface temperatures, shown by Eqs. (18) and (19).

$$T_{1} = T_{f} - \frac{k_{m} \left(\frac{T_{1} - T_{2}}{\delta}\right) + \bar{J}_{T} H_{v} \{(T_{1} + T_{2})/2\}}{h_{f}}$$
(18)

$$T_{2} = T_{p} - \frac{k_{m} \left(\frac{T_{1} - T_{2}}{\delta}\right) + \overline{J}_{T} H_{v} \{(T_{1} + T_{2})/2\}}{h_{p}}$$
(19)

3. Experimental

3.1 Determinations of pore size distributions

The field emission scanning electron microscopy (FESEM) (Hitachi model S-900) was used to image the membranes. The magnifications ranging from 7,000 to 10,000 were employed. The electron beam was accelerated under a 3.0 kV in the vacuum chamber. The images obtained from the FESEM were analyzed by the software 'AnalySIS' provided by Soft Imaging System. The pore area was measured by encircling the membrane pores. The equivalent pore diameter, defined as the diameter that a pore of area A_p should have if it had a circular section on the surface, is evaluated by Eq. (20).

$$d_{p} = 2\sqrt{\frac{A_{p}}{\pi}} \tag{20}$$

The pore size distributions, required for mass transfer calculations, are fitted to lognormal distributions given by frequencies:

$$f_{i} = a \exp \left(-\frac{1}{SD_{log}^{2}} \left(ln \left(\frac{d_{i}}{\overline{d}_{m}} \right) \right)^{2} \right)$$
 (21)

where f_i is frequency obtained by the experiments, SD_{log} is the standard deviation or width of the distribution. SD_{log} and a are determined by the slope and the interception of the fitted curve, and the average pore diameter of membrane (\overline{d}_m) is determined by:

$$\overline{d}_{m} = \frac{\sum_{i=1}^{n} f_{i} d_{i}}{\sum_{i=1}^{n} f_{i}}$$
(22)

3.2 DCMD experiments

The experiments were performed under laminar and turbulent flow conditions with three types of the membranes: GVHP, HVHP and PTFE. The properties of the membranes are shown in Table 1. Pure water was used for feed and permeate solutions. The flat sheet membrane modules characteristics and experimental procedures for both flow conditions were described in our previous work [12].

Table 1. Membrane properties [12,13]

No.	Membrane material	Nominal ore size (µm)	Thickness (µm)	Porosity (ε)	k _m (W/m.K)	Manufacturer
1	GVHP (PVDF)	0.22	126	0.62	0.041	Millipore
2	HVHP (PVDF)	0.45	116	0.66	0.040	Millipore
3	PTFE	0.2	70*	0.7*	0.0382**	Sartorious

^{*} Manufacturer's data

* *calculated by:
$$k_m = \frac{\varepsilon}{k_q} + \frac{(1-\varepsilon)}{k_p}$$
 [12,14].

The flow rates of feed and permeate solutions were adjusted to obtain the same heat transfer coefficients for both feed and permeate channels. The heat transfer correlations used to calculate the heat transfer coefficients and operating conditions in this work were:

- for laminar flow [12,15]:
$$Nu = 4.36 + \frac{0.036 \text{RePr}(d_h/L)}{1 + 0.0011 (\text{RePr}(d_h/L))^{0.8}}$$
(23)

- for turbulent flow [12,16]:
$$Nu = 0.023 Re^{0.8} Pr^{1/3} \left(1 + \frac{6d_h}{L} \right)$$
 (24)

The correlation of turbulent flow was corrected to account for the entrance effect by the term of $\left(1 + \frac{6d_h}{L}\right) [17] \text{ for } 20 < L/d_h < 60.$

4. Flux calculation procedure

The proportions of Knudsen and the transition regions can be evaluated by the accumulative function of lognormal function distribution, Eqs.(5) and (6), respectively.

Fluxes and membrane distillation coefficients were used to assess the performance of mass transfer model and the influences of pore size distribution and air fluxes. The MD coefficient (C) is defined by:

$$C = \frac{\overline{J}_T}{(P_{w,1} - P_{w,2})} \tag{25}$$

The calculations were preformed by using the mass transfer model; Eqs. (7), (8), and (15) if the effects of pore size distribution and air fluxes are included or ;Eq.(17) if both effects are ignored. Initially, molar flux is assumed and used to calculate the membrane surface temperatures (T_1 and T_2) by Eqs.(18) and (19). Subsequently, T_1 and T_2 are used to evaluate molar flux by the mass transfer model (Eq.(7) or Eq.(17)). The procedures are repeated until the difference between assumed molar flux and calculated one is less than 0.1%. The experimental fluxes (J_{exp}) and MD coefficients (C_{exp}) are compared to the calculated values. In the calculations the tortuosity factor (χ) for all membranes was presumably equal to 2 [18].

5. Results and discussions

5.1 Pore size distributions

Various pore shapes were observed from the images such as elliptical, circular, and slit. The images of the membrane surface from FESEM facilitate the determination of the pore sizes. 900 – 1300 pores from total images for each membrane were observed, and their cross-section areas were measured by the image analysis program. The pore size distributions obtained for GVHP, HVHP, and PTFE are reported as bar graphs in Fig. (5). The statistical parameters in Eq.(21) are summarized in Table 4.

Table 4. Mean pore sizes and standard deviation of the membranes calculated from the FESEM images

Membrane	SD_{log}	d _m (μm)	
GVHP	1.037	0.251	
HVHP	0.636	0.414	
PTFE	0.9383	0.253	

As depicted in Fig. (5) and Table 4, the pore size distribution of GVHP is widest. The mean pore size of GVHP is bigger than the nominal pore size of 0.22 μm, reported by the manufacturer. Similar results were found for PTFE membrane. On the other hand, the mean pore size for HVHP is smaller than the nominal pore size, 0.45 μm, and its pore size distribution is narrowest among the membranes tested. In comparison with other methods, the average pore size of HVHP from FESEM was comparable to the results achieved by light transmission, 0.48 μm [19] and fluid displacement, 0.39 μm [20].

5.2 Mass transfer prediction

From Eq.(1), the mean free path of water vapor slightly changed from 0.101 µm at 30 °C to 0.106 µm at 45 °C. The fractions of Knudsen region varied from 19.2 to 20.5 % for GVHP, 16.5 to 17.8 % for PTFE, and 1.4 to 1.6 % for GVHP. This means that the influence of Knudsen region was less important for larger pore size membrane. The majority of membrane area was occupied by transition region. The average

pore diameters of Knudsen and transition region were found to be 0.0646 μm and 0.322 μm for GVHP, 0.086 μm and 0.418 μm for HVHP, and 0.0591 μm and 0.31 μm for PTFE, respectively.

The importance of membrane thickness and pore size on fluxes can be identified by Figs. (6)-(8). PTFE provided remarkably higher fluxes than HVHP although the mean pore size of HVHP is larger than PTFE by 1.7 times. However, the membrane thickness of HVHP is greater than PTFE by 1.6 times. Hence, the mass transfer resistance of the membranes is predominated by the membrane thickness.

Figs. (6) – (8) also compare measured fluxes with calculated fluxes by the mass transfer model including both effects for laminar and turbulent flow conditions. For GVHP, the average discrepancies were 7.1 % for laminar flow and 8.1 % for turbulent flow. The smaller discrepancies were found for PTFE membrane, which were 3.5 % for laminar flow and 4.1 % for turbulent flow. The flux predictions of HVHP provided the smallest disagreement of 2.9 % for laminar flow and 1.4 % for turbulent flow. The success in predicting the fluxes was possibly attributed to using more accurate membrane properties determined experimentally by [13] and to the heat transfer model.

The effects of pore size distribution and air fluxes on mass transport were examined by the comparison of the mass transfer model including and excluding such effects, shown in Figs. (9) - (11). For laminar flow, molar fluxes calculated by the both models were comparable, and for turbulent flow the model excluding such effects gave slightly higher fluxes at high feed temperature.

The MD coefficients calculated by the model excluding the effects evidently increased with increasing feed temperatures (see Fig.12). On the other hand, the measured MD coefficients and the coefficients evaluated by the model including the effects were likely to be independent with the feed temperatures. However, the calculated MD coefficients from both models were very close to the measured ones for all membranes and operating conditions.

5.3 Mass transfer regions in vacuum membrane distillation and gas permeation

The concept of mass transfer regions can also be applied for vacuum membrane distillation (VMD) and gas permeation (GP) in which the continuum region is negligible due to longer mean free path resulting from lower total pressure. As a result, the total flux is contributed by the Knudsen and transition regions, and Eq. (7) can be used to express the average total flux including the effect of pore size distribution. The mass

transport in the Knudsen region is also described by Knudsen diffusion (Eq.(8)). For single gas transport, the parallel connection between Knudsen diffusion and viscous flow is regarded for the transition region:

$$\overline{J}_{Tr} = \frac{1}{RT\delta} \left[\left(\frac{\varepsilon \overline{d}_{Tr}}{3\chi} \right) \left(\frac{8RT}{\pi m_w} \right)^{0.5} + \left(\frac{\varepsilon \overline{d}_{Tr}^2}{32\chi} \right) \left(\frac{P_{avg}}{\mu} \right) \right] (P_1 - P_2)$$
 (26)

Substitute Eqs.(26) and (8) into Eq.(7) and then rearrange to the well-know form [1,2]:

$$\overline{J}_{T} = \frac{1}{RT\delta} \left[K_0 \left(\frac{8RT}{\pi m_w} \right)^{0.5} + B_0 \left(\frac{P_{avg}}{\mu} \right) \right] (P_1 - P_2)$$
(27)

where μ is fluid viscosity, and K_0 and B_0 are the parameters, as shown below,

$$K_{0} = \frac{\varepsilon}{3\chi} \left(\Phi \left\{ \frac{\lambda}{\overline{d}_{m}} \right\} \overline{d}_{Kn} + \left(1 - \Phi \left\{ \frac{\lambda}{\overline{d}_{m}} \right\} \right) \overline{d}_{Tr} \right)$$
 (28)

and
$$B_0 = \left(1 - \Phi\left\{\frac{\lambda}{\overline{d}_m}\right\}\right) \frac{\varepsilon \overline{d}_{Tr}^2}{32\chi}$$
 (29)

From Eqs.(28) and (29), K_0 and B_0 from the concept of mass transfer regions depend on gas property (collision diameter), membrane properties, and experimental conditions, while K_0 and B_0 from the Dusty-Gas Model are a function of membrane properties only ($K_0 = \frac{\varepsilon \overline{d}_m}{3\gamma}$ and $B_0 = \frac{\varepsilon \overline{d}_m^2}{32\gamma}$).

6. Conclusion

The mass transfer model based on the concept of mass transfer regions has been proposed to determine the influences of pore size distribution and air fluxes on the mass transport in DCMD. The pore size distributions of the membranes determined by FESEM with the contribution of the image analysis program were comparable to those determined by other methods and to nominal values reported by the manufacturers. The predictions of the fluxes and MD coefficients showed good agreement with the experimental results for GVHP and excellent agreement for HVHP and PTFE. Additionally, the models predicted fluxes with less than 8% discrepancy. The utilization of more accurate membrane properties such as porosity, thickness, and pore size can offer better agreement with experimental results. The results also showed that the influences of pore size distribution and air fluxes were negligible for DCMD due to using of large pore membranes. The mass transfer model including the effects provided better predictions of MD

coefficients than the model excluding the effects. The approximation of the membrane area fractions by membrane pore number fraction was satisfactory. Moreover, the concept of mass transfer regions in membranes can be applied for other membrane processes such as gas permeation and is also suitable for the situation which only mass transfer in transition region is inadequate to describe overall mass transport.

6. Acknowledgement

The authors would like to thank the Thailand Research Fund (TRF) and the Royal Golden Jubilee Ph.D Program (RGJ) for financial support. Phattaranawik wishes to thank the UNESCO Centre for Membrane Science & Technology and Electron Microscope Unit (EMU), University of New South Wales for kind hospitality..

Nomenclatures

parameter in Eq.(24) a fraction of pore areas for each mass transfer region Α membrane distillation coefficient (mol.m⁻².s⁻¹.Pa⁻¹) C pore diameter (m) d_{p} hydraulic diameter of channel (m) d_h Diffusivity of water vapor-air mixture (m².s⁻¹) D_{w-a} Knudsen diffusion coefficient (m².s⁻¹) D_{Kn} f frequency F fraction of pore numbers heat transfer coefficient (W.m⁻².K⁻¹) h $H_v\{T\}$ vapor enthalpy evaluated at temperature T membrane thermal conductivity (W.m⁻¹.K⁻¹) k_{α} thermal conductivity of air (W.m⁻¹.K⁻¹) $k_{\mathbf{g}}$ thermal conductivity of polymer (W.m⁻¹.K⁻¹) k_{ρ} Flux (mol.m⁻².s⁻¹) J channel length (m) L molecular weight (kg.mol⁻¹) m pore numbers n Nusselt number Nu vapor pressure (Pa) P Prandlt number Рг temperature (K) T R gas constant (8.314 J/mol.K) Reynolds number Re Greek letters porosity ε

membrane thickness

δ

χ membrane tortuosity

Φ cumulative function of lognormal distribution

σ molecule collision diameter (m)

 λ mean free path of gas (m)

α ratio of air flux to water flux in Eq.(11)

Subscripts

1 membrane surface on feed side

2 membrane surface on permeate side

a air

f feed

Kn Knudsen region

p permeate

T Total

Tr Transition region

w water

References

- 1. E.A. Mason and A.P Malinauskas, in S.W. Churchill (Ed.), Gas Transport in Porous Media: The Dusty-Gas Model, Elsevier, Amsterdam, 1983.
- 2. K.W. Lawson, D.R. Lloyd, Membrane distillation. I. Module design and performance evaluation using vacuum membrane distillation, J. Membr. Sci., 120 (1996) 111-121.
- K.W. Lawson, D.R. Lloyd, Membrane distillation. II. Direct Contact MD, J. Membr. Sci., 120 (1996) 123-133.
- 4. F. Lagana, G. Barbieri, and E. Drioli, Direct contact membrane distillation: modeling and concentration experiments, J. Membr. Sci., 166 (2000) 1-11.
- C. Fernandez-Pineda, M.A. Izquierdo-Gil, and M.C. Garcia-Payo, Gas permeation and direct contact membrane distillation experiments and their analysis using different models, J. Membr. Sci., 2002 (198) 33-49.

- W. Kast, C.-R. Hohenthanner, Mass transfer within the gas-phase of porous media, Int. J. Heat & Mass Transfer, 43(2000) 807-823.
- 7. Hands Kuhn and Horst-Dieter Forstering, Principles of Physical Chemistry, Wiley, New York, 2000.
- 8. R.A. Albert and R.J. Silbey, Physical Chemistry, 2nd Edition, Wiley, New York, 1997.
- 9. E.L. Cussler, Diffusion, mass transfer in fluid system, 2nd Edition, Cambridge University Press, New York, 1997.
- 10. A.F. Mills, Mass Transfer, 2nd Edition, Prentice-Hall, New Jersey, 2001.
- R.W.Schofield, A.G.Fane and C.J.D.Fell, Gas and vapour transport though microporous membrane. II.
 Membrane Distillation, J.Membr. Sci., 53(1990) 173-185.
- 12. J. Phattaranawik, R. Jiraratananon, A.G. Fane, Heat Transport and Membrane Distillation Coefficient in Direct Contact Membrane Distillation, submitted to Journal of Membrane Science.
- 13. M.A. Izquierdo-Gil, M.C. Garcia-Payo, and C. Fernandez-Pineda, Air gap membrane distillation of surcose aqueous solution, J. Membr. Sci., 155(1999) 291-307.
- 14. S.B. Warner, Fiber Science, Prentice Hall, New Jersey, 1995.
- M.Gryta and M. Tomaszewska, Heat transport in the membrane distillation process, J. Membr. Sci., 144
 (1998) 211-222.
- 16. K.P. Hagan, Heat transfer with application, Prentice Hall, New Jersey, 1990.
- 17. J.R. Welty, C.E. Wicks, and R.E. Wilson, Fundamentals of Momentum, Heat and Mass Transfer, 3rd Ed, Wiley&Sons, 1984.
- R.W. Schofield, A.G. Fane, and C.J.D. Fell, Gas and vapour transport through Microporous membranes.II. Membrane Distillation, J. Membr. Sci., 53(1990) 173-185.
- 19. I.J. Youn, J. Jeong, T. Kim, Jae-chum Lee, Light transmission study for determination of pore size distribution in Microporous membranes, J. Membr. Sci., 145 (1998) 265-269.
- Y. Lee, J. Jeong, I.J. Youn, W.H. Lee, Modified liquid displacement method for determination of pore size distribution in porous membranes, J. Membr. Sci., 130 (1997) 149-156.

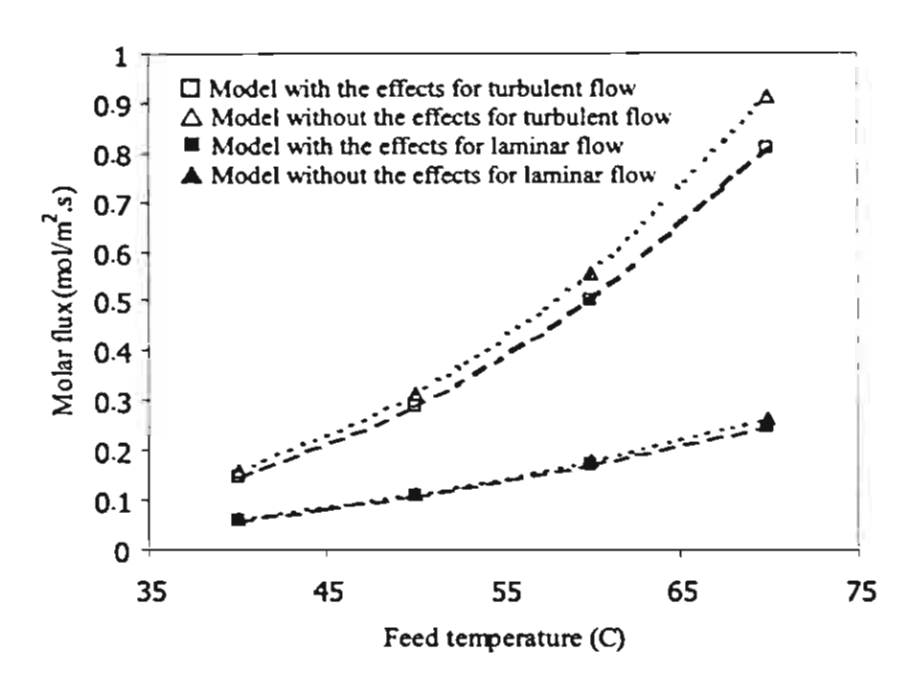


Figure 11. Predictions of molar fluxes by the models with and without the effect of pore size distribution and air flux for PTFE at. $h = 1,054.29 \text{ W/m}^2$.K for laminar flow and $h = 17,026.3 \text{ W/m}^2$.K for turbulent flow.

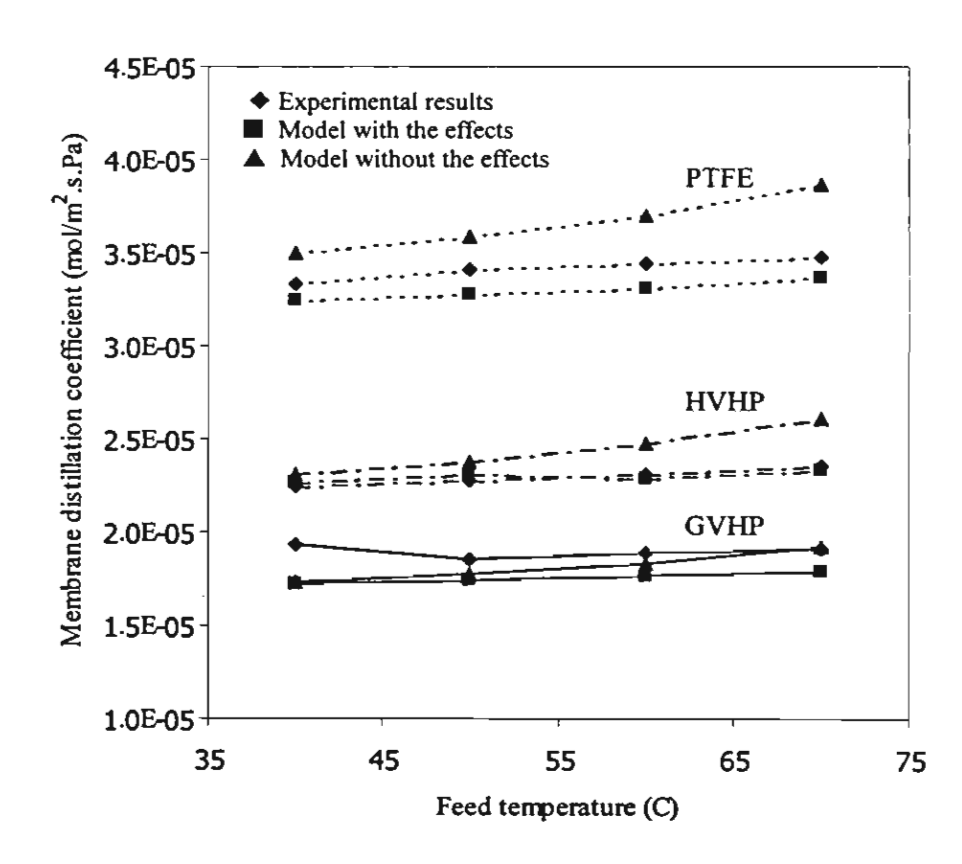


Figure 12. Experimental and predicted membrane distillation coefficients for GVHP, HVHP, and PTFE at $h = 1,498.87 \text{ W/m}^2.\text{K}$.

List of figures.

- Figure 1. Regions and mechanisms of mass transport the membrane with pore size distribution
- Figure 2. Electrical analogical circuit for multi pore size model
- Figure 3. Electrical analogical circuit for single pore size model: (a) The Dusty gas model and (b) Schofield's model
- Figure 4. Electrical analogue circuit for transition region
- Figure 5. Pore size distributions: (a) GVHP, (b) HVHP, and (c) PTFE
- Figure 6. Experimental and predicted flux for GVHP at $h = 1,281.88 \text{ W/m}^2$.K for laminar flow and $h = 19,261 \text{ W/m}^2$.K for turbulent flow.
- Figure 7. Experimental and predicted flux for HVHP at $h = 1,281.88 \text{ W/m}^2$.K for laminar flow and $h = 19,261 \text{ W/m}^2$.K for turbulent flow.
- Figure 8. Experimental and predicted flux for PTFE at $h = 1,281.88 \text{ W/m}^2$.K for laminar flow and $h = 19,261 \text{ W/m}^2$.K for turbulent flow.
- Figure 9. Predictions of molar fluxes by the models with and without the effect of pore size distribution and air flux for GVHP at. $h = 1,054.29 \text{ W/m}^2$.K for laminar flow and $h = 17,026.3 \text{ W/m}^2$.K for turbulent flow.
- Figure 10. Predictions of molar fluxes by the models with and without the effect of pore size distribution and air flux for HVHP at. $h = 1,054.29 \text{ W/m}^2$.K for laminar flow and $h = 17,026.3 \text{ W/m}^2$.K for turbulent flow.
- Figure 11. Predictions of molar fluxes by the models with and without the effect of pore size distribution and air flux for PTFE at. h = 1,054.29 W/m².K for laminar flow and h = 17,026.3 W/m².K for turbulent flow.
- Figure 12. Experimental and predicted membrane distillation coefficients for GVHP, HVHP, and PTFE at $h = 21,432.4 \text{ W/m}^2.\text{K}$.

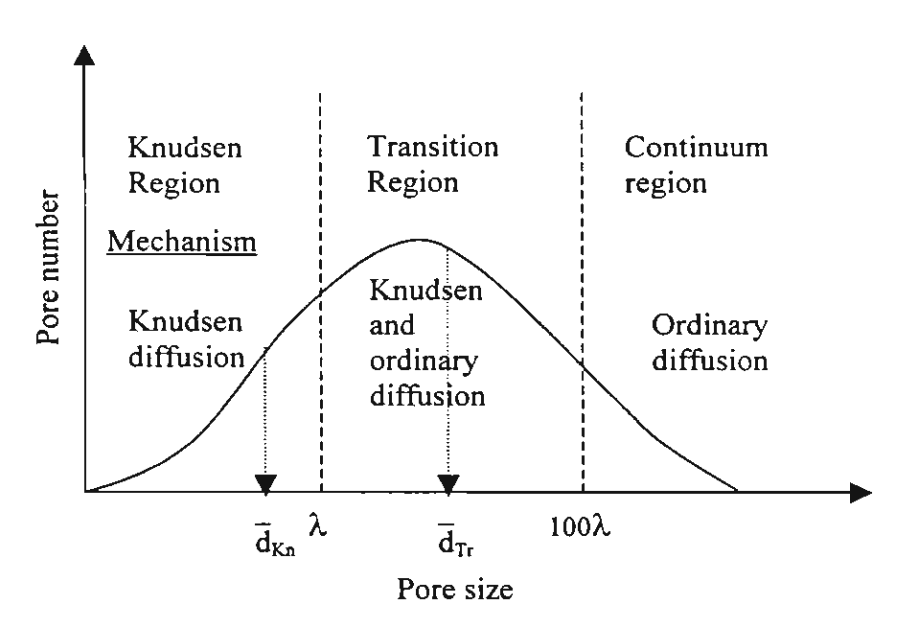


Fig.1. Regions and mechanisms of mass transport in the membrane with pore size distribution

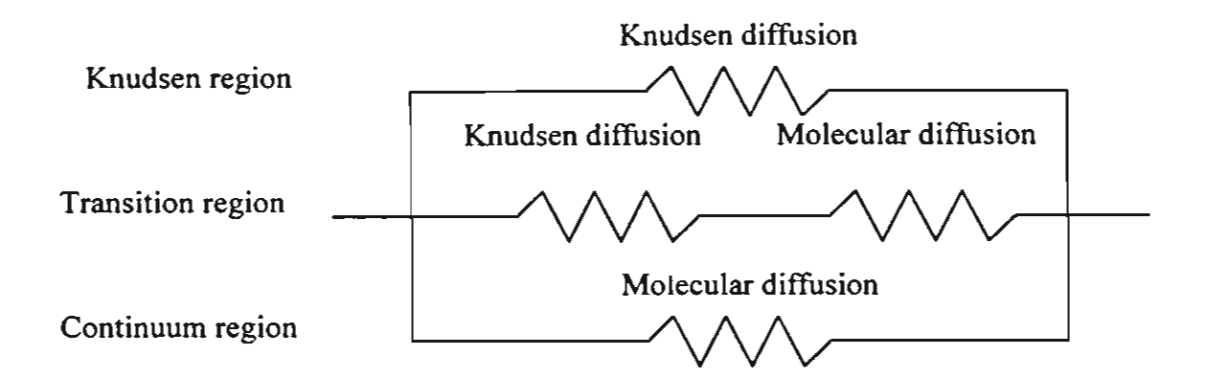
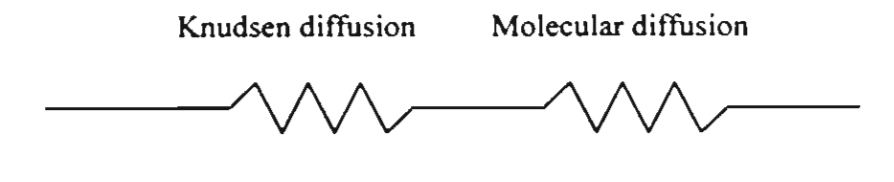
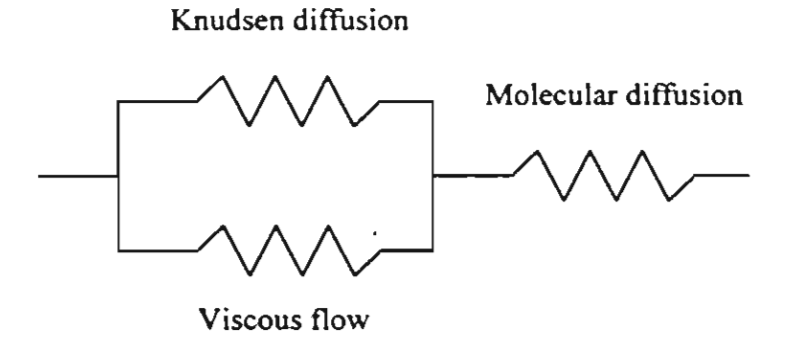


Fig.2. Electrical analogical circuit for multi pore size model



(a) Dusty Gas model



(b) Schofied's model

Fig.3. Electrical analogical circuit for single pore size model:

(a) Schofield's model, (b) Dusty Gas model

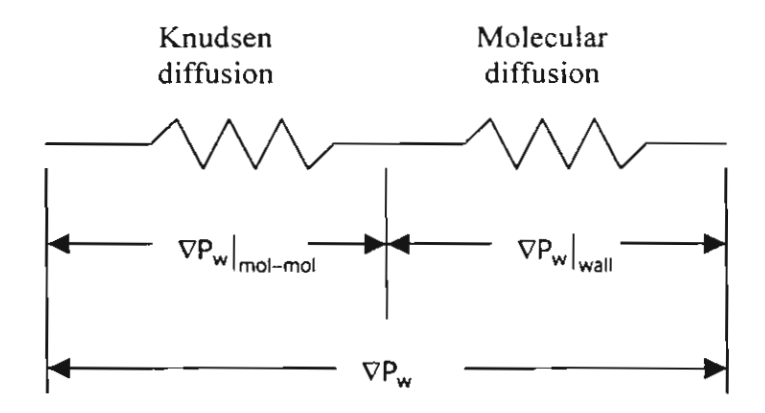


Fig. 4. Electrical analogue circuit for the transition region

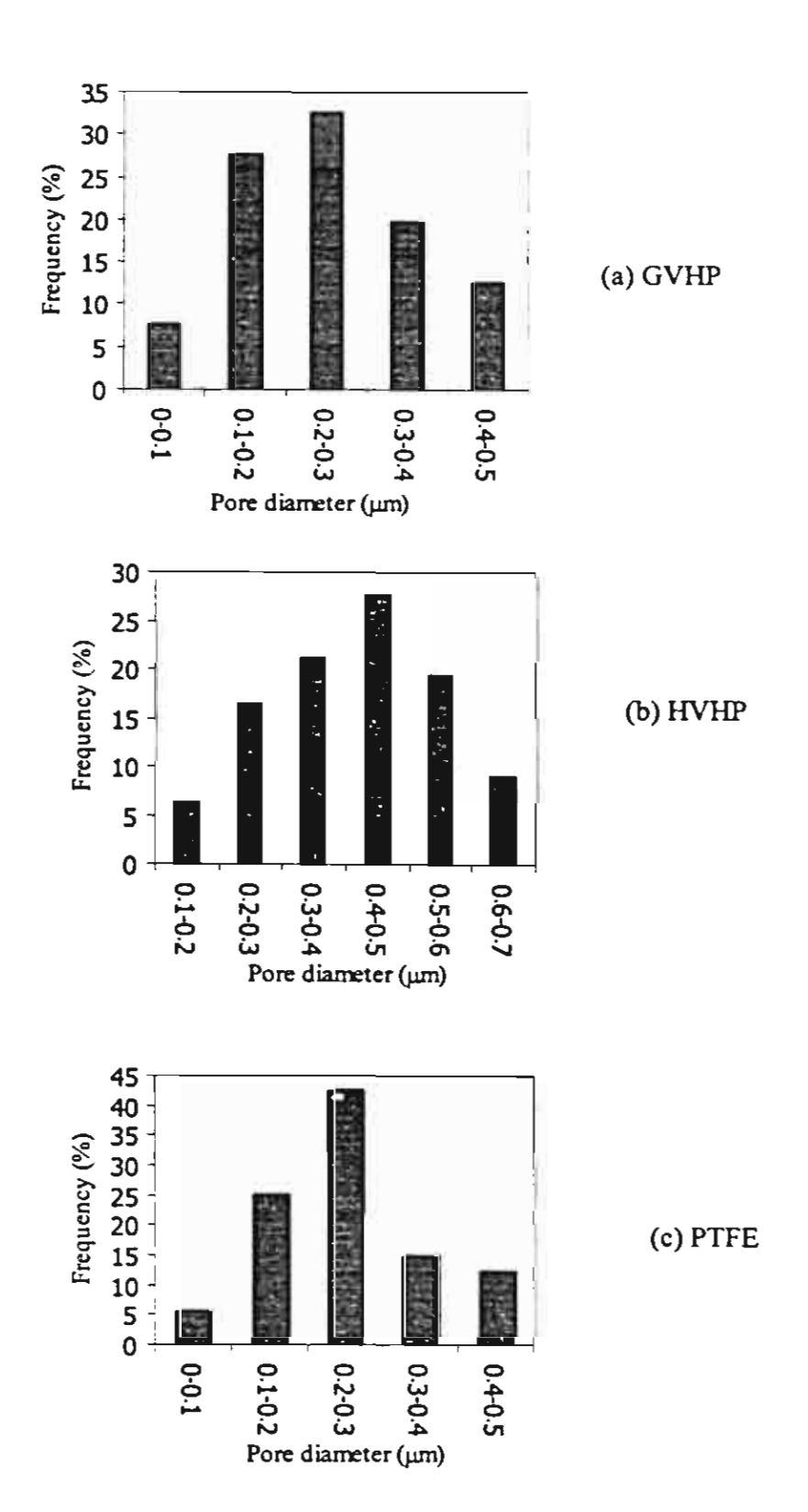


Fig.5. Pore size distributions: (a) GVHP, (b) HVHP, and (c) PTFE

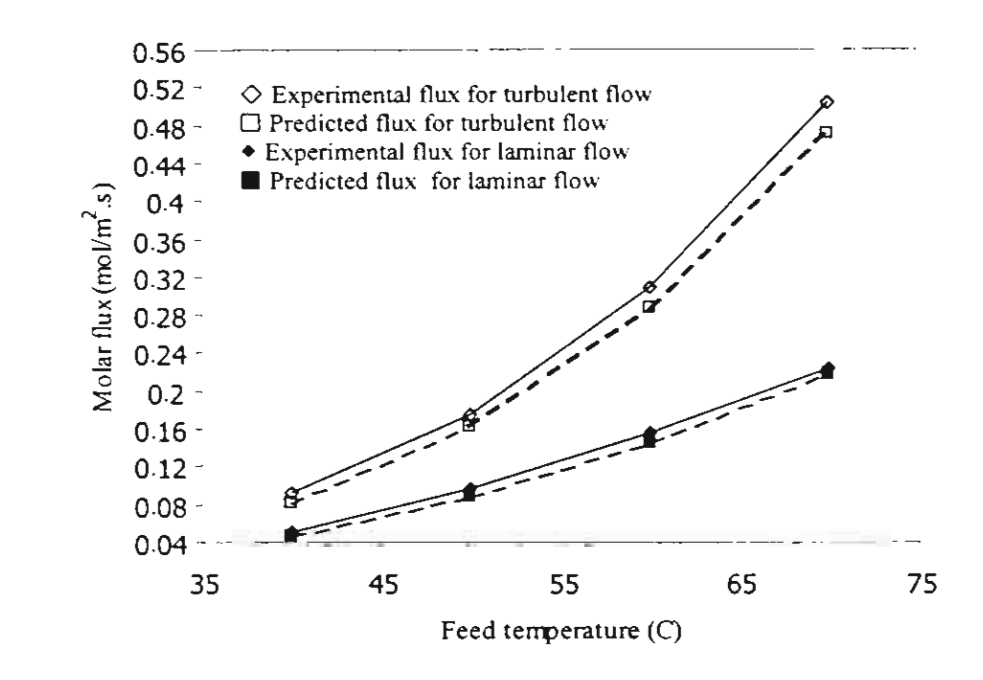


Figure 6. Experimental and predicted flux for GVHP at $h = 1,281.88 \text{ W/m}^2$.K for laminar flow and $h = 19,261 \text{ W/m}^2$.K for turbulent flow.

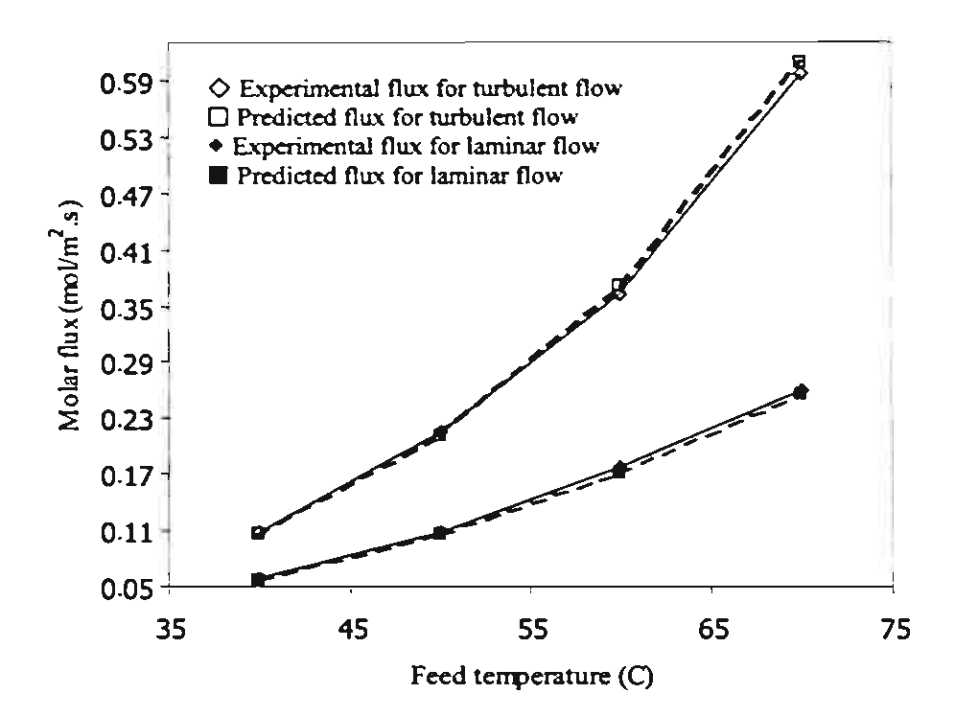


Figure 7. Experimental and predicted flux for HVHP at $h=1,281.88~W/m^2.K$ for laminar flow and $h=19,261~W/m^2.K$ for turbulent flow.

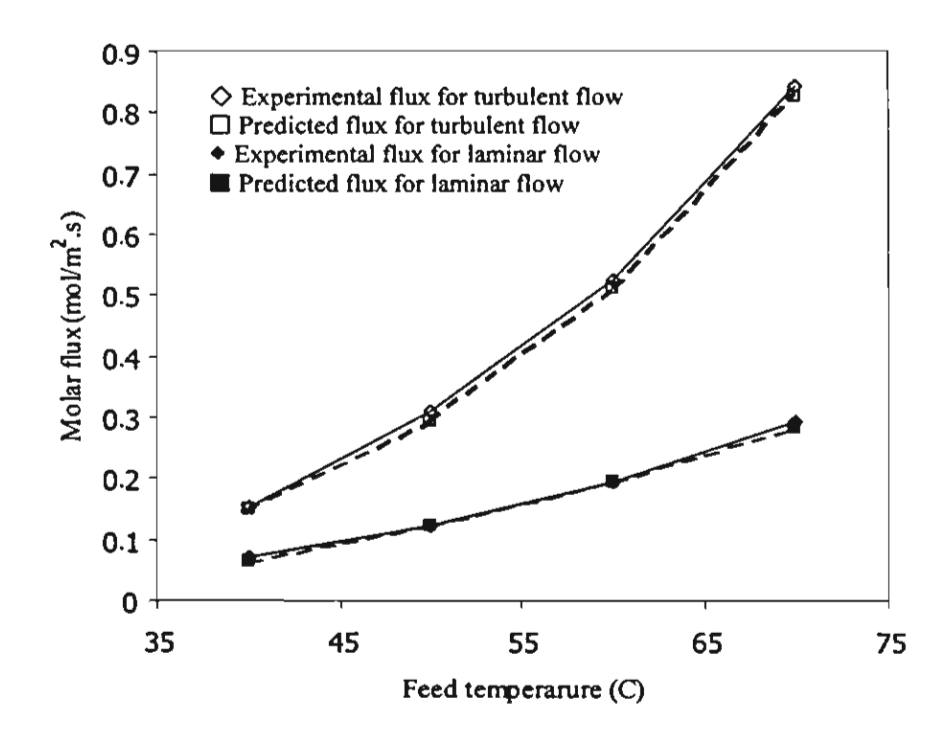


Figure 8. Experimental and predicted flux for PTFE at $h = 1,281.88 \text{ W/m}^2$.K for laminar flow and $h = 19,261 \text{ W/m}^2$.K for turbulent flow.

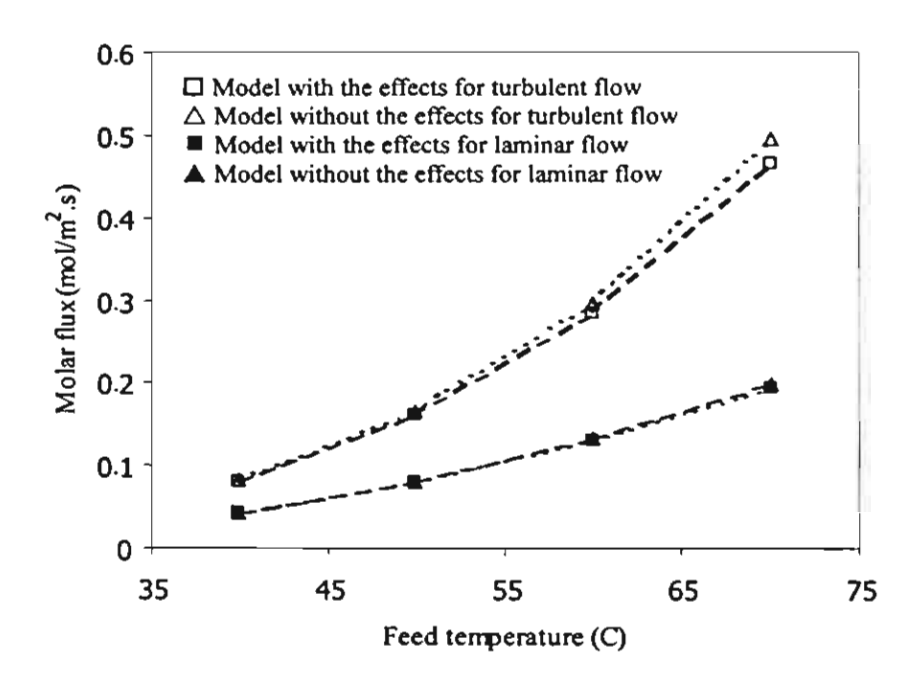


Figure 9. Predictions of molar fluxes by the models with and without the effect of pore size distribution and air flux for GVHP at. $h = 1,054.29 \text{ W/m}^2$.K for laminar flow and $h = 17,026.3 \text{ W/m}^2$.K for turbulent flow.

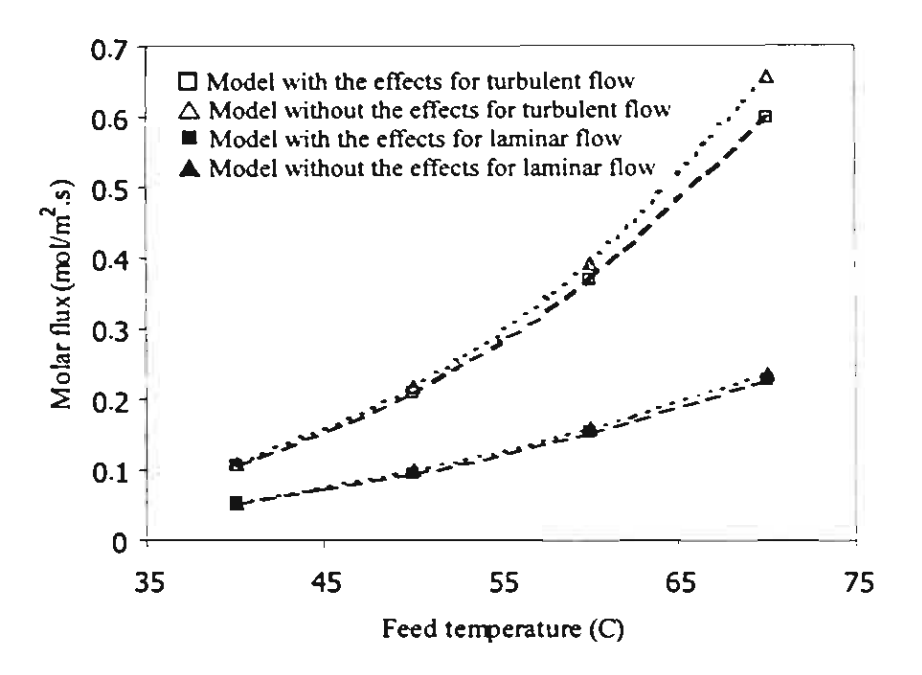
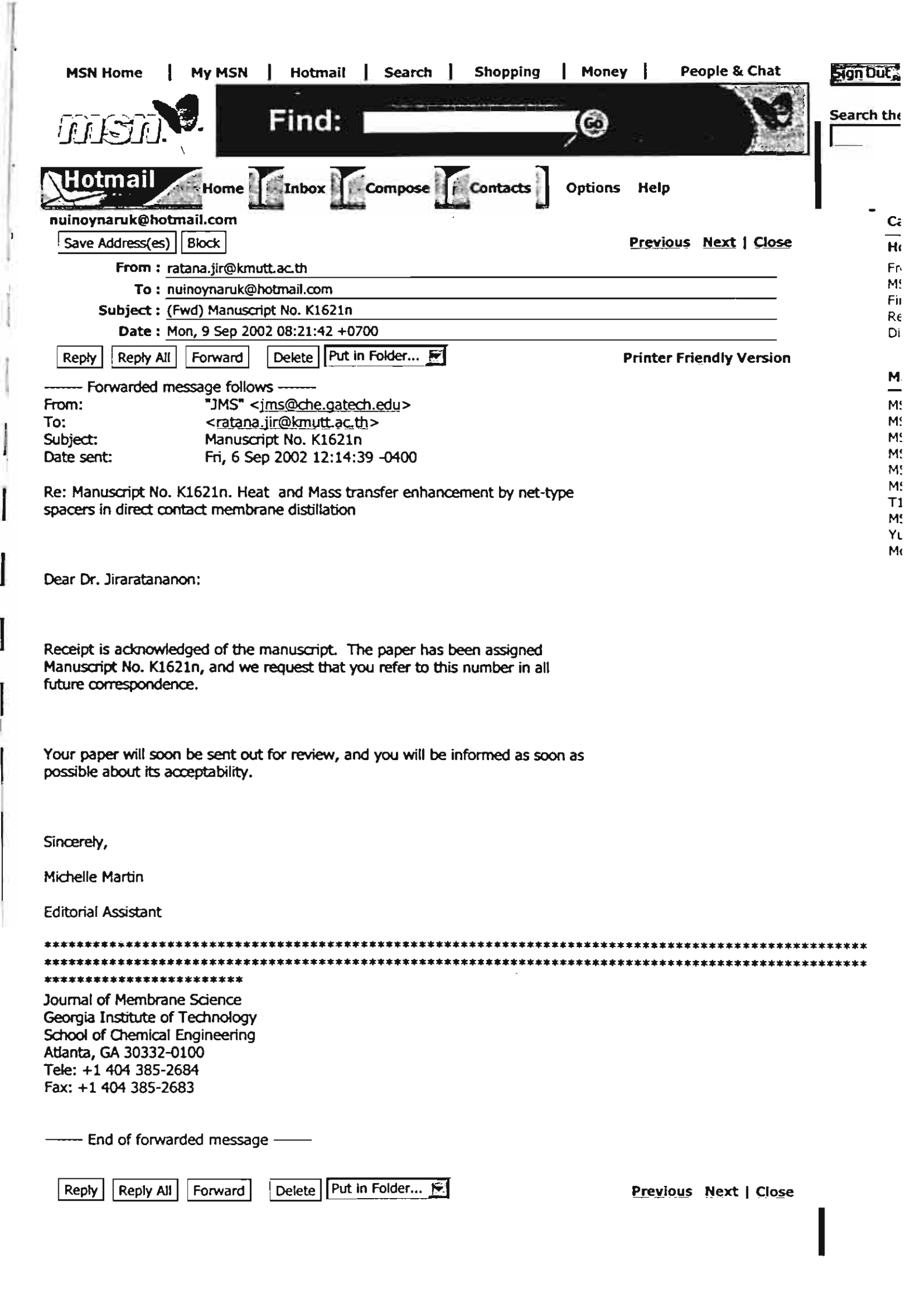


Figure 10. Predictions of molar fluxes by the models with and without the effect of pore size distribution and air flux for HVHP at. $h = 1,054.29 \text{ W/m}^2$.K for laminar flow and $h = 17,026.3 \text{ W/m}^2$.K for turbulent flow.



Heat and Mass transfer enhancement by net-type spacers in direct contact membrane

distillation

J. Phattaranawik a, R. Jiraratananon a, and A.G. Fane b

^a Department of Chemical Engineering, King Mongkut's University of Technology Thonburi, Toongkru,

Bangkok, Thailand, 10140

b UNESCO Centre for Membrane Science & Technology, School of Chemical Engineering and

Industrial Chemistry, The University of New South Wales, Sydney, NSW, Australia, 2052

Abstract

The study of heat and mass transfer enhancement in direct contact membrane distillation

(DCMD) by the net-type spacers was intended to develop the heat transfer correlation for the spacer-

filled channels. DCMD experiments performed with 20 spacers different in voidages and hydrodynamic

angles were used to determine the spacer performance in heat and mass transfer enhancement. The

effect of high mass transfer rates on heat and mass transfer coefficients was also investigated to explain

the experimental results compared with ultrafiltration (UF) with the spacers.

The results showed that spacers enhanced mass fluxes up to 60% and increased heat transfer

coefficients by approximately 2 times over the empty channels. The optimum spacer geometry was

found at the voidage and hydrodynamic angle of 0.6 and 90°, respectively. The heat transfer correlation

for spacer-filled channel was obtained. The analysis of high mass transfer rate convection showed that

the effect of high mass transfer rates on mass transfer coefficients was remarkable for ultrafiltration but

was insignificant for membrane distillation.

Keywords: Spacers; Membrane distillation; Flux enhancement; Temperature polarization

1. Introduction

Direct contact membrane distillation (DCMD) is the potential process for many applications such as desalination and fruit juice concentration. In DCMD, vapor-liquid equilibrium exists at the hot feed-membrane surface where the vapor is produced, driven by trans-membrane vapor pressure through porous hydrophobic membrane, and then condense into the cold permeate. The existence of temperature gradient in DCMD means that the membrane surface temperatures always contrast with bulk temperatures. This phenomenon, called temperature polarization, occurs in both feed and permeate channels and may cause a considerable loss of the thermal driving force leading to lower rates of mass transfer. The influence of this phenomenon is determined by temperature polarization coefficient (τ) [1] defined in Eq.(1).

$$\tau = \frac{\mathsf{T_1} - \mathsf{T_2}}{\mathsf{T_f} - \mathsf{T_p}} \tag{1}$$

where T_1 and T_2 are membrane surface temperatures on feed and permeate sides, and T_f and T_p are bulk temperatures of feed and permeate, respectively. Attempts to reduce the effect of temperature polarization have been made by improving the flow characteristic. Higher flow rates or turbulent flow conditions are usually used to decrease this effect. However, larger energy consumption by pumps is not appealing in economic viewpoint.

Recently, an alternative method to reduce the temperature polarization without increase of flow rates, but by using the spacers was proposed [2]. Similar to ultrafiltration (UF) and reverse osmosis (RO), spacers or turbulence promoter put into flow channels can promote wakes and eddy in laminar flow regime. Hence, heat and mass transfers are enhanced.

There are several types of spacers used in the membrane processes, for example net-type spacers [3] and zigzag spacers [4]. For DCMD spacers raised mass fluxes 30 - 60% [2,5], meanwhile 2-5 times of mass flux enhancement was reported in UF with spacers [4,6]. Furthermore, the mass transport in RO [7] and the pressure drop in UF [3,4] with the spacer-filled channels were best described by the turbulent flow correlation, although the Reynolds numbers were in the laminar flow region (Re < 2,000). Hence, the flow characteristic in spacer-filled channels was claimed to be turbulent [6,7] or upper transition regimes [4].

Phattaranawik et al [5] proposed the method to predict the mass flux enhancement by the spacers and reported large disagreement between experimental and calculated results. In addition, the heat transfer coefficients acquired by using analogy between mass transfer in UF and heat transfer in DCMD were relatively higher than those obtained from conventional heat transfer correlation. Likewise, the mass transfer coefficients determined experimentally from ultrafiltration process [4] seem to be much higher than those obtained from conventional mass transfer correlations. The reason for the unusually high transfer coefficients in UF has not been discussed in details.

From above discussions, it is evident that the flow condition in DCMD performed with spacers has not been clearly identified. The values of heat transfer coefficients for spacer-filled channels in DCMD have not been evaluated, and the validity of the analogy between mass transfer in UF and heat transfer in DCMD has not been proven. Therefore, it is the objective of this work to investigate the heat and mass transfer enhancement by net-type spacers in DCMD to propose the heat transfer correlation for spacer-filled channel. In addition, the experimental results will be compared to those from the UF performed with spacers so as to demonstrate the influence of high mass transfer rates in DCMD and in UF.

2. Theory

2.1 Heat and mass transfer for DCMD with and without spacers

The general relation of mass flux (J) and the driving force for DCMD is written by Eq. (2).

$$J = C (P_1 - P_2)$$
 (2)

The difference in vapor pressures at membrane surfaces $(P_1 - P_2)$ between feed and permeate sides is evaluated at the membrane surface temperatures $(T_1 \text{ and } T_2, \text{ as shown in Fig.1})$. The linear relation between mass flux and vapor pressure difference with constant slope was reported [8]. As a result, membrane distillation coefficients (C), determined from the slope, are dependent upon membrane properties, i.e. pore size, porosity, membrane thickness, and membrane material but are independent on temperatures and flow rates. Hence, MD coefficient remains unchanged when the spacers are put into flow channels.

~

Better flow characteristic arises from the presence of turbulence or eddy current induced by the spacers. As a result, the thickness of thermal boundary layer in spacer-filled channel (Δ^s_T) is less than that in empty channel (Δ_T) which allows the membrane surface temperatures to be closer to bulk temperatures, shown in Fig.1. Temperature polarization is thus reduced, and mass fluxes are enhanced due to larger difference of vapor pressures.

The expressions for the membrane surface temperatures was previously reported [8] as;

$$T_{1} = T_{f} - \frac{JH_{v}\left\{\frac{T_{1} + T_{2}}{2}\right\} + k_{m}\left(\frac{T_{1} - T_{2}}{\delta}\right)}{h_{f}}$$
(3)

$$T_{2} = T_{p} + \frac{JH_{v}\left\{\frac{T_{1} + T_{2}}{2}\right\} + k_{m}\left(\frac{T_{1} - T_{2}}{\delta}\right)}{h_{p}}$$
(4)

The second terms of right hand sides of Eqs.(3) and (4) are the temperature polarization terms. H_v is vapor enthalpy evaluated at average membrane temperature ($(T_1+T_2)/2$), k_m is membrane thermal conductivity, δ is the membrane thickness, and h_f and h_p are heat transfer coefficients for feed and permeate sides, respectively. For the spacer-filled channels, T_1 increases and T_2 decreases, but MD coefficient remains unchanged for the same membrane. Therefore, flux equations and membrane surface temperatures for spacer-filled channel are similar to those of empty channels, as the followings.

$$J^{s} = C\left(P_1^{s} - P_2^{s}\right) \tag{5}$$

$$T_{1}^{S} = T_{f} - \frac{J^{S}H_{V}\left\{\frac{T_{1}^{S} + T_{2}^{S}}{2}\right\} + k_{m}\left(\frac{T_{1}^{S} - T_{2}^{S}}{\delta}\right)}{h_{f}^{S}}$$
(6)

$$T_{2}^{s} = T_{p} - \frac{J^{s}H_{v}\left\{\frac{T_{1}^{s} + T_{2}^{s}}{2}\right\} + k_{m}\left(\frac{T_{1}^{s} - T_{2}^{s}}{\delta}\right)}{h_{p}^{s}}$$

$$(7)$$

Eqs.(5) - (7) can be used to calculate the heat transfer coefficients for spacer-filled channels with the procedure shown in section 4.

2.2 Heat transfer correlation for spacer-filled channel

Da Costa et al [3] obtained mass transfer coefficient for spacer-filled channels which can be transformed to the heat transfer correlation by assuming an analogy between heat and mass transfer [5], expressed as;

$$Nu^{s} = 0.664k_{dc} \left(Re^{s} \right)^{0.5} Pr^{0.33} \left(\frac{2d_{h}^{s}}{l_{m}} \right)^{0.5}$$
 (8)

where
$$k_{dc} = 1.654 \left(\frac{d_f}{H}\right)^{-0.039} \epsilon^{0.75} \left(\sin\left(\frac{\theta}{2}\right)\right)^{0.086}$$

The definition of Reynolds numbers for spacer-filled channel (Re⁵) is expressed by Eq.(9).

$$Re^{s} = \frac{u^{s}d_{h}^{s}}{v} \tag{9}$$

The velocity of fluid passing through the spacers (u^s) is increased since spacers provide lower cross-section area, which is calculated by Eq.(10).

$$u^{s} = \frac{u_{empty}}{\varepsilon}$$
 (10)

where spacer voidge (ϵ) is the void volume available in spacer-filled channels, calculated by Eq.(11). [3].

$$\varepsilon = 1 - \frac{\pi d_f^2}{2l_m h_{sp} \sin \theta} \tag{11}$$

where hsp is spacer thickness, and df is filament diameter.

Hydraulic diameter for spacer-filled (dsh) [7] is defined in Eq.(12),.

$$d_{h}^{s} = \frac{4\epsilon}{(2/h_{sp}) + (1-\epsilon)(4/d_{f})}$$
 (12)

A simple relationship between Nu^s (the Nusselt number for spacer-filled channel) and Nu_{laminar} (the Nusselt number for laminar flow in empty channel) from Eq.(8) is

$$Nu^{s} = \alpha^{s} Nu_{laminar}$$
 (13)

where α^s is the spacer factor depending on spacer geometry and describes the spacer efficiency.

Eq.(13) can be used to correlate the heat transfer correlation for spacer-filled channels from experimental results.

2.3 High mass transfer rate convection [9,10]

The heat and mass transfer analysis by boundary layer theory is generally based on the assumption that the rates of mass transfer across the boundary layers are so small that they do not affect the velocity, temperature, and concentration profiles. The result achieved from that assumption shows that Nusselt or Sherwood number is a function of Reynolds and Prandlt or Schmidt number. However, when the rates of mass transfer are high enough that they can distort the velocity, temperature, and concentration profiles, friction factors, convective heat transfer coefficients and mass transfer coefficients become dependent upon the rates of mass transfer [9,10]. Theoretically, high mass transfer rates can either increase or decrease the transfer coefficients. Only heat and mass transfer coefficients are focused in this work.

The basic equations for the heat and mass transfer coefficients are expressed by Eqs.(14) and (15).

$$h = -k \frac{\left(\frac{dT}{dy}\right)|_{s}}{T_{b} - T_{s}}$$
 (14)

$$K = -D \frac{\left(\frac{dC}{dy} \right)|_{s}}{C_{b} - C_{s}}$$
 (15)

Here, T and C are temperature and concentration at various positions along the distant from the surface; b and s refer to bulk and surface positions. K and h are mass and heat transfer coefficients, and k and D are thermal conductivity and diffusivity, respectively. The above expressions state that heat and mass transfer coefficients increase with the slopes of temperature and concentration profiles at the surface. For low mass transfer rates, the temperature and concentration profiles from the laminar boundary layer theory are in algebraic equations below [11].

$$\frac{\mathsf{T} - \mathsf{T}_{\mathsf{b}}}{\mathsf{T}_{\mathsf{s}} - \mathsf{T}_{\mathsf{b}}} = 1 - \frac{3}{2} \frac{\mathsf{y}}{\Delta_{\mathsf{T}}} + \frac{1}{2} \left(\frac{\mathsf{y}}{\Delta_{\mathsf{T}}} \right)^{3} \tag{16}$$

$$\frac{C - C_o}{C_s - C_o} = 1 - \frac{3}{2} \frac{y}{\Delta_C} + \frac{1}{2} \left(\frac{y}{\Delta_C} \right)^3 \tag{17}$$

 Δ_{T} and Δ_{C} are thermal and concentration boundary layer thicknesses, and y is the distance from the surface. Since both Δ_{T} and Δ_{C} are the inverse function of Reynolds number, the boundary layer thickness decreases with increasing flow rate. As a result, heat and mass transfer coefficients increase due to the steeper slopes of the profiles, but the profile expressions do not change. The heat and mass transfer coefficients for low mass transfer rate condition (h_L and K_L) are obtained by substituting Eqs.(16) and (17) into Eqs.(14) and (15), respectively.

The analysis of high mass transfer rates is based on the energy and mass balances in the boundary layers that are represented by Eq. (18) for heat transfer and Eq.(19) for mass transfer [9,10].

$$\frac{d}{dy}\left(JC_{p}T - k\frac{dT}{dy}\right) = 0 {(18)}$$

$$\frac{d}{dy}\left(J_{V}C - D\frac{dC}{dy}\right) = 0 \tag{19}$$

By integration twice with the boundary conditions y = 0 (at surface), $T = T_s$ or $C = C_s$ and $y = \Delta_T$ or Δ_C , $T = T_b$ or $C = C_b$, the temperature and concentration profiles under the influence of high mass transfer rates are:

$$\frac{\mathsf{T} - \mathsf{T}_{\mathsf{s}}}{\mathsf{T}_{\mathsf{b}} - \mathsf{T}_{\mathsf{s}}} = \frac{\exp(\mathsf{JC}_{\mathsf{p}}\mathsf{y}/\mathsf{k}) - 1}{\exp(\mathsf{JC}_{\mathsf{p}}\Delta_{\mathsf{T}}/\mathsf{k}) - 1} \tag{20}$$

$$\frac{C - C_s}{C_b - C_s} = \frac{\exp(J_V y / D) - 1}{\exp(J_V \Delta_C / D) - 1}$$
 (21)

Comparison of Eqs.(16) and (17) with Eqs.(20) and (21) shows that the profiles for low mass transfer rates are in algebraic forms, whereas the profiles under high mass transfer rate condition, Eqs. (20) and (21), are expressed in the exponential forms. By Eqs.(14) and (15), heat and mass transfer coefficients for high mass transfer rates (h_H and K_H) are:

$$h_{H} = \frac{JC_{p}}{\exp(JC_{p}\Delta_{T}/k) - 1}$$
 (22)

$$K_{H} = \frac{J}{\exp(J_{V}\Delta_{C}/D) - 1}$$
 (23)

The limits of Eqs.(22) and (23) as flux approaches zero (low mass transfer rates), are [9,10];

$$\lim_{J \to 0} h_{H} = \frac{k}{\Delta_{T}} = h_{L} \tag{24}$$

$$\lim_{J \to 0} K_{H} = \frac{D}{\Delta_{C}} = K_{L} \tag{25}$$

Combination of Eq.(22) and Eq.(24), and of Eq.(23) and Eq.(25) yield the ratio of the transfer coefficients under high mass transfer rates to those under low mass transfer rates (ψ_T and ψ_C), expressed by Eqs.(26) and (27).

$$\psi_{T} = \frac{h_{H}}{h_{L}} = \frac{JC_{p} / h_{L}}{\exp(JC_{p} / h_{L}) - 1}$$
 (26)

$$\psi_{C} = \frac{K_{H}}{K_{L}} = \frac{J_{V}/K_{L}}{\exp(J_{V}/K_{L}) - 1}$$
 (27)

 ψ_T and ψ_C are correction factors which rectify the heat and mass transfer coefficients calculated from the conventional Nusselt and Sherwood correlations when the effect of high mass transfer rates on heat and mass transfer coefficients are regarded.

As mentioned previously, high mass transfer rates can increase or reduce the transfer coefficients due to change of the slopes of the profiles (see Eqs.(14) and (15)). In the case that high mass transfer rates increase the transfer coefficients (ψ_T and $\psi_C > 1$), there is the increase of the slopes (of the profiles) and of the differences in temperatures or concentrations between bulk and surface. Mathematically, the sign of mass flux in Eqs.(26) and (27) is minus for this situation. Based on theory of high mass transfer rate convection described in [9,10], if there is removal of mass from the system [9] or suction effect [10], the negative sign of flux is employed. On the other hand, the positive sign of mass flux is used in in Eqs.(26) and (27) when the mass transfer lowers the transfer coefficients. For the later case, there is the addition of mass into the system [9] or blowing effect [10]. Mass transfer reduces the slopes of the profiles and also the temperature (or concentration) differences between the membrane surface and bulk.

For MD, the influence of high mass transfer rates on heat transfer coefficient in hot feed channel is demonstrated in Fig.2. The removal of energy due to mass fluxes lessens the membrane surface temperature, and the slope of the temperature profile becomes steeper. Thus, the minus sign of

7

the mass fluxes is used to evaluate the effect of high mass transfer rates. From Eq. (26), the minimum mass flux $(J_{min,T})$ that begins to affect the heat transfer coefficient can be estimated. ψ_T approaches unity when the ratio of JC_p to h_L is equal to 0.15. Hence, $J_{min,T}$ can be expressed by;

$$J_{\min,T} = \frac{0.15h_L}{C_p} \tag{28}$$

The typical value of C_p for water is 4,000 J/kg.K. By Eq.(28), $J_{min,T}$ is 0.0375 kg/m².s at $h_L = 1000$ W/m².K (laminar flow) and is 0.375 kg/m².s at $h_L = 10,000$ W/m².K (turbulent flow). From the calculations, $J_{min,T}$ is much higher than the maximum mass flux reported in [12 – 15]. Therefore, the effect of high mass transfer rates on heat transfer coefficient is theoretically negligible.

High mass transfer rates in pressure-driven membrane processes such as reverse osmosis (RO) and ultrafiltration (UF) can result in the large difference in concentration between bulk and surface and steepen the slope of the concentration profile (see Fig.3). There is the removal of mass from the feed side. Therefore, the high mass transfer rates enhance mass transfer coefficients ($K_H > K_L$) for UF and RO. As a result, the mass transfer coefficients evaluated from the convectional mass transfer correlation are always lower than those obtained from the UF experiments due to the effect of high rates of mass transfer. Similar to Eq.(28), the minimum mass flux that begin to affect mass transfer coefficient ($J_{min,C}$) is expressed below.

$$J_{\text{min.C}} = 0.15K_{L} \tag{29}$$

The typical value of mass transfer coefficients for UF is 1.5×10^{-6} m/s (at Re = 1,000) [4,6], and by Eq. (29) the $J_{mun,C}$ is equal to 2.25×10^{-7} m³/m².s which is much lower than the typical fluxes reported in UF [4,6], i.e. 1.4×10^{-5} m³/m².s. Therefore, the mass transfer coefficient can be affected by the high mass transfer rates.

3. Experimental

The DCMD experiments were carried out with empty channels under laminar flow conditions and with 20 spacers different in hydrodynamic angles (θ) and voidages (ϵ) as summarized in Table 1. All spacers were fabricated from cylindrical polypropylene rods with a diameter of 3 mm. The fabrication procedure was mentioned in our previous work [8]. The average error of the fabrication was

. ..

less than 8 % (see Table 1). In all experiments the spacers exactly fitted in the flow channels in order to minimize the leak or by-pass flow that can diminish the spacer performance.

Table 1. Spacer characteristics

Spacer Number	Hydrodynamic angle (θ)	Voidage (ε)	Mesh size (l _m) (mm)	Hydraulic diameter (d _{b.s}) (mm)
1		0.39±8%	7.0±8%	1.3±8%
2		0.525±7%	9.0±8%	2.1±6%
3	45±7%	0.612±8%	11.0±8%	2.7±5%
4		0.695±7%	14.0±7%	3.5±5%
5		0.797±6%	21.0±7%	4.8±4%
6		0.363±8%	5.0±8%	1.2±8%
7	70±7%	0.468±7%	6.0±8%	1.7±6%
8		0.596±6%	8.0±7%	2.6±7%
9		0.709±6%	11.0±8%	3.7±5%
10		0.799±6%	16.0±7%	4.8±5%
11		0.4±8%	5.0±8%	1.4±8%
12		0.5±7%	$6.0\pm8\%$	1.9±7%
13	90±5%	0.623±8%	8.0±7%	2.8±5%
14		0.697±7%	10.0±7%	3.5±4%
15		0.799±5%	15.0±6%	4.8±4%
16		0.42±8%	6.0±8%	1.5±7%
17		0.5±7%	7.0±8%	1.9±7%
18	120±6%	0.613±5%	9.0±7%	2.7±7%
19		0.709±6%	12.0±8%	3.7±7%
20		0.806±4%	18.0±6%	5.0±7%

Note: Spacer thickness (H) = $5 \pm 8\%$ mm.

Pure water was used as feed and permeate solutions. The bulk feed temperatures ranging from 50 to 70 °C were employed with constant permeate temperature at 20 °C. The feed and permeate streams arranged in parallel flow were driven by the peristaltic pumps into the top of the module. The hot water bath and the cooler with digital temperature controllers were used to maintain the feed and permeate solutions at the required temperatures.

The PVDF membranes used are namely, GVHP and HVHP provided by Millipore. Their properties are reported in Table 2 [16,8]. The membrane module with square channels machined from

polymethylmethacrylate (PMMA) was held in vertical position. The channel dimensions are 50 mm for width, 100 mm for length (L), and 5 mm for height with the effective membrane area of 5×10^{-3} m². The hydraulic diameter of the channel (d_h) is 9.09×10^{-3} m.

Table 2. Membrane properties [16,8]

No.	Membrane	Pore size (µm)	Thickness (µm)	Porosity (ε)	k _m (W/m.K)	MD coefficient (kg/m².s.Pa)
l	GVHP	0.22	126	0.62	0.041	3.459×10 ⁻⁷
2	HVHP	0.45	116	0.66	0.040	4.169×10 ⁻⁷

In this work, the heat transfer coefficients for spacer-filled channels for each side were kept equal $(h_f^s = h_p^s)$ by adjusting the flow rates of each flow channel. It is valid to assume that if the heat transfer coefficients of empty channels of both sides are the same $(h_f = h_p)$, the heat transfer coefficients for spacer-filled channels of both flow channels at same flow rates should be equal. (This assumption was used for the calculation in section 4.) The required flow rates were then calculated from the laminar flow heat transfer correlation previously shown [8], Eq.(30).

$$Nu_{la\,min\,ar} = 4.36 + \frac{0.036\,Re\,Pr(d_h\,/L)}{1 + 0.0011(Re\,Pr(d_h\,/L))^{0.8}}$$
(30)

The experimental conditions for empty and the spacer-filled channels were shown in Table 3. The experimental conditions for spacer-filled channels were similar to those for empty channels except that the spacers were filled into the flow channels. Furthermore, the mass fluxes for both channel conditions were measured so as to assess the spacer performance.

Table 3. Experimental conditions

Temperature (°C)		Flow rate (m ³ .s ⁻¹)		Reynolds number of empty channel		Heat transfer coefficient for empty
Feed	Permeate	Feed	Permeate	Feed	Permeate	channel (W.m ⁻² .K ⁻¹)
50	20	1.58×10 ⁻⁵	1.58×10 ⁻⁵	1,039.2	571.1	
60	20	1.58×10 ⁻⁵	1.58×10 ⁻⁵	1,148.2	571.1	1,054.3
70	20	1.50×10 ⁻⁵	1.58×10 ⁻⁵	1,320.6	571.1	
50	20	2.08×10 ⁻⁵	2.1×10 ⁻⁵	1,367.3	761.5	
60	20	2.08×10 ⁻⁵	2.1×10^{-5}	1,594.7	761.5	1,281.9
70	20	2.08×10 ⁻⁵	2.1×10 ⁻⁵	1,834.1	761.5	
50	20	2.50×10 ⁻⁵	2.63×10 ⁻⁵	1,640.8	951.9	
60	20	2.50×10 ⁻⁵	2.63×10 ⁻⁵	1,913.7	951.9	1,498.9
70	20	2.42×10 ⁻⁵	2.63×10 ⁻⁵	2,127.6	951.9	

4. The procedure for evaluating heat transfer coefficients of spacer-filled channels.

Heat transfer coefficients for spacer-filled channels were evaluated from heat and mass transfer expressions for spacer-filled channel, Eqs.(5)-(7). The data required for the calculations are the mass fluxes for spacer-filled channels (J^s), the membrane properties, thermodynamic properties for liquid and vapor, and the bulk temperatures. The procedure of calculating the heat transfer coefficients is comprised of two loops, i.e. inner and outer loops, displayed in Fig.4. The inner loop is used for calculating the membrane surface temperatures from the assumed heat transfer coefficients of spacer-filled channels. The outer loop is used to examine the assumed heat transfer coefficients by comparison between the calculated and the experimental MD coefficients.

In the inner loop, the membrane surface temperatures (T_1 and T_2) are first evaluated by Eqs.(31) and (32).

$$T_{1,N=0}^{s} = T_{f} - \frac{2J^{s}H_{v}\left\{\frac{T_{f} + T_{p}}{2}\right\}}{h_{f}^{s}}$$
 (31)

٠.

 $T_{2,N=0}^{s} = T_{p} + \frac{2J^{s}H_{v}\left\{\frac{T_{f} + T_{p}}{2}\right\}}{h_{p}^{s}}$ (32)

The membrane temperature is approximated by average bulk temperature. N refers to the number of reiteration and N=0 for the first trial. The presence of number 2 in Eqs.(31) and (32) refer to the equal significance of heat conduction (q_c) and the heat transfer due to vapor flow (q_v) [8]. T₁ and T₂ from the first step are used in Eqs.(33) and (34) where the terms q_c and q_v are included.

$$T_{1,N+1}^{s} = T_{f} - \frac{J^{s}H_{v}\left\{\frac{T_{1,N}^{s} + T_{2,N}^{s}}{2}\right\} + k_{m}\left(\frac{T_{1,N}^{s} - T_{2,N}^{s}}{\delta}\right)}{h_{f}^{s}}$$
(33)

$$T_{2,N+1}^{s} = T_{p} + \frac{J^{s}H_{v}\left\{\frac{T_{1,N}^{s} + T_{2,N}^{s}}{2}\right\} + k_{m}\left(\frac{T_{1,N}^{s} - T_{2,N}^{s}}{\delta}\right)}{h_{p}^{s}}$$
(34)

 T_{N+1} is determined from T_N by the expressions Eqs.(33) and (34). The calculations were repeated until the difference between T_N and T_{N+1} is less than 0.1%. The trans-membrane vapor pressure $(P_1 - P_2)$ was evaluated at T_1 and T_2 and was then used to evaluate the MD coefficient by Eq.(5).

In the outer loop, the MD coefficient is compared with experimental MD coefficient (C_{exp}). The heat transfer coefficient will be assumed again if the calculated MD coefficient differs from the measured MD coefficient over 0.1%. The measured MD coefficient for each membrane are available in Table 2.

The calculated heat transfer coefficients for spacer-filled channels were correlated by multiple linear regressions to obtain the heat transfer correlation for spacer-filled channels. Da Costa et al. [3] suggested the following form of spacer factor (α ^s).

$$\alpha^{s} = a \left(\frac{d_{f}}{H}\right)^{-0.039} f(\theta).f(\epsilon)$$
 (35)

 $f(\theta)$ and $f(\epsilon)$ are the relationship between spacer factor and hydrodynamic angle and spacer voidage, determined from the experiments. When spacer-filled channels are employed, Nu_{lamunar} needs minor adjustment. Re and d_h in Eq.(30) were replaced by Re^s and d_h^s , respectively. In addition, channel length (L) was employed in the correlation instead of the mesh size (l_m) [3] because the channel flow

ب ء

was found in spacer-filled channels and the bulk fluid flow did not follow a zigzag path as claimed in [17]. The effect of all spacer geometries is included in spacer factor (α^{s}).

5. Results and discussions

5.1 The enhancement of mass and heat transfer.

Mass fluxes are shown in Figs.5. At spacer voidage of approximately 0.6, the mass flux enhancements were 30 – 62 % for the angle of 90°, 29 – 58 % for the angle of 70°, 23 – 48 % for the angle of 120°, and 11 – 36 % for the angle of 45°. Similar results were reported for UF [3]. The optimum hydrodynamic angle obtained was therefore at 90°. Fig. 6 depicts the effect of spacer voidage on the enhancement. The voidage of approximately 0.6 provided highest increase in mass fluxes for all hydrodynamic angles. The effect of flow rates on flux enhancement (spacer efficiency) is displayed in Fig.7. Lower flux enhancements were obtained with higher flow rates because the better heat transfer in empty channels was obtained at higher flow rates. Thus, the role of spacers on heat and mass transfer improvement fades away at higher flow rate where turbulent flow is approached. Similarly, the influence of spacers on flux improvement becomes more evident at higher temperatures (Fig.8) where temperature polarization coefficients were low. Therefore, spacers play the important role under the operating conditions that provide poor heat transfer or high temperature polarization (low temperature polarization coefficient). Similar situation was also found in UF process [18]. Flux enhancement in UF process was observed more evidently in the high concentration polarization situation.

The heat transfer in feed and permeate streams control and also limits mass fluxes in MD. On the other hand, most of UF processes are controlled by the mass transfer resistance due to concentration polarization and fouling that are reduced by better fluid management or by spacers.

5.2 The heat transfer correlation

The heat transfer coefficients for each spacer and experimental condition were obtained from the procedures described in section 3.1. Figs. 9 and 10 display the calculated heat transfer coefficients of spacer-filled channels at maximum and minimum flow rates, respectively. Similar results were found for medium flow rate. As shown in Fig.10, the maximum heat transfer coefficient obtained by this

study was 3,577.4 W/m².K or 2.4 fold over empty channels for the equivalent condition. The heat transfer coefficients obtained were correlated with spacer characteristics by the multiple linear regressions. The best-fitted curve (Eq.(36)) was achieved with the squared correction coefficient 0.985.

$$Nu^{s} = \alpha^{s} \left[4.36 + \frac{0.036 \, \text{Re}^{s} \, \text{Pr}(d_{h}^{s} / L)}{1 + 0.0011 (\text{Re}^{s} \, \text{Pr}(d_{h}^{s} / L))^{0.8}} \right]$$
where
$$\alpha^{s} = 1.88 \left(\frac{d_{f}}{H} \right)^{-0.039} (\sin(\theta))^{1.33} \exp \left(-4.05 \left(\left[\ln \left(\frac{\epsilon}{\epsilon_{m}} \right) \right]^{2} \right) \right)$$

$$(\epsilon_{m} = 0.6 \text{ for this work})$$
(36)

The advantage of Eq.(36) over Eq.(8) is that the optimum spacer geometry can be directly observed from the expression of α^s . Fig. 11 shows that temperature polarization coefficients (τ^s) for spacer-filled channels (obtained from the calculation in Fig. 4). were increased by 30-40%. For turbulent flow (Re >10,000) and laminar flow (Re < 2,100), the typical heat transfer coefficients are approximately 10,000 and 1,500 W/m².K, respectively. Therefore, the flow characteristic in spacer-filled channels for MD is likely to be the lower transition regime because the calculated heat transfer coefficient for spacer-filled channels is only 3,577.4 W/m².K (maximum).

5.3 The effect of high mass transfer rates in UF processes.

The reason for unusually high mass transfer coefficients in UF may be illustrated by theory of high mass transfer rate convection. The effect of high mass transfer rates on mass transfer coefficients in UF processes can be illustrated by the comparison between mass transfer coefficients calculated from the conventional Sherwood correlation for laminar flow, Eq.(37), and the correlation obtained from UF experiments, Eq.(38), summarized in Table 4 and shown in Fig. 12. The mass transfer coefficients for the UF process included the effect of high mass transfer rates and were higher than those calculated by the conventional mass transfer correlation for laminar flow by approximately 5 folds. Thus, the effect of high mass transfer rates can be regarded as the possible reasons for unusually high mass transfer coefficient in UF process.

The influence of high mass transfer rates in UF was also assessed by Eq. (27), displayed in Fig.13. The comparison in Fig.13 reveals that the presence of high mass transfer rates increases the

mass transfer coefficients (upper line) by 12 times. However, the high mass transfer rate theory over predicted the increase of mass transfer coefficients because only 4 times increase was found from the experiment (lower line).

Table 4. Mass transfer correlations for empty channels and laminar flow condition.

Туре	Correlation	Equation	References
Laminar flow	Sh = 0.664 Re ^{0.5} Sc ^{0.33} $\left(\frac{d_h}{L}\right)^{0.5}$	(37)	[19]
UF with empty channel	Sh = 2.69 Re ^{0.44} Sc ^{0.33} $\left(\frac{d_h}{L}\right)^{0.33}$	(38)	[4]
	(at $c = 10 \text{ g/L for dextran}$)		

Likewise, the friction factors which are used to calculate the pressure drop in UF can be increased by the effect of high mass transfer rates for several folds. The relationship between pressure drop and (flow rate)^{1.7 to 1.8} [4,6] was found and led to the conclusion of the presence of turbulent flow in spacer-filled channels, although Reynolds numbers were lower than 2,100 [4,6].

Because of the high mass transfer effect in UF process, the heat transfer correlation for spacer-filled channels achieved by the analogy (Eq.(9)) was also expected to provide very high heat transfer coefficients. The comparisons between Eq.(9) and the heat transfer correlation from this work is shown in Fig.14. The heat transfer coefficients from the analogy were approximately 2 times higher than those obtained by this work.

Therefore, the effect of high mass transfer rates can be a possible reason for high values of mass transfer coefficients and friction factors and for why the pressure drop and mass transfer in UF with spacers was best described by the turbulent flow correlation [3] at low Reynolds numbers (Re < 2,100).

6. Conclusions

The performance of the spacers on the mass flux enhancement in DCMD was determined. The maximum flux enhancement was at 60% with optimum geometry at hydrodynamic angle of 90° and voidage of 0.6. The heat transfer coefficients were evaluated and correlated with the spacer geometries the angle and voidage. The correlation obtained can be used to evaluate heat transfer coefficients for any spacer geometry. The increase of temperature polarization coefficients after the spacers are filled into the channels meant that there was the improvement of heat transfer in the flow channels. In addition, the effect of the spacers on mass flux enhancement became more important for the higher polarization situation (poor heat transfer). In this work the net-type spacers possibly operated in the lower transition regime.

The comparison of the mass transfer correlations showed that the influence of high mass transfer rates on mass transfer coefficients in UF process was considerable. On the other hand, such effect on heat transfer coefficients in DCMD was negligible. The analogy between heat transfer in MD and mass transfer in UF may be invalid because of the presence of high mass transfer rates in UF processes. Moreover, the difference of fluid flow in ultrafiltration and membrane distillation can be explained by the theory of high mass transfer rate convection.

However, this work provided only the preliminary results in the effect of high mass transfer rates on the transfer coefficients in UF and DCMD. Such effect may considerably raise the mass transfer coefficient and friction factor due to a change of the velocity and concentration profiles. More accurate simulation results from CFD [17,20] to visualize the fluid flow in UF with spacer-filled channels can be achieved if theory of high mass transfer rate convection is included. The effect of high mass transfer rates can be a new topic for membrane research.

Acknowledgements

The authors would like to thank the Thailand Research Fund and the Royal Golden Jubilee Ph.D Program for financial support. Phattaranawik wishes to thank the UNESCO Centre for Membrane Science & Technology for hospitality.

Nomenclature

a constant in Eq.(35)

С	membrane distillation coefficient (kg.m ⁻² .s ⁻¹ .Pa ⁻¹)
d_{f}	filament diameter (m)
$\mathbf{d_h}$	hydraulic diameter (m)
D	diffusivity (m ² .s ⁻¹)
h	heat transfer coefficient (W.m ⁻² .K ⁻¹)
Н	spacer thickness (m)
$H_v\{T\}$	vapor enthalpy evaluated at temperature T
K	mass transfer coefficient (m.s ⁻¹)
J	mass flux (kg.m ⁻² .s ⁻¹)
J_v	volumetric flux (m ³ .m ⁻² .s ⁻¹)
L	channel length (m)
Nu	Nusselt number
P	vapor pressure (Pa)
Pr	Prandlt number
Re	Reynolds number
Sc	Schmidt number
Sh	Sherwood number
T	temperature (K)
Greek letters	
τ	temperature polarization coefficient
ε	voidage
δ	membrane thickness
α^s	spacer factor
Ψс	correction factor for mass transfer coefficient
Ψτ	correction factor for heat transfer coefficient
θ	hydrodynamic angle

thickness of concentration boundary layer

 Δ_{C}

Δ_{T}	unickness of thermal boundary layer
Subscripts	
1	membrane surface on feed side
2	membrane surface on permeate side
f	feed
p	permeate
v	vapor
Н	high mass transfer rates
L	low mass transfer rates
Superscript	

spacer-filled channel

References

S

- R.W. Schofield, A.G. Fane, and C.J.D. Fell, Heat and mass transfer in membrane distillation, J. Membr. Sci., 33 (1987) 299-313.
- 2. L. Martinaz-Diez, M.I Vazquez-Gonzalez, F.J. Florido-Diaz, Study of membrane distillation using channel spacers, J. Membr. Sci., 144 (1998) 45-56.
- A.R. Da Costa, A.G. Fane, D.E. Wiley, Spacer characterization and pressure drop modeling in spacer-filled channels, J. Membr. Sci., 87 (1994) 79-98.
- 4. J. Schwinge, D.E. Wiley, A.G. Fane, R.Guenther, Characterization of a zigzag spacer for ultrafiltration, J. Membr. Sci., 172 (2000) 19-31.
- J. Phattaranawik, R. Jiraratananon, A.G. Fane, C. Halim, Mass flux enhancement using spacer filled channels in direct contact membrane distillation, J. Membr. Sci., 187 (2001) 193-201.
- A.R. Da Costa, A.G. Fane, C.J.D. Fell and A.C.M. Fraken, Optimal channel spacer design for ultrafiltration, J. Membr. Sci., 62 (1991) 275-291.
- G. Shock and A. Miquel, Mass transfer and pressure loss in spiral wound modules, Desalination, 64 (1987) 339-352.

- 8. J. Phattaranawik, R. Jiraratananon, A.G. Fane, Heat Transport and Membrane Distillation Coefficient in Direct Contact Membrane Distillation, Submitted to Journal of Membrane Science.
- 9. R.B. Bird, W.E. Stewart and E.N. Lightfoot, Transport Phenomena, Wiley, New York, 1960.
- 10. A.F. Mills, Mass Transfer, 2nd Edition, Prentice-Hall, New Jersey, 2001.
- J.R. Welty, C.E. Wicks, and R.E. Wilson, Fundamentals of Momentum, Heat and Mass Transfer, 3rd Ed, Wile, New York, 1984.
- K.W. Lawson, D.R. Lloyd, Membrane distillation. I. Module design and performance evaluation using vacuum membrane distillation, J. Membr. Sci., 120 (1996) 111-121.
- K.W. Lawson, D.R. Lloyd, Membrane distillation. II. Direct Contact MD, J. Membr. Sci., 120 (1996) 123-133.
- R.W. Schofield, A.G. Fane and C.J.D. Fell, Gas and vapor transport through Microporous membranes. II. Membrane distillation, J. Membr. Sci., 53 (1990) 173-185.
- M. Gryta, M. Tomaszewska, Heat transport in membrane distillation process, J. Membr. Sci., 144
 (1998) 211-222.
- M.A. Izquierdo-Gil, M.C. Garcia-Payo, and C. Fernandez-Pineda, Air gap membrane distillation of surcose aqueous solution, J. Membr. Sci., 155(1999) 291-307.
- S.K. Karode and Ashwani Kumar, Flow visualization through spacer filled channels by computational fluid dynamics I. Pressure drop and shear rate calculations for flat sheet geometry.
 J. Membr. Sci., 193 (2001) 69-84.
- A.R. Da Costa, A.G. Fane, D.E. Wiley, Ultrafiltration of whey protein solutions in spacer-filled flat channels, J. Membr. Sci., 76 (1993) 245-254.
- H. Grober, S.Erk and U. Grigull, Fundamentals of heat transfer, McGraw-Hill, New York, NY,
 1961.
- Z. Cao, D.E. Wiley, A.G. Fane, CFD simulations of net-type turbulence promoters in a narrow channel, J. Membr. Sci., 185 (2001) 157-176.

List of figures

- Figure 1. Temperature polarization for empty channels and spacer-filled channels.
- Figure 2. High mass transfer rate convection for heat transfer in DCMD.
- Figure 3. High mass transfer rate convection for mass transfer in UF.
- Figure 4. Flowchart of heat transfer coefficient calculations.
- Figure 5. Mass fluxes for various hydrodynamic angles ($\varepsilon \approx 0.6$) and for empty channels.

(Permeate flow rate = 1.58×10^{-5} m³/s, GVHP membrane)

- Figure 6. Effect of voidage on fluxes. (Permeate flow rate = 1.58×10^{-5} m³/s, for GVHP membrane at $T_f = 70$ °C)
- Figure 7. Effect of flow rates on mass flux enhancement ($T_f = 70 \, ^{\circ}\text{C}$, $\theta = 90^{\circ}$, $\epsilon = 0.632$)
- Figure 8. Effect of feed temperatures on mass flux enhancement.

(Permeate flow rate = $1.58 \times 10^{-5} \text{ m}^3/\text{s}$, $\theta = 70^\circ$, $\epsilon = 0.596$)

- Figure 9. Calculated heat transfer coefficients for spacer-filled channel at flow rate = 1.58×10^{-5} m³/s.
- Figure 10. Calculated heat transfer coefficients for spacer-filled channel at flow rate = $2.63 \times 10^{-5} \text{ m}^3/\text{s}$.
- Figure 11. Temperature polarization coefficient for empty and spacer-filled channels.

(for GVHP membrane, permeate flow rate = 2.63×10^{-5} m³/s)

- Figure 12. Comparisons of mass transfer coefficients.
- Figure 13. ψ_T and ratio of mass transfer coefficient.
- Figure 14. Comparison of heat transfer coefficients.

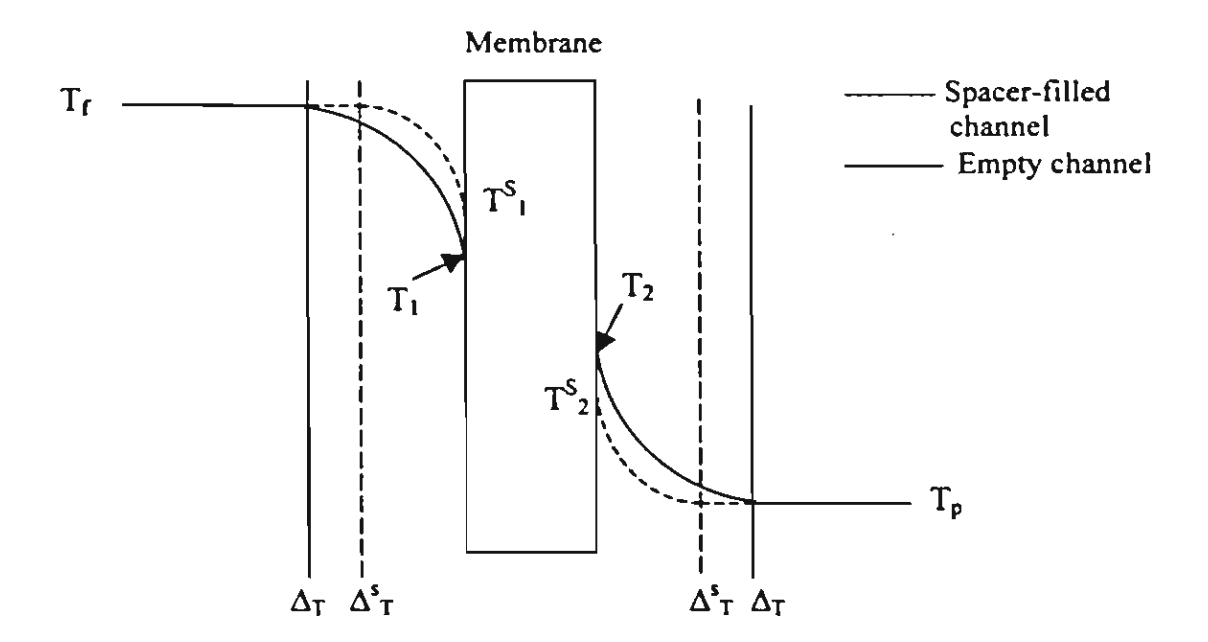


Fig.1. Temperature polarization for empty channels and spacer-filled channels.

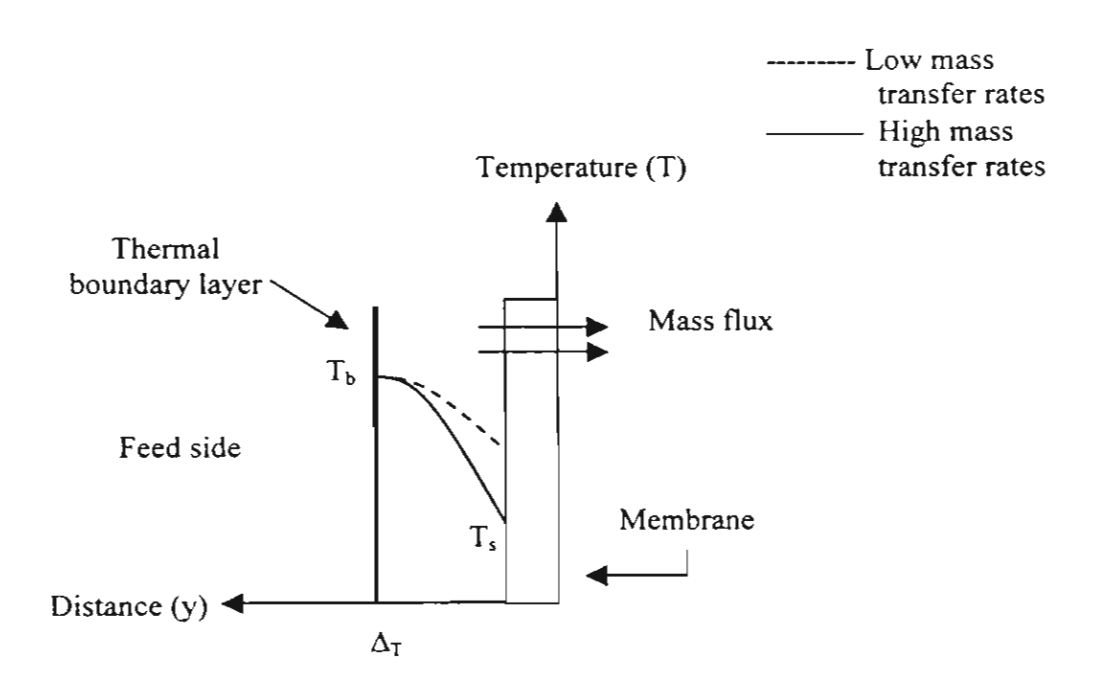


Fig.2. Effect of high mass transfer rates for heat transfer in DCMD.

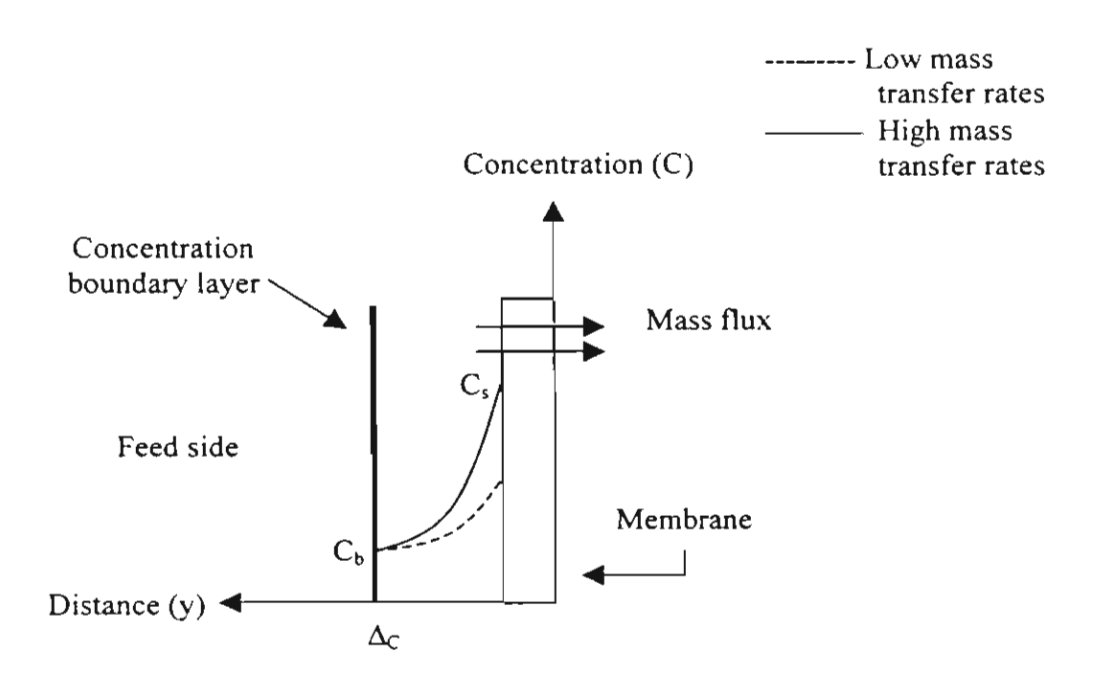


Fig.3. Effect of high mass transfer rates for mass transfer in UF.

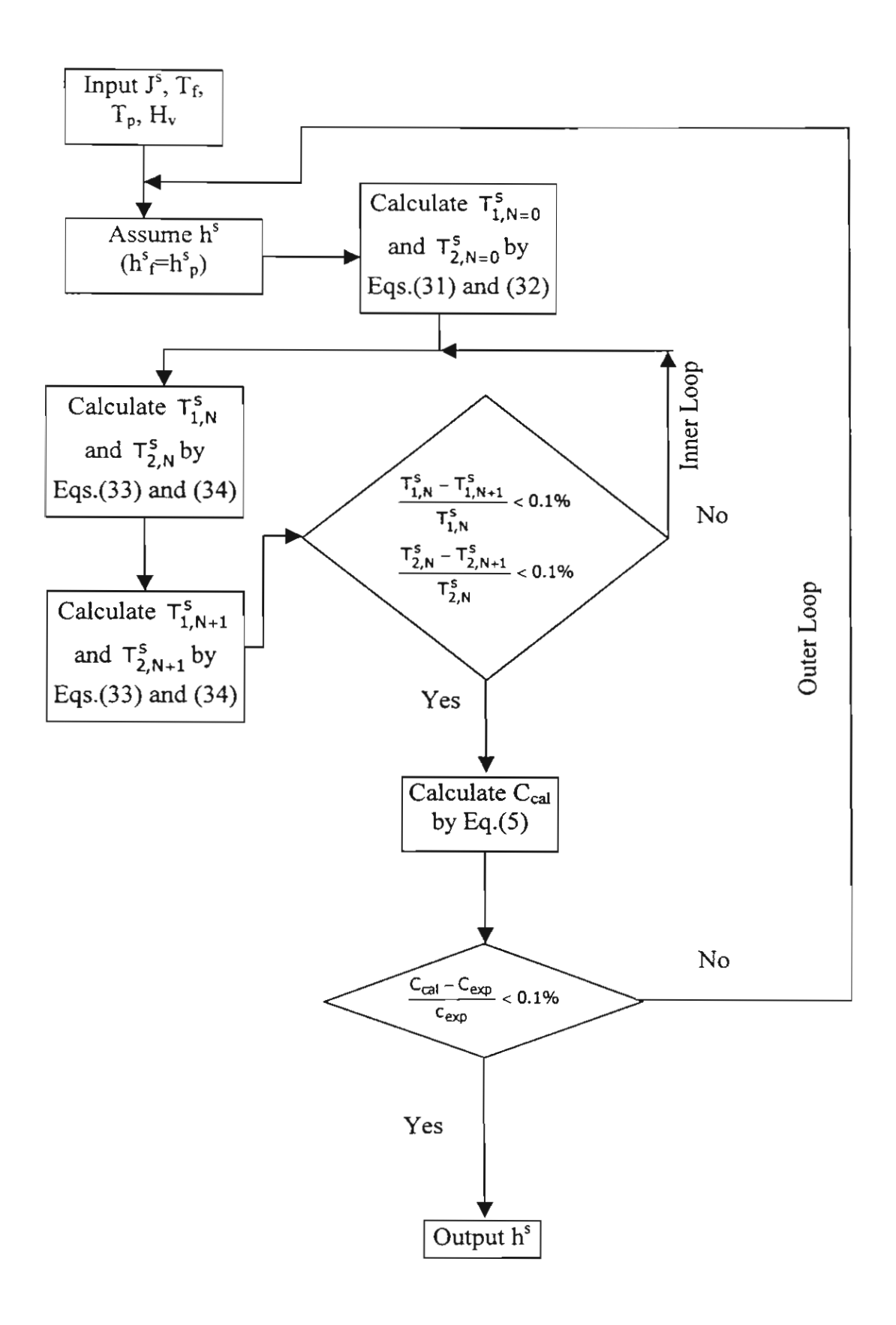


Fig. 4. Flowchart of heat transfer coefficient calculations.

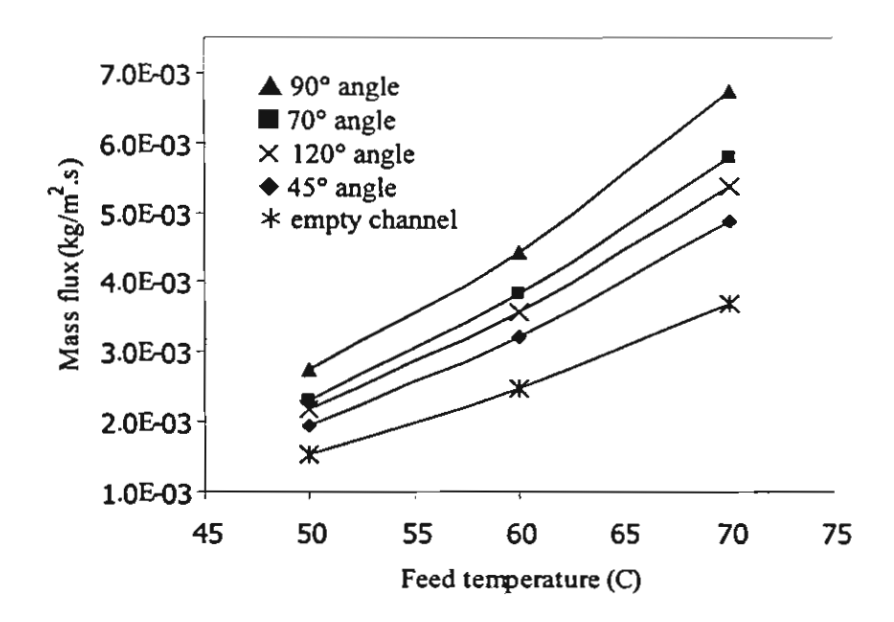


Fig. 5. Mass fluxes for various hydrodynamic angles ($\epsilon \approx 0.6$) and for empty channels. (Permeate flow rate = 1.58×10^{-5} m³/s, for GVHP membrane)

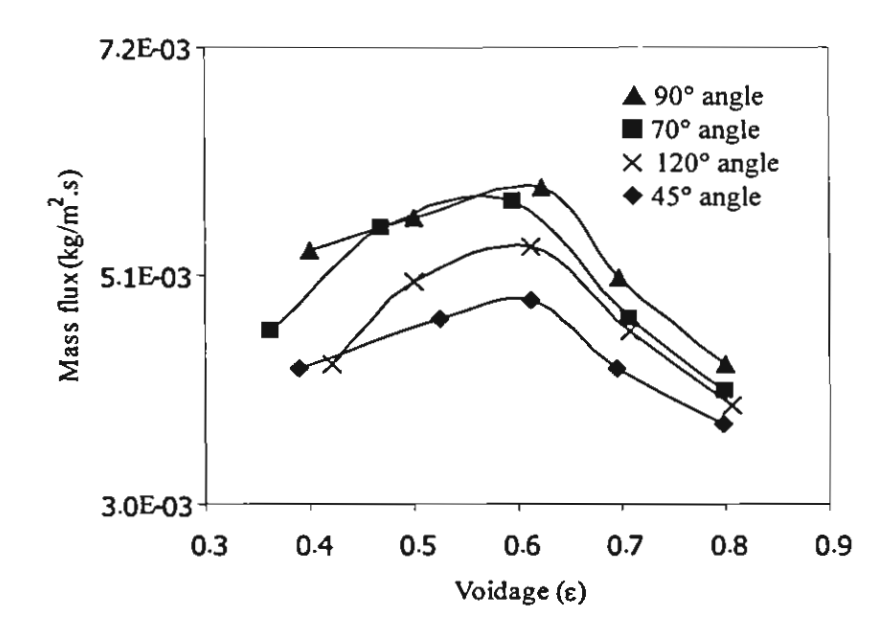


Fig. 6. Effect of voidage on fluxes. (Permeate flow rate = 1.58×10^{-5} m³/s, for GVHP membrane and $T_f = 70$ °C)

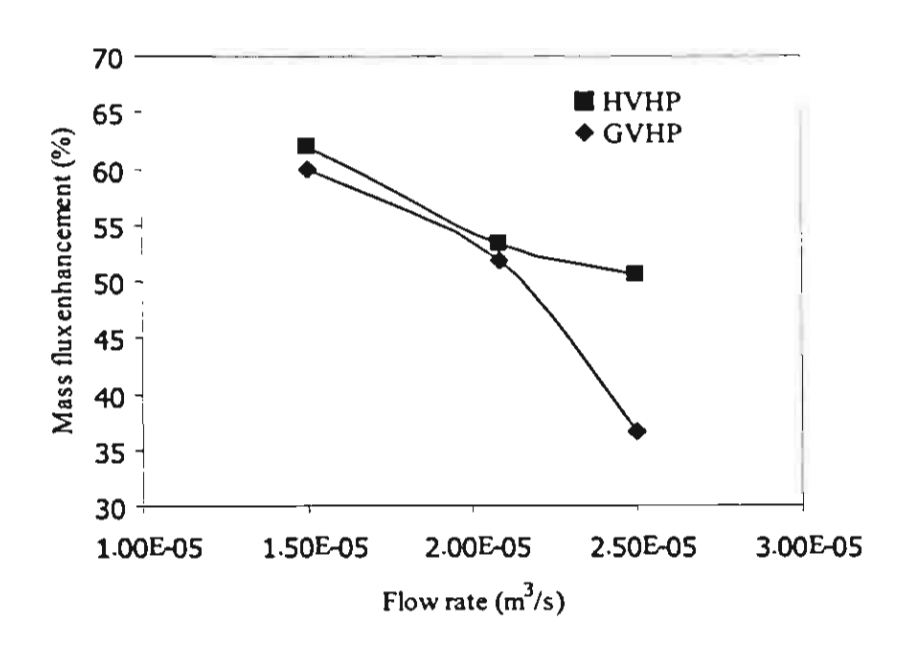


Fig. 7. Effect of flow rates on mass flux enhancement ($T_f = 70$ °C, $\theta = 90$ °, $\epsilon = 0.632$)

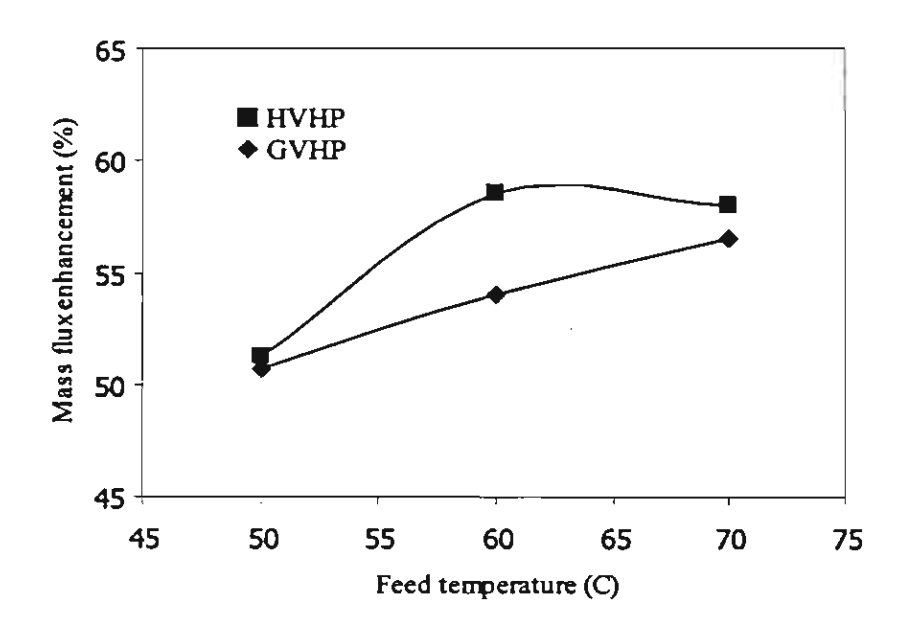


Fig. 8. Effect of feed temperatures on mass flux enhancement (Permeate flow rate =1.58×10⁻⁵ m³/s, θ = 70°, ϵ = 0.596)

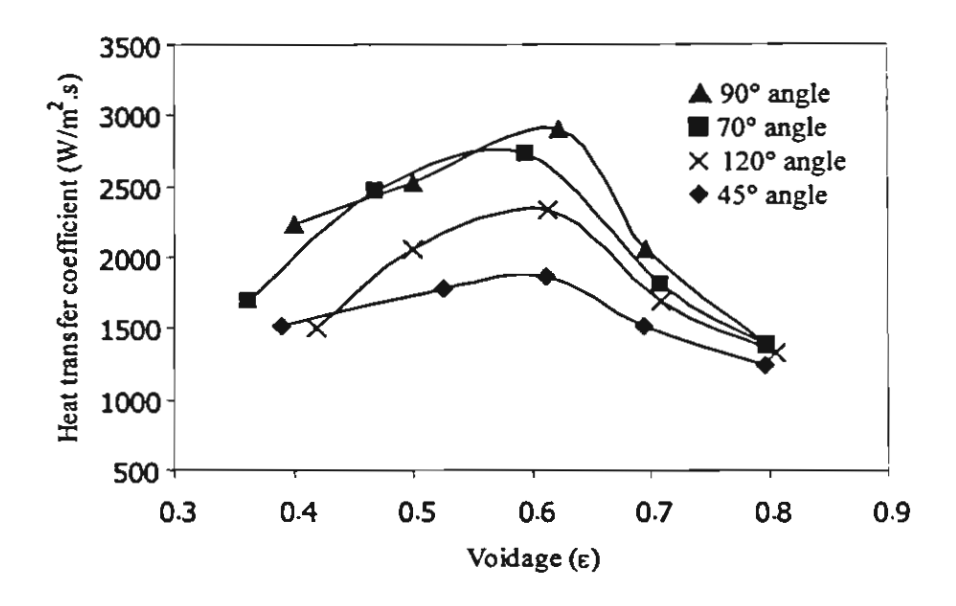


Fig. 9. Calculated heat transfer coefficients for spacer-filled channel at flow $rate = 1.58 \times 10^{-5} \text{ m}^3/\text{s}$

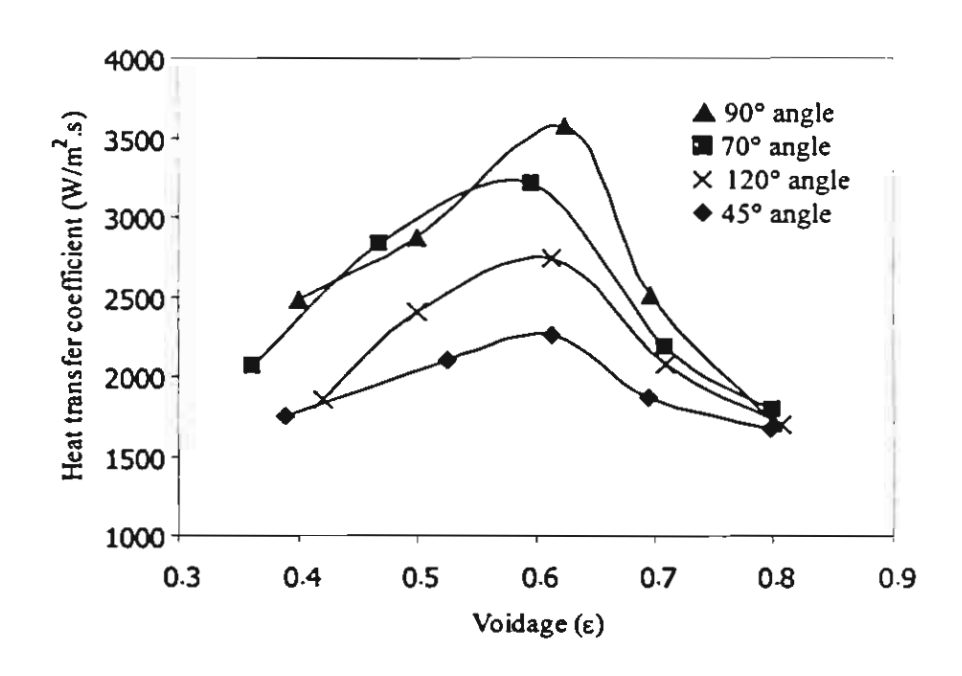


Fig. 10. Calculated heat transfer coefficients for spacer-filled channel at flow rate = 2.63×10^{-5} m³/s

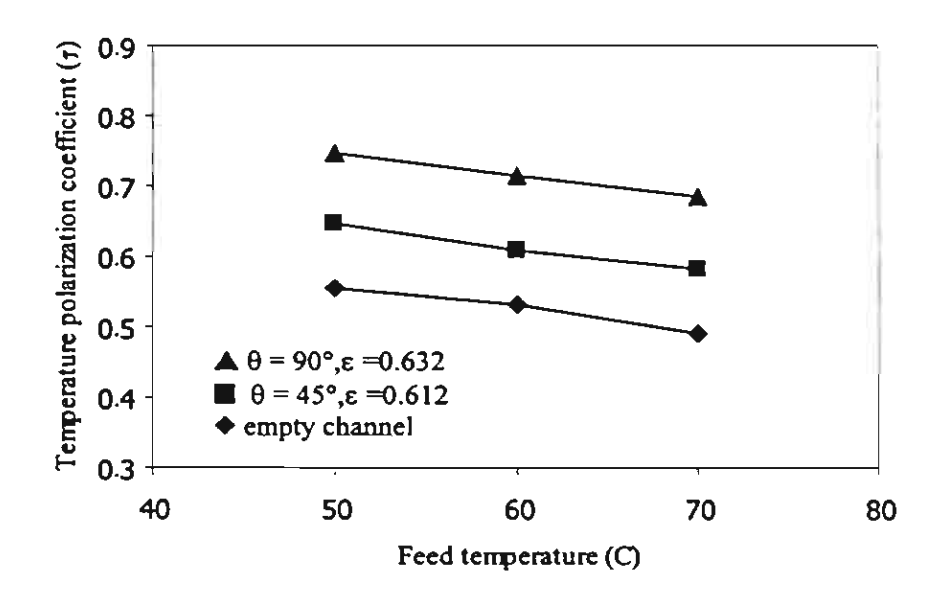


Fig. 11. Temperature polarization coefficient for empty and spacer-filled channels (for GVHP membrane, permeate flow rate = 2.63×10^{-5} m³/s)

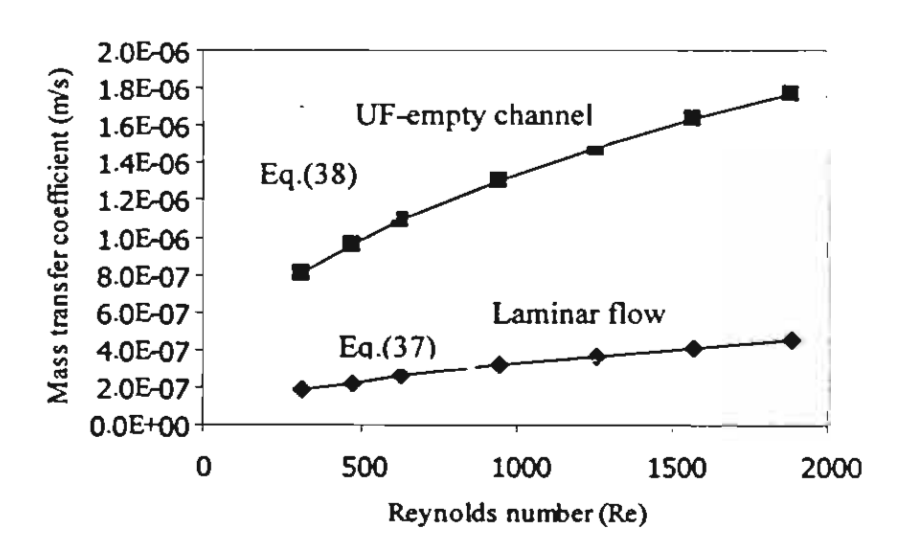


Fig. 12. Comparisons of mass transfer coefficients

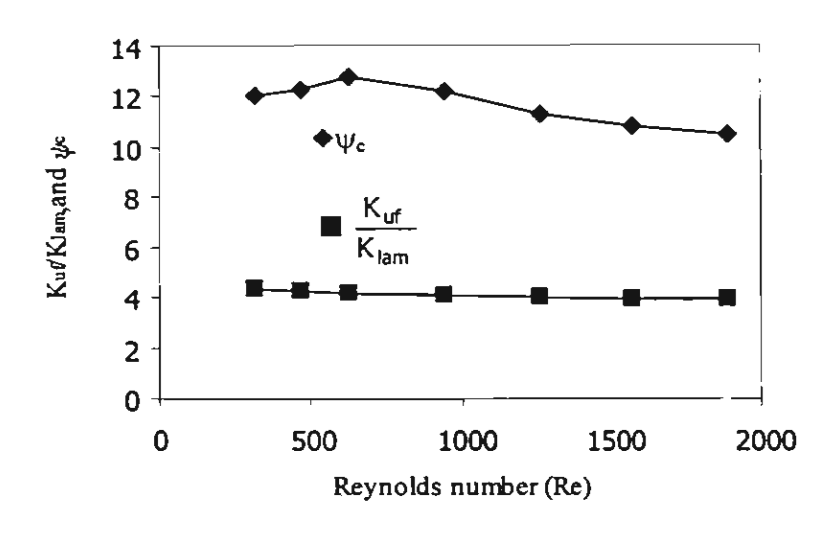


Fig. 13. ψ_T and ratio of mass transfer coefficient

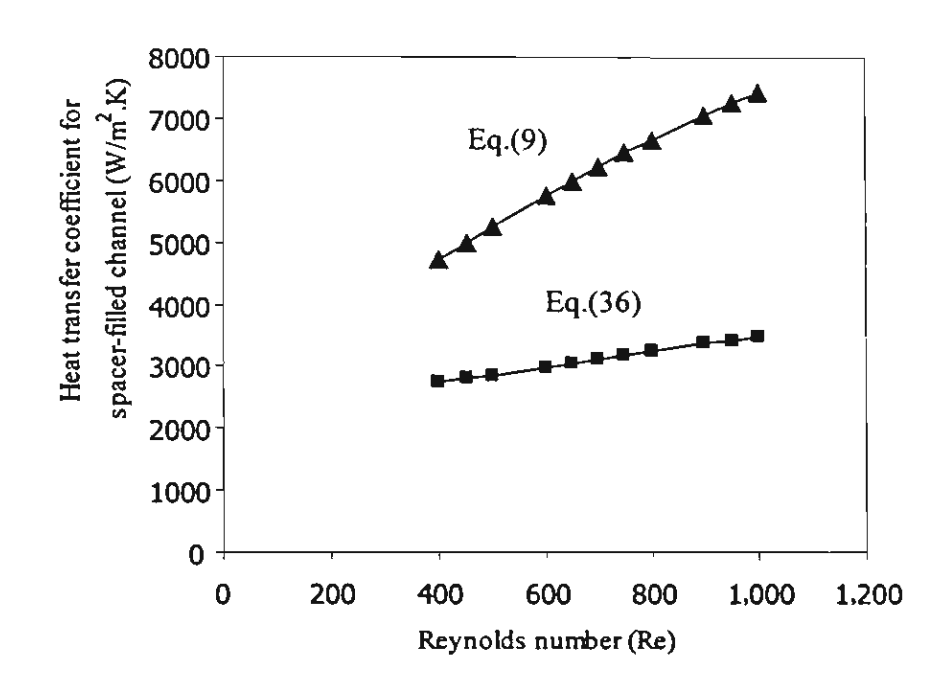


Fig. 14. Comparison of heat transfer coefficients ($\theta = 90^{\circ}$, $\epsilon = 0.632$)